Dielectrophoretic cytometry for measurement of live cell dielectric signatures on population level

Pavel Fikar

University of West Bohemia

Department of Applied Electronics and Telecommunications

Faculty of Electrical Engineering

Dissertation thesis submitted in fulfilment of the requirements for the degree of Doctor of Philosophy.

Université Paris-Est

Mathématiques, Sciences de l'Information et de la Communication (MSTIC)

École Doctorale

Thèse pour obtenir le grade de Docteur de l'Université Paris-Est.

Dielectrophoretic cytometry for measurement of live cell dielectric signatures on population level

Cytométrie diélectrophorétique pour les mesures des signatures diélectriques de cellules vivantes au niveau d'une population

---

Author

Pavel Fikar

Supervisors

Doc. Dr. Ing. Vjačeslav Georgiev

Prof. Gaëlle Lissorgues

Jury

Mustapha Nadi, Professeur, Univ Lorraine	Rapporteur
Antoine Pallandre, Professeur, Univ Paris 11	Rapporteur
Daniel Georgiev, Chargé de Recherche, UWB, République Tchèque	Examinateur
Thibault Honneger, Chargé de Recherche, CEA, Grenoble	Examinateur

March 2017

Declaration of Authorship

I, Pavel Fikar, declare that this thesis titled, 'Dielectrophoretic cytometry for measurement of live cell dielectric signatures on population level' and the work presented in it are my own. I confirm that:

- This work was done wholly or mainly while in candidature for a research degree at the University.
- Where any part of this thesis has previously been submitted for a degree or any other qualification at this University or any other institution, this has been clearly stated.
- Where I have consulted the published work of others, this is always clearly attributed.
- Where I have quoted from the work of others, the source is always given. With the exception of such quotations, this thesis is entirely my own work.
- I have acknowledged all main sources of help.
- Where the thesis is based on work done by myself jointly with others, I have made clear exactly what was done by others and what I have contributed myself.

Signed: _____

Date: _____

UNIVERSITY OF WEST BOHEMIA
UNIVERSITÉ PARIS-EST

Abstract in English

Doctor of Philosophy

Dielectrophoretic cytometry for measurement of live cell dielectric signatures on population level

by Pavel Fikar

Flow cytometry in combination with staining and antibody labelling presents one of the most valuable tools in current biotechnology providing information about cell population heterogeneity, cell size and volume, as well as expression of certain surface and intracellular molecules. The increased cost and the fundamental difficulty of these methods, however, are attributed to the requirement of the surface marker molecules. Attractive alternatives to flow cytometry are label-free methods, such as micro-filtration, Dielectric Spectroscopy (DS), and electro-kinetic methods. Out of these methods, Dielectrophoresis (DEP) was selected as the most promising approach. This thesis focuses on improvements of current DEP-based technologies, and development and establishment of a new method to address the issues of Dielectrophoretic (DEP) cytometry enabling label-free non-invasive probabilistic measurement of cell Dielectric (DE) signatures on population level, as well as enabling identification of reliable biomarkers for cell changes.

First, improvements of DEP cytometry based on DEP-induced lateral cell translation through fabrication are explored. A novel highly precise SU-8 fabrication technology is employed to construct microfluidic devices for sensitive DEP manipulation of budding *Saccharomyces cerevisiae* (*S. cerevisiae*) cells. A benchmark microfluidic live cell sorting system is presented, and the effect of microchannel misalignment above electrode topologies on live cell DEP is discussed in detail. Simplified model of budding *S. cerevisiae* cell is presented and validated experimentally in fabricated microfluidic devices. A novel fabrication process enabling rapid prototyping of microfluidic devices with well-aligned integrated electrodes is presented and the process flow is described. Identical devices were produced with standard soft lithography processes. In comparison to standard Poly(dimethylsiloxane) (PDMS) based soft lithography, an SU-8 layer was used to construct the microchannel walls sealed by a flat sheet of PDMS to obtain the microfluidic channels. Direct bonding of PDMS to SU-8 surface was achieved by efficient wet chemical silanization combined with oxygen plasma treatment of the contact surface. The

presented fabrication process significantly improved the alignment of the microstructures. According to the benchmark study, the standard PDMS procedure fell well outside the range required for reasonable cell sorting efficiency. In addition, PDMS delamination above electrode topologies was significantly decreased over standard soft lithography devices. The fabrication time and costs of the proposed methodology were found to be roughly the same.

In the second part of the PhD project, a method called Distributed Dielectrophoretic Cytometry (2DEP Cytometry) was developed. It uses a DEP-induced vertical translation of live cells in conjunction with Particle Image Velocimetry (PIV) in order to measure probabilistic distribution of live cell DE signatures on an entire cell population. The method was integrated in a micro-fluidic device. The bottom of the micro-fluidic channel is lined with an Interdigitated (ID) electrode array. Cells passing through the micro-channel are acted on by sedimentation forces, while DEP forces either oppose sedimentation, support sedimentation, or neither, depending on the DE signatures of the cells. The heights at which cells stabilize correspond to their DE signature and are measured indirectly using PIV. The presented method is similar to all-electric DEP cytometry [80], however it is based on PIV analysis, which enables simultaneous and high-throughput collection of hundreds of single-cell responses in a single frame. In addition, PIV may be further integrated with fluorescence measurements yielding correlations between DE signatures and intracellular processes.

Experimental data quantify the DE signature of a *S. cerevisiae* population and Human Immortalised Myelogenous Leukemia (K562) cell line. It is shown that DEP-induced cell translation along the parabolic velocity profile can be measured by PIV with submicron precision, enabling identification of individual cell DE signatures. It is possible to analyse more than 5 thousand cells within 1 minute with the actual experimental setup. The high-throughput enables measurement of DE signatures at 20 different frequencies in almost real-time. The experimental results are consistent with other studies [68, 100]. Applications of 2DEP Cytometry in synthetic biology and cancer research were demonstrated. 2DEP Cytometry was used to detect differences in molecular expression on cells by differential analysis of *a*) *S. cerevisiae* cells, and *b*) K562 cell line. First, the effect of over-expression of certain membrane protein was studied in *S. cerevisiae* cells. Measured distribution of DEP forces was compared to distribution of DEP forces of *S. cerevisiae* cell population expressing a cytoplasmic protein at the same rate. Second, 2DEP Cytometry was applied to, and validated on, K562 cell line. Effects of stress response triggered by various inducers (heat shock and pH variations) on the DE signature of the cell population were analysed.

Finally, statistical data analysis defined adjusted Kernel Density Estimation (KDE) to overcome the finite nature of the measured data, and in combination with Wasserstein pseudometrics from sampled data, the Wasserstein distance spectra, denoted as Wasserstein signatures, were quantified and linked to certain cell changes. These signatures identify frequencies, where less and more significant differences between the measured DE signatures are observed, and may be used as reliable biomarkers for cell changes measurable by 2DEP Cytometry.

In conclusion, 2DEP Cytometry showed it is sensitive enough to identify certain changes in cell states. The novel 2DEP Cytometry device is therefore a promising alternative to conventional flow cytometry.

ZÁPADOČESKÁ UNIVERZITA V PLZNI
UNIVERSITÉ PARIS-EST

Abstrakt v češtině - Abstract in Czech

Doktor Filozofie

Dielektroforetická cytometrie pro měření dielektrických podpisů živých buněk na populační úrovni

Pavel Fikar

Průtoková cytometrie v kombinaci s barvením a značením pomocí protilátek představuje v současnosti jeden z nejcennějších nástrojů na poli biotechnologií a poskytuje informace o heterogenitě populace buněk, velikosti buněk a jejich objemu, jakož i expresi některých povrchových a intracelulárních molekul. Nicméně vysoké pořizovací i provozní náklady a základní obtížnost těchto metod je připisována právě potřebnosti protilátek k povrchovým markerům. Atraktivními alternativami k průtokové cytometrii jsou tedy metody, které nevyžadují značení, mezi které se řadí mimo jiné mikro-filtrace, dielektrická spektroskopie či elektro-kinetické metody. Z těchto metod byla vybrána dielektroforéza (DEP) jako nejslibnější. Tato práce se zaměřuje na zvýšení efektivity stávajících technologií založených na DEP efektu a na vývoj a zavedení nové metody pro řešení problémů DEP cytometrie umožňující neinvazivní pravděpodobnostní měření buněčných Dielektrických (DE) podpisů na populační úrovni bez potřeby značení pomocí protilátek, a v neposlední řadě na zavedení metriky umožňující identifikaci spolehlivých biomarkerů pro buněčné změny.

První část práce je zaměřena na vylepšení metod DEP cytometrie založené na laterální translaci buněk skrze optimalizaci výrobního postupu. Nová precizní výrobní technologie využívající SU-8 je využita ke konstrukci mikrofluidního zařízení pro citlivou DEP manipulaci pučících kvasinkových buněk *Saccharomyces cerevisiae* (*S. cerevisiae*). Benchmark mikrofluidní systém pro třídění živých buněk je prezentován a účinnost DEP vychylování živých buněk nad elektrodovými topologiemi je podrobně rozebrána. Zjednodušený model pučící *S. cerevisiae* buňky je prezentován a ověřen experimentálně ve vyrobených mikrofluidních zařízeních. Nový proces výroby umožňující rychlé prototypování mikrofluidních zařízení s perfektně zarovnanými integrovanými elektrodami je prezentován a výrobní proces je detailně popsán. Identická zařízení byla vyrobena pomocí standardních procesů měkké litografie. Na rozdíl od standardní Poly(dimethylsiloxane) (PDMS) měkké litografie byla pro konstrukci stěn mikrofluidních kanálů použita vrstva SU-8.

Mikrofluidní kanál byl posléze zapouzdřen jednoduchou vrstvou PDMS. Přímé vazby mezi PDMS a SU-8 bylo dosaženo efektivní mokrou chemickou silanizací v kombinaci s ošetřením kontaktních povrchů kyslíkovou plazmou. Předkládaný výrobní proces výrazně zlepšil relativní zarovnání mikrostruktur. Podle srovnávací studie, standardní postup založený na PDMS měkké litografii spadá výrazně mimo rozsah požadovaný pro efektivní třídění buněk. Využitím nového výrobního postupu došlo mimo jiné ke snížení delaminace PDMS ve srovnání se standardní měkkou litografií. Doba zhotovení a náklady porovnávaných metodik zůstávají zhruba stejné.

V druhé části disertační práce byla vyvinuta nová metoda nazvaná Distribuovaná Dielektroforetická Cytometrie (2DEP Cytometrie). Ta využívá DEP-indukovanou vertikální translaci živých buněk ve spojení s Částicovou Velocimetrií (PIV) k měření pravděpodobnostních distribucí DE podpisů živých buněk v rámci celé buněčné populace. Metoda byla integrována v mikrofluidním zařízení. Dno mikrofluidního kanálu je lemováno řadou Interdigitálních (ID) elektrod. Buňky procházející mikrokanálem sedimentují, zatímco DEP síly působí buď proti sedimentaci, sedimentaci podporují, nebo nepůsobí vůbec, v závislosti na konkrétním DE podpisu buněk. Výšky, ve kterých se buňky stabilizují odpovídají jejich DE podpisům a jsou měřeny nepřímo pomocí PIV. Tato metoda funguje na podobném principu jako kompletně elektrická DEP cytometrie [80], avšak je založena na PIV analýze, která umožňuje současný sběr až stovek DE podpisů jednotlivých buněk v rámci jednoho PIV snímku. PIV lze mimo jiné dále kombinovat s měřením fluorescence přinášející možnosti korelace DE podpisů a intracelulárních procesů.

Experimentální data kvantifikují DE podpisy populace *S. cerevisiae* a imortalizované leukemické buněčné linie (K562). Bylo prokázáno, že DEP-indukovaná buněčná translace podél parabolického rychlostního profilu může být měřena pomocí PIV se sub-mikronovou přesností, což umožňuje identifikaci jednotlivých DE buněčných podpisů. S aktuální experimentální sestavou je možné analyzovat více než 5 tisíc buněk během 1 minuty. Takto vysoká rychlost zpracování umožňuje měření DE podpisů na 20 různých frekvencích elektrického pole v téměř reálném čase. Experimentální výsledky jsou v souladu s jinými studiemi [68, 100]. Dále byly demonstrovány aplikace 2DEP Cytometrie v syntetické biologii a výzkumu rakoviny. 2DEP Cytometrie byla použita ke zjištění rozdílů v molekulární expresi pomocí diferenciální analýzy a) buněk *S. cerevisiae* b) buněčné linie K562. Nejdříve byl zkoumán účinek nadměrné exprese konkrétního membránového proteinu v buňkách *S. cerevisiae*. Naměřená distribuce rozložení DEP sil byla srovnána s distribucí DEP sil populace buněk *S. cerevisiae* exprimujících cytoplazmatický protein stejnou rychlostí. Následně byla 2DEP Cytometrie aplikována a ověřena na buněčné linii K562. Zde byly analyzovány účinky stresové reakce vyvolané různými induktory (tepelným šokem a kolísáním hodnoty pH) na změnu DE podpisu této buněčné linie.

V poslední řadě byla provedena detailní statistická analýza experimentálních dat. Ta definuje nejprve přizpůsobenou Metodu Jádrových Odhadů (KDE), která slouží ke kompenzaci konečné povahy naměřených experimentálních dat. A následně je definována přizpůsobená Wassersteinova pseudometrika ze vzorkovaných dat. Kombinace KDE a spektra Wassersteinových vzdáleností, označených jako Wassersteinův podpis, byly kvantifikovány a spojeny s konkrétními změnami buněk. Tyto podpisy určují frekvence elektrického pole, při kterých jsou pozorovány méně či více významné rozdíly mezi naměřenými DE podpisy a mohou být použity jako spolehlivé biomarkery pro změny buněk měřitelné pomocí 2DEP Cytometrie.

Závěrem lze říci, že 2DEP Cytometrie ukázala, že je dostatečně citlivá pro identifikaci určitých změn v buněčných stavech. 2DEP Cytometrie je tedy slibnou alternativou k běžné průtokové cytometrii.

UNIVERSITÉ PARIS-EST
UNIVERSITY OF WEST BOHEMIA

Abstract en Français - Abstract in French

Docteur de l'Université Paris-Est

Cytométrie diélectrophorétique pour les mesures des signatures diélectriques de cellules vivantes au niveau d'une population

Pavel Fikar

La cytométrie en flux en association avec la coloration et le marquage d'anticorps présente l'un des outils les plus précieux en biotechnologie actuelle fournissant des informations sur l'hétérogénéité des populations cellulaires, la taille et le volume des cellules, ainsi que l'expression de certaines molécules de surface et intracellulaires. L'augmentation du coût et la difficulté fondamentale de ces méthodes, cependant, sont attribués à l'exigence des molécules de marquage de surface. Des méthodes sans marquage sont des alternatives attrayantes en cytometrie en flux comme la micro-filtration, la spectroscopie diélectrique et les méthodes électro-cinétiques. Parmi ces méthodes, la Diélectrophorèse (DEP) a été choisi comme l'approche la plus prometteuse. Cette thèse porte sur l'amélioration des technologies basée sur les DEP actuelles, et le développement et la création d'une nouvelle méthode pour aborder les questions de cytometrie Diélectrophorétique (DEP) permettant la mesure probabiliste des signatures Diélectriques (DE) non-invasive sans marquage de cellules vivantes au niveau dune population, ainsi que de permettre l'identification de biomarqueurs fiables pour les changements cellulaires.

Tout d'abord, les améliorations de la cytometrie DEP sur la translation de cellules latérales induites par DEP sont explorées par fabrication. Une nouvelle technologie de fabrication de haute précision basée sur SU-8 est utilisée pour construire des dispositifs microfluidiques pour la manipulation DEP sensible de cellules *Saccharomyces cerevisiae* (*S. cerevisiae*). Un système de tri cellulaire benchmark microfluidique est présenté, et l'effet des désalignements des microcanaux sur les topologies des électrodes des cellules DEP vivantes est discuté en détail. Un modèle simplifié de cellule *S. cerevisiae* bourgeonnant est présenté et validé expérimentalement dans des dispositifs microfluidiques fabriqués. Un nouveau procédé de fabrication permettant le prototypage rapide de dispositifs microfluidiques avec des électrodes intégrées bien alignées est présenté et le flux de processus est décrit. Des dispositifs identiques ont été fabriqués avec des procédés standards de lithographie douce. En comparaison avec le procédé standard de

lithographie douce basé sur Poly(dimethylsiloxane) (PDMS), une couche SU-8 a été utilisé pour construire les murs des microcanaux scellés par une feuille plate de PDMS pour obtenir les canaux microfluidiques. La liaison directe du PDMS sur la surface SU-8 a été réalisée par une efficace silanisation humide chimique combinée avec un traitement au plasma d'oxygène de la surface de contact. Le procédé de fabrication présenté a amélioré de manière significative l'alignement des microstructures. Selon l'étude benchmark, la procédure standard PDMS est tombée bien en dessous de la gamme nécessaire pour le tri des cellules vivantes par DEP. En outre, le délaminage du PDMS sur les topologies d'électrodes était diminué significativement par rapport aux dispositifs standard de lithographie douce. Le temps de fabrication et les coûts de la méthode proposée se sont révélés être à peu près les mêmes.

Dans la deuxième partie du projet de doctorat, une nouvelle méthode appelée Cytométrie Diélectrophorétique Distribuée (2DEP Cytométrie) a été développée. Elle utilise un effet de diélectrophorèse induite par translation verticale de cellules vivantes en liaison avec la Vélocimétrie par Image de Particules (PIV) afin de mesurer la répartition probabiliste de forces DEP sur une population cellulaire entière. La méthode a été intégrée dans un dispositif microfluidique. Le fond du canal microfluidique est bordée d'une matrice d'électrodes Interdigitées (ID). Les cellules passant à travers le micro-canal sont sollicitées par des forces de sédimentation, tandis que les forces DEP soit sopposent a la sédimentation, prennent en charge la sédimentation, ou aucun des deux, en fonction des signatures DE des cellules. Les hauteurs à laquelle les cellules se stabilisent correspondent à leur signature DE et sont mesurées indirectement en utilisant PIV. La méthode présentée est similaire à tout-électrique cytométrie DEP [80], mais elle est basée sur l'analyse PIV, qui permet la collecte simultanée et à haut débit de centaines de réponses cellulaires unique en un coup PIV unique. En outre, PIV peut encore être combiné avec des mesures de fluorescence donnant des corrélations entre signatures DE et les processus intracellulaires.

Les données expérimentales quantifient la signature DE d'une population de *S. cerevisiae* et la lignée cellulaire Human immortalise leucemie myeloide (K562). Il est montré que la translation de la cellule induite par DEP le long du profil de vitesse parabolique peut être mesurée par PIV avec une précision inférieure au micron, ce qui permet l'identification des signatures DE de cellules individuelles. Il est possible d'analyser plus de 5 mille cellules en moins de 1 minute avec la configuration expérimentale actuelle. Le haut débit permet de mesurer les signatures DE à 20 fréquences différentes presque en temps réel. Les résultats expérimentaux sont en accord avec d'autres études [68,100]. Les applications de 2DEP Cytométrie en biologie synthétique et en recherche sur le cancer ont été démontrées. 2DEP Cytométrie a été utilisée pour détecter des différences dans l'expression moléculaire sur les cellules par analyse différentielle de a) cellules *S. cerevisiae*, et b) la lignée cellulaire K562. Tout d'abord, l'effet de la surexpression de certaines protéines membranaires a

été étudié dans des cellules *S. cerevisiae*. La répartition mesurée des forces DEP a été comparée à la répartition des forces DEP dune population de cellules *S. cerevisiae* exprimant une protéine cytoplasmique au même taux. Deuxièmement, 2DEP Cytométrie a été appliquée à, et validée sur, la lignée cellulaire K562. Les effets de la réponse à un stress provoqué par divers inducteurs (choc thermique et variations de pH) sur la signature DE de la population cellulaire ont été analysées.

Enfin, l'analyse statistique des données définies Estimation par Noyau (KDE) ajustées pour surmonter la nature finie des données mesurées. En combinaison avec des pseudometriques Wasserstein à partir des données échantillonnées, les spectres en distance de Wasserstein, notés signatures Wasserstein, ont été quantifiés et liée à certains changements cellulaires. Ces signatures identifient des fréquences, où des différences plus ou moins significatives entre les signatures DE mesurées sont observées, et peuvent être utilisées comme marqueurs biologiques fiables pour certains changements cellulaires mesurables par 2DEP Cytométrie.

En conclusion, 2DEP Cytométrie a montré être suffisamment sensible pour identifier certains changements détats cellulaires. Le nouveau dispositif 2DEP Cytométrie est donc une alternative prometteuse à la cytométrie en flux classique.

Acknowledgements

First of all, I want to thank immeasurably to my supervisors Vjačeslav Georgiev and Gaëlle Lissorgues, who were so brave and took the responsibility for such a young injudicious student like me, and gave me the opportunity to gain new experience and develop new skills in the fields of electrical engineering, biotechnology and micro-technologies.

I would like to express deepest gratitude to my advisor Daniel Georgiev, who introduced me to the amazing world of synthetic biology and fed my passion for science with his visionary and enthusiasm. He was of great inspiration for me on daily bases, and he helped me to overcome the hard times throughout my doctoral studies. Without his expert guidance and supervision, which required significant amount of patience, this thesis would get hardly finished.

It would be difficult to carry on working on the thesis without my colleagues, the core members of the Georgiev lab, and members of the iGEM 2015 Czech Republic team, Martin Cienciala, Jiri Fatka, Hynek Kasl, Katerina Pechotova, Tereza Puchrova and Pavel Zach. Thank you for your enthusiasm, and the energy your bring to the lab every new day.

My sincere thanks to Faculty of Electrical Engineering membres who helped me with the initial prototype device fabrication, introduction to numerical modelling, and electronic design. These thanks go, but are not limited to Vladimír Pavlíček, Pavel Karban, Richard Linhart and colleagues Jiří Žahour, Jindřich Křivka, Pavel and Jan Broulím, and others.

To Lionel Rousseau who was of a great help throughout my period spent at ESIEE Paris, and who helped and guided me in CAD design and micro-fabrication processes, that were crucial parts of this doctoral project.

To Olivier Français and Bruno Le Pioufle from ENS Cachan, Laboratory of Systems & Applications of Information & Energy Technologies (SATIE), who have done amazing job on applications of numerous dielectric methods in cell biology, and were opened to discussion, collaboration and contribution to this thesis.

Thanks also go to the faculty hospital in Pilsen, the department of hematology and oncology, namely Monika Holubova and Daniel Lysak, who provided live cell samples, were opened to collaboration and did not fear to step over the barriers between different disciplines.

Last but not least, I want to thank to my parents, who gave me the opportunity to follow my dreams and motivated me throughout my life by their infinite love and support.

Contents

List of Figures

Acronyms

2DEP Cytometry Distributed Dielectrophoretic Cytometry 109

∇E^2 Gradient of the Square of the Electric Field 42

APTMS (3-Aminopropyl)trimethoxysilane 35

HCO_3- Bicarbonate 76

CDC Communication Device Class 62

cDEP-FFF Continuous Flow Dielectrophoresis Field Flow Fractionation 12

CO_2 Carbon Dioxide 93

CTCs Circulation Tumor Cells 12

DAC Digital-to-Analog Converter 60

DC Direct Current 40

DDS Direct Digital Synthesis 93

DE Dielectric 92

DEP Dielectrophoresis 109

DEP Dielectrophoretic 109

DEP-FFF Dielectrophoresis Field Flow Fractionation 82

DOS Distance Of Separation 30

DRIE Deep Reactive Ion Etching 58

DS Dielectric Spectroscopy 97

GUI Graphical User Interface 40

Chapter 1

Introduction

1.1 Motivation

Identification and isolation of cells with specific structural or dynamic properties is essential in engineering biological technology. Conventional techniques rely on identification of surface markers using antibodies, or fluorescent reporter proteins linked to functional products, often used in combination with laser detection and flow cytometry [33, 77].

Specific immunochemical signature of cells enables antibodies and aptamer molecules have to be designed to attach to specific cells. Antibody and aptamer coated surfaces are produced to trap the cells of interest while non-target cell are flushed away, or vice versa [55]. This method may be combined with Dielectrophoresis (DEP) to attract or repel cells towards the surface covered by antibodies/aptamers [110]. Throughput of the method is determined by the surface/volume ratio.

Fluorescence Activated Cell Sorting (FACS) enables high throughput serial cell sorting. It exploits fluorescence of either the cells themselves or the fluorescent markers attached to the cells. Typically, sample purity ranges between 90% and 100%. The cells can be characterized at rates between 100,000 and 1,000,000 cells each minute [23]. However, standard flow cytometric analysis combined with antibody labeling may be highly invasive to analyzed cells [35] not permitting repeated measurements or subsequent cultivation of analyzed cells.

Methods which rely on surface marker antibodies for cell detection and separation are sufficient for current practice and with proper training their regular application is observed in fields such as medical diagnosis and cancer treatment. The increased cost and the fundamental difficulty of these methods, however, are attributed to the requirement of the surface marker antibody molecules. In addition, surface marker antibodies are

not universal and need to be custom tailored for many novel cell types leaving some cell types undetectable [4, 94]. On the other hand, more universal marker antibodies may lack specificity leading to overly contaminated isolates and unreliable results. Therefore, there is need for a universal label-free, non-invasive method for efficient and specific cell characterization or isolation.

Alternative methods that do not require cell labelling are based on micro-filtration, Dielectric Spectroscopy (DS), or electro-kinetic methods. Several architectures of micro-filters were proposed and tested based on difference in size of the cells of interest. The micro-filters trap cells larger than the rest of the cells in suspension. This technique is often used to extract rare cancer cells out of blood sample [18]. The viability of the cancer cells might be decreased significantly due to the deformation and forces that act on the cells when trapped in the filter [18]. Its low specificity leads to decreased output sample purity due to the fact that only cell size differences are considered [2, 4]. Hence, it is not possible to use micro-filters to probe cells on the sub-cellular level.

DS, sometimes called impedance spectroscopy, is a characterization technique generally applied to cell suspensions or single cells. It is popular for its experimental simplicity. The DS measures the impedance of suspension/cell in a given frequency range. From obtained results, it is possible to evaluate the Dielectric (DE) properties of characterized cells.

The DS was successfully used to characterize DE properties of buddying yeasts [8], and normal and malignant white blood cells [85]. DS enables dynamic characterisation under physiological conditions. For instance, dynamic impedance variations were mapped during growth of Bacillus thuringiensis [31].

If applied to cell suspensions, cell synchronization is required to obtain relevant data. In addition, DS on cell population is valid for low concentrations only, while reasonable analysis of permittivity value requires higher cell concentrations. The principle of DE spectroscopy is illustrated in Figure 1.1.

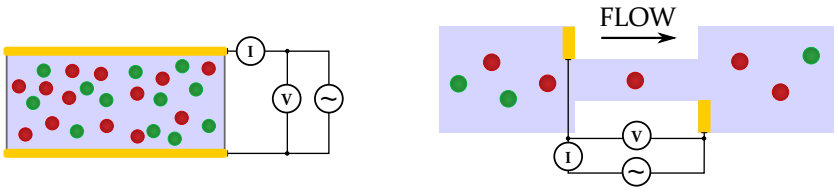

FIGURE 1.1: Illustration of DE spectroscopy performed on cell suspension (left), and single cell DE spectroscopy (right).

Novel approaches exploit microfluidic technology enabling single cell DS. Such approaches require fabrication of small pores of size close to the cell diameter. The precision of the DS is strongly size-dependent as the ratio of the cell size to the pore size determines

the sensitivity of the measurement. Smaller particles require smaller dimensions of the pore. The limit is set by noise in the system. Hence DS is suitable for use with cells comparable in size. In limit case, cell clogging may lead to device failure. β-dispersion due to interfacial polarization must be taken into account in the lower frequency range [7]. It is possible to implement the DS in cell sorting applications. However DS is responsible for the characterization step only, and additional technique responsible for cell manipulation needs to be employed on top of the DS. Theoretical background suggests single cell DS as straightforward characterization method. However, it is difficult to apply the measurement method to cells of the standard size of 10 μm [7]. Instead, electromechanical methods, such as DEP and Electrorotation (ER) are often used for single cell DE characterization resulting in electric field induced cell movement.

ER enables label-free dynamic single cell characterization, but is significantly more time-consuming, and requires extensive experiment control [15, 90]. It is a controlled rotation of an object in rotating electric field. The rotating electric field is generated by four-electrode arrangement. The same electrodes are used for precise cell positioning creating Dielectrophoretic (DEP) trap. The rotation speed and direction depend on the DE properties of the analyzed cell structural parts and their geometry, DE properties of the surrounding medium, frequency of the electric field, and intensity of the electric field. ER is non-invasive and requires no cell preparation. The principle of electro-rotation is illustrated in Figure 1.2.

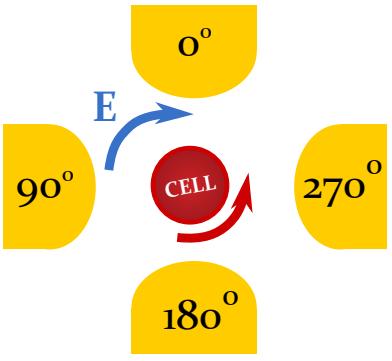

FIGURE 1.2: Simplified illustration of DE cell characterisation by ER.

ER was extensively used to estimate the cell DE properties [37, 51, 53, 103]. Recently, ER was used to study DE variations of *Saccharomyces cerevisiae* (*S. cerevisiae*) cells during the cell life cycle [91]. It has been used to reveal the link between variations of the DE properties and over-expression of HER2/neu in MFC-7 breast cancer cell lines [24], or study effects of antibiotics on *S. cerevisiae* cells [52].

Despite the indisputable precision of single cell analysis, the method focuses on individual cells ignoring the diversity in cell population. It results in precise, but highly subjective results. The rotation speed measurement may be automated with computer

controlled video microscopy and image recognition algorithm [89]. An important part of the frequency spectrum lies in the higher frequency range (above 100 MHz). It therefore increases the requirements on the electric field amplitude and phase control, as the wavelength becomes comparable to the length of cables and electrodes.

DEP induces a cell movement in a non-uniform electric field based on the DE properties of the cell independently on the cell concentrations. DEP is capable of quantifying the distribution of cell characteristic properties amongst whole cell population, and therefore provide more complete quantitative understanding of cellular processes. DEP has more recently proven capable in separating out specific cell phenotypes out of heterogeneous mixtures [3, 46]. Most sorting and characterization methods require cell labeling and thus rely on two or more stages. Biological cells need to be marked with labels. Labeled cells are then measured, e.g., by laser detection, in a separate stage. Cells are finally sorted, e.g., using static electric forces, based on the measurement results. DEP sorting, on the other hand, couples all stages into one. No additional cell suspension or auxiliary detection is required suggesting this approach to be potentially more cost efficient and flexible. DEP is label-free technique, which exploits the physiological information which is encapsulated within a cell. It is generally applicable to a wide spectrum of objects, such as red blood cells, bacterial cells, polystyrene beads or proteins. The responses of the objects to the electric field differ since all structural elements of the particular object manifest themselves in the aggregate response to the electrical stimulus. Hence, differences DEP responses may potentially serve as reliable biomarkers for certain cell types, or even cell states measurable within a single cell population. The non-invasive character of DEP implies the method may be applied repeatedly to obtain dynamic cell characterisation or enable efficient post-analytical cultivation.

Despite the advantages, DEP cytometry is not yet considered as general identification and sorting tool in biotechnology. DEP-based methods are often extensively custom tailored for given application, while general population statistics providing robustness and versatility is still missing. Most of the currently used methods do not permit continuous mode of operation and the frequency range in which they operate is limited, require complex fabrication processes or provide low throughput. In addition, conventional DEP techniques used to measure the cell DE signatures neglect the cell-cell interactions, which are in fact unavoidable using techniques based on cell concentration at the electrode structures due to DEP.

The motivation of this PhD project is to overcome the current limitations of DEP cytometry, to show that DEP can be used reliably to measure probabilistic distribution of live cell DE signatures on population level, and to identify reliable biomarkers for cell changes.

1.2 Objectives

Every cell that is exposed to a non-uniform electric field exhibits a specific DEP response. Differences in DEP responses of individual cells are based on differences in their structural and DE properties. The set of these properties is denoted as the DE signature of the cell. Although DE signatures of cells of the same phenotype are similar, every cell has its own DE signature that is unique. The DE signature is frequency-dependent, and varies according to the cell internal state. In general, it is dependent on the whole molecular structure of the cell. Hence measurements of DE signatures may potentially be used to indirectly measure many intracellular processes themselves. Although the DE signatures may contain whole set of useful biomarkers, there is no efficient and universal method enabling measurement of the live cell DE signatures on a population level.

The main objectives of this work is to investigate the state of the art label-free DEP technologies used for cytometry purposes, to identify their limitations, and improve the state of the technology. Conventional DEP-based methods require complex and expensive fabrication processes to be employed, do not permit continuous analysis resulting in lower throughput and difficult automation, while they often neglect the cell-cell interactions decreasing the method sensitivity. To overcome these shortcoming, first, improvements of the current state of the art methods is searched through fabrication of the microfluidic devices. Second, novel method enabling label-free, non-invasive, continuous probabilistic measurements of live cell DE signatures is developed to show DEP is sensitive enough to be used for cytometry purposes, and for identification of reliable biomarkers for cell changes. The work includes theoretical research, description of the fabrication process, experimental protocols, and analysis of the data obtained by the newly developed method.

1.3 Organisation

The thesis is organized into six chapters. Introduction of the thesis explains the motivation and states the main focus of the thesis.

Chapter 2 contains the literature survey and lists state of the art DEP cytometry methods. Concepts of the DEP analytical and sorting methods are detailed. DEP is described in detail, and the analytical solution of DEP is presented including the cell structure simplification process required for analytical solution of live cell DEP. Numerical simulations are used to show that optimization of electrode topologies is necessary in order to increase DEP efficiency in frequency ranges where the DEP efficiency would be otherwise low. Models of *S. cerevisiae* and Human Immortalised Myelogenous Leukemia (K562)

cells are presented and used for simulation of live cell DEP. Finally, integration of DEP cytometry in microfluidic lab-on-chip devices is discussed.

Chapter 3 searches improvements of DEP cytometry requiring high precision through improvements of the fabrication technology. It formulates the importance of precise alignment in DEP-based cytometry and cell sorting applications. A benchmark problem of DEP-driven cell sorting in microfluidics is defined. The chapter focuses on sorting of *S. cerevisiae* cells according to their life cycle phase in a specific microfluidic topology. A simplified model of a budding *S. cerevisiae* yeast cell is presented and experimentally validated. The benchmark problem is characterised numerically to show that high sorting efficiencies can be achieved only with precise alignment. A novel fabrication process enabling rapid prototyping of microfluidic devices with integrated electrodes and with high precision alignment is presented in detail.

Chapter 4 is dedicated to a newly developed method called Distributed Dielectrophoretic Cytometry (2DEP Cytometry). It describes how a DEP-induced vertical translation of live cells in conjunction with Particle Image Velocimetry (PIV) is used in order to measure probabilistic distribution of live cell DE signatures on an entire cell population. The chapter includes details on numerical simulations, model-based optimizations, and resolution and sensitivity analysis. The 2DEP Cytometry HW platform is presented describing the design of the 2DEP Cytometry microfluidic device and the corresponding micro-fabrication process is described, as well as the development of the customized electric signal generator used to drive the integrated micro-electrodes, and the interface platform providing mechanical support, fluidic and electrical interconnections. Experimental results showing DE signatures of *S. cerevisiae* cell population and K562 cell line are presented. Applications of 2DEP Cytometry in comparative cell analysis are demonstrated on genetically modified *S. cerevisiae* strain over-expressing certain membrane protein. The data are compared to the DE signature of cell population expressing a cytoplasmic protein at the same expression rate. Similar comparison was done on K562 cell line under various types of stress (heat shock and pH variations).

Chapter 5 focuses on statistical analysis of the 2DEP Cytometry data. Custom Kernel Density Estimation (KDE) is introduced to overcome the finite nature of the 2DEP Cytometry data. Subsequently, adjusted Wasserstein pseudometrics on sampled data is described as a measure of dissimilarity of the measured live cell DE signature distributions. The Wasserstein distance spectra, denoted as Wasserstein signatures, were quantified and linked to certain cell changes. These signatures identify frequencies, where less and more significant differences between the measured DE signatures are observed, and may be used as reliable biomarkers for cell changes measurable by 2DEP Cytometry.

The thesis concludes in Chapter 6.3.

1.4 International collaboration

An integral part of the presented PhD project was the international collaboration of the faculties and laboratories presented below.

The design of electronics was performed at the Faculty of Electrical Engineering, University of West Bohemia, as well as the modeling, simulation, and optimization of the electric field generated by electrode structures. The faculty provided technical facilities and software support for computer-aided design, electronic design, and software tools for physical and electrical simulation for the presented work.

Design and fabrication related to microfluidic devices was done at ESIEE Paris, University of East Paris, the Laboratory of Electronics, Communication Systems and Microsystems (ESYCOM). The silicon masters for the soft-lithography process were fabricated in available cleanroom equipped with necessary resources. ESIEE Paris provided licensed software suites for computer aided design.

Microfluidic experiments with integrated DEP cell sorting and handling systems were performed at the Faculty of Applied Sciences, University of West Bohemia, Department of Cybernetics, at the Georgiev Lab. The laboratory is equipped with microscopic station enabling fluorescence imaging and live cell microscopy with incubation chamber allowing precise atmosphere composition and humidity control. The laboratory was responsible for the biology related work including cell cultivation and verification, and DNA synthesis and transformation.

Finally, the SU-8 silanization and the subsequent oxygen plasma treatment required for direct bonding of Poly(dimethylsiloxane) (PDMS) to SU-8 was performed in ENS Cachan, Laboratory of Systems & Applications of Information & Energy Technologies (SATIE).

Chapter 2

DEP cytometry

2.1 Introduction

In this chapter, the idea of Dielectrophoretic (DEP) cytometry is introduced, as well as the individual concepts standing behind it. Dielectrophoresis (DEP) is described in detail, and the analytical solution of DEP is presented including cell structure simplification problem, which is required so that the analytical solution of DEP can be used in combination with heterogenous structures, such as live cells. Numerical simulations based on Finite Element Method (FEM) and analytical solution of DEP were used to optimize electrode topologies in order to increase efficiency of DEP, and to explore DEP response of *Saccharomyces cerevisiae* (*S. cerevisiae*) and Human Immortalised Myelogenous Leukemia (K562) cells, and its dependence on various parameters (e.g., frequency of the electric field and medium electrical conductivity). The cell models are further used and extended in the following chapters for the purpose of modelling of the influence of *S. cerevisiae* cell budding cycle on its DEP response, and DEP-induced levitation of *S. cerevisiae* and K562 cells. Finally, the integration of DEP cytometry methods in microfluidic lab-on-chip devices is discussed.

2.2 DEP cytometry for analysis of live cells

Cytometry in general, is the measurement of characteristics of cells. Flow cytometry quantifies light scattered from cells and their fluorescence while passing through a laser beam in order to analyze cells size and volume, expression of cell surface and intracellular molecules, differentiate between cell types in heterogenous populations, and identify cells with specific structural and dynamic properties. Where conventional flow cytometry requires staining or labelling with antibodies, DEP is able to differentiate between cell

types and cells in certain cell states by measuring differences in their Dielectric (DE) signatures.

DE properties that dictate cell interactions with external electric fields are strongly linked to the cell structural properties, and the cell internal state. Experimental results show DE properties present valuable biomarkers for various cellular events ranging from cell growth, proliferation, response to drug molecules, apoptosis, and cell death. These processes are often mapped to different parts of the cell and thereby manifest as DE changes in different parts of the frequency spectrum. Hence spectral analysis of DE properties can uncover specific physiological changes and provide insight into cellular processes that are otherwise difficult to measure.

Correlations between the DE properties and cell physiology were studied by DEP extensively and registered significant progress in the last decade. It was shown that it is possible to measure progression of cell apoptosis by dynamic mapping of cell DE properties using DEP microwells [76], DEP cell profiler [83], and eventually by simple estimation of the 1^{st} crossover frequency in the cells DEP response and its variation with the degree of apoptosis quantified by Annexin V assay in combination with ethidium bromide staining of DNA [105]. Therein the changes of DE properties were linked to changes in plasma membrane capacitance, its permeability, and the corresponding change of Ca^{+} and K^{+} ion levels in cytoplasm resulting in change in plasma membrane and cytoplasm electrical conductivity. Another real-time microfluidic DEP analysis of B16F10 melanoma cells response to small-molecule drugs (e.g., N-ethylmaleimide) demonstrated that efficiency of small-molecule drugs can be correlated with variation of the DEP response, which was attributed to activation or deactivation of K^{+} and Cl^{-} co-transporter channels in the cell membrane [82]. DEP was also able to show that cytoplasm conductivity and plasma membrane DE properties and their variations play an important role in development of Multidrug Resistance (MDR) in leukemic [32] and breast cancer cells [22], which is one of the major causes resulting in failure of cell response to standard treatment by increasing efflux of the drugs preventing proper diffusion into the cells. In other studies, conventional DEP analysis of the 1^{st} crossover frequency in Red Blood Cells (RBCs) DEP response showed that plasma membrane electrical conductivity changes significantly enabling DEP discrimination of RBCs following malarial infection [41].

Although significant progress was registered throughout the last decade in the DEP field, methods that are used to obtain the live cell DEP spectra are not universally applicable and often need to be custom tailored for given application. In the next section, the specific concepts of DEP cytometry are presented and discussed.

2.3 Concepts

Two main DEP cytometry approaches can be distinguished. First, non-equilibrium methods based on DEP concentration and lateral deflection of cells by potential barriers. And second, equilibrium methods, that are based on balancing forces acting in opposite directions (e.g., gravitational force and DEP force).

2.3.1 Non-equilibrium methods

Non-equilibrium DEP methods are often based on concentration of target cells in potential wells [42]. The target cells remain concentrated in these wells during the sorting until the remaining cells are flushed away. The target cells are released by turning off the electric field or by applying a Negative Dielectrophoresis (N-DEP), and can be subsequently collected at the outlet. Eventually, cell DEP spectra can be obtained by quantifying the concentration rates according to the frequency of the electric field if cell separation is not required.

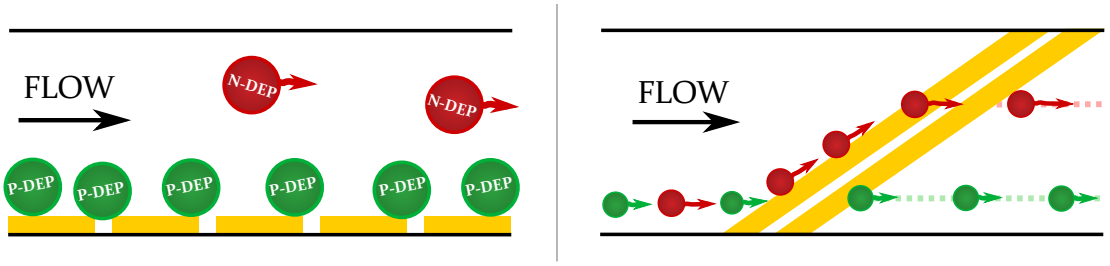

FIGURE 2.1: Illustration of conventional DEP cell sorting based on cell concentration at the electrode structures (left); and lateral displacement (right).

With non-equilibrium methods based on concentration of cells in the locations of electric field maxima, it is difficult to avoid the cell-to-cell interactions due to the immobilization of target cells at the electrode edges. For the same reason, such methods do not permit continuous collection of data and are difficult to automate and the throughput is low. In addition, methods based on concentration are limited to frequency range, where Positive Dielectrophoresis (P-DEP) dominates.

Unlike the concentration methods, methods based on lateral deflection only work properly in the N-DEP frequency range. Lateral displacement with parallel electrodes may also be challenging as cells may tend to jump over the potential barriers. The relative position of microchannels to the electrode structures may play a significant role in the sorting efficiency, which increases the requirements on the selected fabrication processes.

Despite these shortcomings, the conventional non-equilibrium DEP-based methods were successfully used to distinguish between different cell phenotypes as well as cells in different cell states or cells undergoing certain cell changes suggesting DEP has great potential in sensitive cytometry applications.

2.3.2 Equilibrium methods

The equilibrium methods are based on either DEP-induced cell levitation such as Dielectrophoresis Field Flow Fractionation (DEP-FFF), Isodielectric Cell Separation (IDS) enabling separation of cells according to their DE signatures in electrical conductivity gradient within microfluidic channel, or DEP opacity using two lateral DEP forces acting in opposite directions.

2.3.2.1 Isodielectric Cell Separation (IDS)

IDS exploits DEP and gradient of the electrical conductivity across microchannel. All cells are initially located at one side of microchannel. During the sorting, cells are pushed to the other side of the microchannel by N-DEP across the conductivity gradient until they reach their isodielectric point[1], eventually, the point where the drag force exceeds the DEP force acting against it.

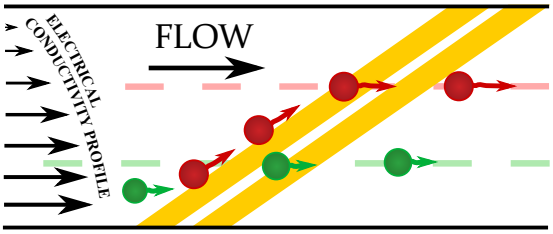

FIGURE 2.2: Illustration of iso-dielectric cell sorting.

IDS has been used to successfully identify specific *S. cerevisiae* cells from the *S. cerevisiae* knock-out library based on their single-gene differences in otherwise identical genotype [99]. In order to achieve high enough efficiency, it requires the parallel electrodes to be patterned on both, bottom and ceiling of the microchannel making the fabrication processes more challenging and expensive. The experiment parameters, such as the flow-rate and the gradient of the medium electrical conductivity, need to be selected carefully not to trap the cells at the location of the isodielectric point by P-DEP. Additionally, the flow-rate and the length of the active sorting regions must be of a reasonable order

[1]Isodielectric point is defined as position where fluid DE properties match the DE properties of the cell

of magnitude, so that the gradient of the medium electrical conductivity in the active region is not degraded by diffusion.

2.3.2.2 Dielectrophoresis Field Flow Fractionation (DEP-FFF)

In batch DEP-FFF, Interdigitated (ID) electrodes are patterned at the bottom of the microchannel. When electric field is applied, the cells are levitated to different heights across the microchannel [104]. The cells gain velocity regarding the parabolic flow profile. In long enough microchannel, even the cells with relatively small differences can be separated without overlapping out of a mixed solution. The conventional DEP-FFF operates in batch mode and can not be operated continuously.

Recently, the DEP-FFF method was improved and transformed by sophisticated design into Continuous Flow Dielectrophoresis Field Flow Fractionation (cDEP-FFF). In cDEP-FFF, cells are introduced through a slit in a bottom of the microchannel. Subsequently, array of electrodes is used to levitate the cells according to their DE properties. Cells that are not levitated above specific critical height are then skimmed off through another slit in the bottom of the microchannel.

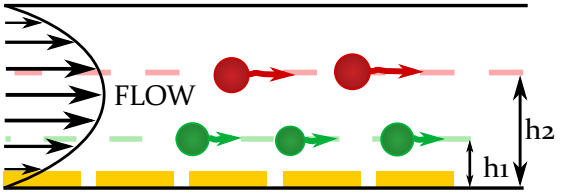

FIGURE 2.3: Illustration of a) conventional DEP field flow fractionation.

The cDEP-FFF achieved isolation of Circulation Tumor Cells (CTCs) from blood sample with sorting efficiency around 70% with approximately 10% sample purity [93]. The method was able to process a 10 ml blood sample in less than 60 minutes, which is required for routine clinical testing. Although the throughput of the method is now sufficient for clinical testing, the sample purity and sorting efficiency and sensitivity needs to be improved significantly.

2.3.2.3 DEP opacity

DEP opacity is a continuous microfluidic cell separation based on two lateral DEP forces acting in opposite directions. Identical electrode arrays are patterned along both sides of a microchannel. Electrodes at one side are energized by AC signal of one specific amplitude and frequency. Electrodes at the opposite side of the microchannel are energized by an AC signal of different frequency and amplitude. Together, these signals are

responsible for shift of the cells across the microchannel. Direction and magnitude of the shift corresponds to the shape, size and DE properties of the cells.

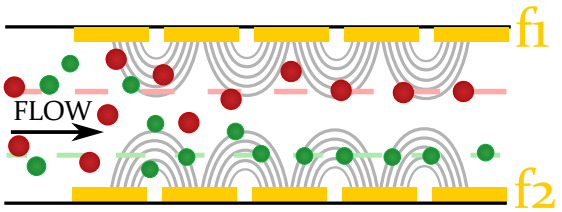

FIGURE 2.4: Illustration of DEP opacity.

DEP opacity was tested on sorting of dividing from non-dividing *S. cerevisiae* cells achieving cell synchronization, and viable from non-viable *S. cerevisiae* cells with nearly 100% sample purity. Sorting of *B. bovis* infected RBCs from non-infected RBCs yielded approximately 50% sample purity and enrichment by factor of 7 [1].

2.3.3 Summary

Concepts of non-equilibrium and equilibrium DEP cytometry methods were presented. Although DEP is already capable of discriminating different phenotypes and even subpopulations within cells of the same phenotype based on the differences in cell DE signatures, there are shortcomings that limit the efficiency and sensitivity of DEP-based methods from further progress and make it difficult to adopt these methods by broader audience in the biotechnology field. The non-equilibrium methods mostly suffer from lower throughput, non-continuous mode of operation, cell-to-cell interactions, difficulty to automate, and lower efficiency and sensitivity. The equilibrium methods on the other hand require complex and thus expensive fabrication processes in order to achieve reasonable sensitivity and reproducibility. The only exception is the DEP-FFF, which does not require complex fabrication process. On the other hand, it only operates in batch mode. In this PhD project, improvements of the DEP cytometry are searched through both, micro-fabrication techniques (see Chapter 3), as well as adopting completely new approach to DEP cytometry (see Chapter 4).

2.4 Mathematical background

2.4.1 Analytical solution of DEP

2.4.1.1 Solution of Laplace equation

Analytical solution of DEP comes from solution of Laplace equation. Presence of no free charge is considered. Therefore, Laplace equation in the following form is expected:

$$\phi^2 = 0 \tag{2.1}$$

A general solution for potential in spherical coordinates is expressed using infinite series of Legendre polynomials. An origin of the coordinate system is located in the center of the sphere. An external electrical field variable with the z component of the coordinate system is considered. The simplification in the form of axial symmetry enables the analytical derivation of the DEP to be soluble. The coordinate system and our model space is illustrated in Figure 2.5

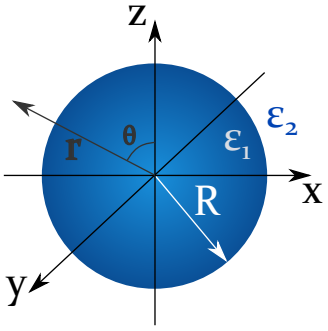

FIGURE 2.5: Axial symmetry model space used for analytical solution of DEP.

The external electric field is applied and the potential distribution is characterized in the presented model space. Boundary condition for continuity of electric potential, and continuity of electric displacement are used. Assuming relatively small variations of the electric field in respect to the diameter of the particle, the higher order terms are neglected. In case of larger variations of the electric field over the cell diameter, effects of induced multipoles must be taken into account [14]. Keeping the first order terms only, sphere is approximated as a dipole, and the effective dipole moment p is determined.

$$p_{eff} = 4\pi R^3 \epsilon_2 \epsilon_0 Re[K(\omega)]E \tag{2.2}$$

In Equation 2.2 $K(\omega)$ stands for Clausius-Mossotti Factor ($K(\omega)$) and is expressed by the following formula:

$$K(\omega) = \frac{\epsilon_1^* - \epsilon_2^*}{2\epsilon_2^* + \epsilon_1^*} \tag{2.3}$$

The permittivities ϵ^* introduced in $K(\omega)$ are frequency dependent complex variables. They are dependent on the DE properties of the material which they consist of. The complex permittivity is expressed as:

$$\epsilon^* = \epsilon_0\epsilon_r - j\frac{\sigma}{\omega}, \tag{2.4}$$

where ϵ_0 is the permittivity of vacuum, ϵ_r is the relative permittivity of the material, σ is the electrical conductivity of the material, and ω stands for the angular frequency of the applied electric field. Force acting on an electric dipole is directly proportional to the value of its dipole moment and the gradient of the electric field.

$$F_{dipole} = p\nabla E \tag{2.5}$$

The solution of Laplace equation yields a general expression of the time-averaged DEP force acting on spherical particle in non-uniform electric field [14, 58]:

$$F_{DEP} = 2\pi R^3\epsilon_0\epsilon_2 Re[K(\omega)]\nabla E^2. \tag{2.6}$$

In this expression R stands for radius of the particle, ϵ_0 stands for permittivity of the vacuum, ϵ_2 stands for relative permittivity of the surrounding medium, $Re[K(\omega)]$ stands for the real part of $K(\omega)$ and it is frequency dependent, ∇E^2 stands for gradient of electric field square. The imaginary part of the $K(\omega)$ then corresponds to torque and is related to phenomenon known as Electrorotation (ER) [58].

2.4.1.2 Positive vs. negative DEP

The Equation 2.6 expressing the time-averaged DEP force acting on spherical particle in non-uniform electric field can be divided into several parts. The first part is dependent on cell size and relative permittivity of the surrounding medium. This part is considered constant. Subsequently, the gradient of the electric field is given by the electrode design, and in general is considered constant as well. Although the magnitude of the electric

field intensity can be controlled, change in its polarity does not change the direction of the force as the DEP force depends on the square of electric field. However, the real part of $K(\omega)$ provides the flexibility of the DEP force thanks to its frequency dependence. Value of the real part of $K(\omega)$ is within the range $< -0.5; 1.0 >$. This means that not only the magnitude of the force, but even its direction can be controlled by controlling the frequency of the electric field. Hence, two types of DEP are distinguished:

1. Positive Dielectrophoresis (P-DEP) - for $Re[CM_f] > 0$
2. Negative Dielectrophoresis (N-DEP) - for $Re[CM_f] < 0$

Therefore, the frequency dependence of the force, and its dependence on specific DE properties, provides the versatility of DEP and gives DEP the potential to be used in cell/particle characterisation, fractionation, concentration and sorting applications. For instance, in specific frequency range, DEP can be used to guide the cells to their initial positions within a microchannel by N-DEP; and different frequency range may be used to trap cancer cells in potential wells with P-DEP while remaining cells are repelled and are being washed away.

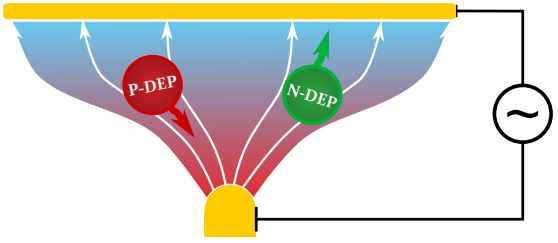

FIGURE 2.6: Positive and negative dielectrophoresis.

Situation showing P-DEP and N-DEP is illustrated in Figure 2.6. In case of P-DEP, cell is pushed to the region with higher intensity of the electric field. In case of N-DEP, cell is pushed to the region with lower intensity of the electric field.

2.4.2 Cell structure simplification

Analytical solution of DEP presented in Section 2.4.1.1 with the $K(\omega)$ given by Equation 2.3 is however applicable only to homogeneous spherical particles made of single material of single electrical permittivity and conductivity. This is not the case of biological cells. Biological cells are always represented as objects with one or even multiples shells that encapsulate the interior (cytoplasmic) space. And the individual layers have different DE properties. However, it has been shown that a non-homogenous particle can be transformed to a homogenous sphere of an effective permittivity. Such homogenous

particle exerts exactly the same induced potential, the same dipole moment, and the same force interactions with the electric field [56, 58]. Such transformation allows subsequent use of the general analytical solution of DEP for spherical particles presented in Section 2.4.1.1.

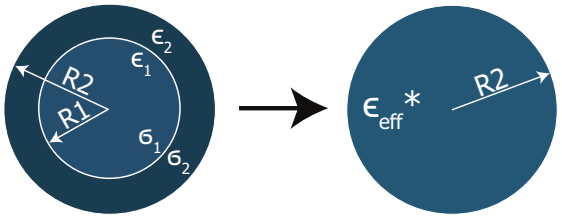

FIGURE 2.7: Cell structure simplification.

To transform the non-homogenous spherical particle into homogenous spherical particle, boundary conditions for continuity of potential and continuity of electric displacement are used. Relatively small variations of the electric field in respect to the diameter of the particle are assumed. Hence, the higher order terms are neglected. The effective permittivity is then provided by Equation 2.7.

$$\epsilon_{eff} = -\epsilon_2 \frac{2K_{std}(\omega)\left(\frac{R_1}{R_2}\right)^3 + 1}{K_{std}(\omega)\left(\frac{R_1}{R_2}\right)^3 - 1}, \tag{2.7}$$

where $K(\omega)$ stands for the standard Clausius-Mossotti Factor of the form:

$$K_{std}(\omega) = \frac{\epsilon_1^* - \epsilon_2^*}{\epsilon_1^* + 2\epsilon_2^*}. \tag{2.8}$$

The homogenous spherical particle consisting of material of effective permittivity induces the same dipole moment as the multilayered cell model. This effective permittivity is obtained by step by step simplification of the cell model from the inner layer to the outer layer. The two most inner layers are always replaced with homogenous layer of the effective permittivity. The process is repeated until the multilayered model is successfully transformed to a homogenous spherical particle. The cell structure simplification process of multi-shelled cell model is illustrated in Figure 2.8.

2.4.3 Summary

An analytical axial symmetry solution for DEP force acting on spherical particle in an external electric field was described. This theory is used in following chapters to show the influence of misalignment of Poly(dimethylsiloxane) (PDMS) microchannel above

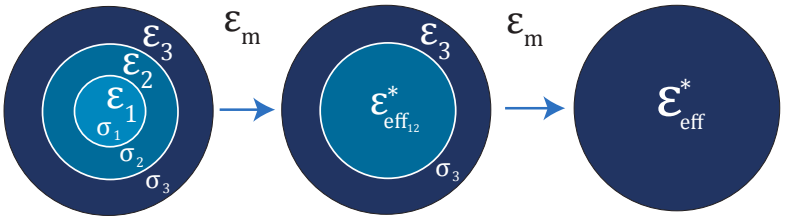

FIGURE 2.8: Illustration of multishelled cell structure simplification.

micro-electrodes in DEP-based sorting, in simulations of Distributed Dielectrophoretic Cytometry (2DEP Cytometry), to optimize 2DEP Cytometry design parameters, and to estimate sensitivity limit of the developed 2DEP Cytometry.

2.5 Numerical simulation and modelling framework

In this section, electrode topologies are modelled, simulated, and optimized by FEM. Models of *S. cerevisiae* and K562 cells are developed and used in numerical simulations of live cell DEP. The results are used to illustrate the effect of the frequency of the electric field, the electrical conductivity of the medium, and the DE properties of the individual cell parts (e.g., plasma membrane and cytoplasm) on the DEP response of cells, as well as to illustrate the frequency ranges, in which these parameters manifest themselves. The developed models are later extended and used in the subsequent chapters for various purposes.

2.5.1 Optimization of electrode topology

DEP force is directly proportional to the Gradient of the Square of the Electric Field (∇E^2). The non-uniformity of the electric field is defined by specific electrode design. Figure 2.9 provides illustration of simple electrode configuration generating a non-uniform electric field.

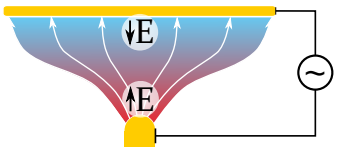

FIGURE 2.9: Shape of electrodes creating a nonuniform electric field.

Optimization of electrode topology is necessary in order to increase the efficiency of the DEP in the frequency range where values of $K(\omega)$ are low. The optimal topology balances the tradeoff between the electric field gradient and its active domain to generate high enough forces for longer periods of time. The topological parameter space of ID

electrode array for live cells DEP was characterized. Nevertheless, there is a limit value of the electric field intensity. Once this value is reached, the transmembrane voltage increases above the permitted value (typically 0.15-1.0 V) which leads to electroporation or even cell death caused by the dielectric breakdown of the plasma membrane [98].

A parametric simulation was performed in Comsol Multiphysics with LiveLink™for Matlab module studying ID electrodes. Electric field distribution was evaluated by FEM. The data from FEM were post-processed by Matlab and the ∇E^2 was evaluated. All following simulation results correspond to electric potential difference of $1V$ applied to electrodes.

The effect of inter-electrode gap dimensions was studied on parallel or ID electrode topologies. The parallel electrode topologies are suitable for general cell handling in microfluidics as well as IDS [99]. The ID electrodes are often used for cell trapping, Traveling Wave Dielectrophoresis (twDEP) [74], and cell sorting techniques based on DEP-FFF [93, 104] as well as for 2DEP Cytometry presented in Chapter 4. The ∇E^2 is independent on the length of the electrodes. The ID electrode array model and the potential distribution is shown in Figure 2.10. Thickness of the medium layer corresponds to the identified optimal height of the microchannel 40 μm. The selection of the microchannel height is discussed later in Section 4.3.2.2.

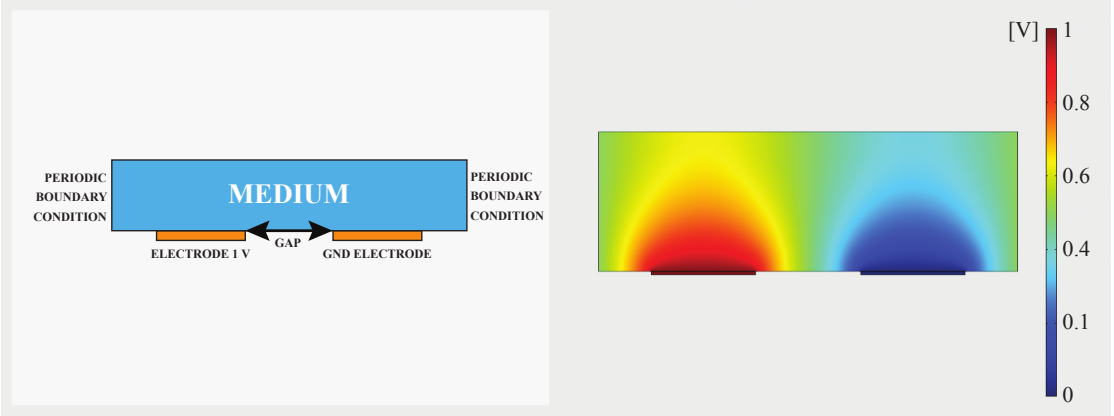

FIGURE 2.10: Geometry of the ID electrodes model (left), and the electric potential distribution for 30 micron gap between electrodes simulated by Comsol Multiphysics (right).

The electric field distribution and the corresponding ∇E^2 in the vertical direction are shown in Figure 2.11. The simulation results denote significant increase of the ∇E^2 with decreasing gap width.

Simulation results showing ∇E^2 in Figure 2.11 denote the ∇E^2 generated by 10 μm inter-electrode gap dominates significantly below 15 μm. At larger distances, the ∇E^2 is lower than with larger inter-electrode gaps. Such behavior is beneficial in the 2DEP Cytometry application discussed in Chapter 4. This means that the ∇E^2 dominates in the lower

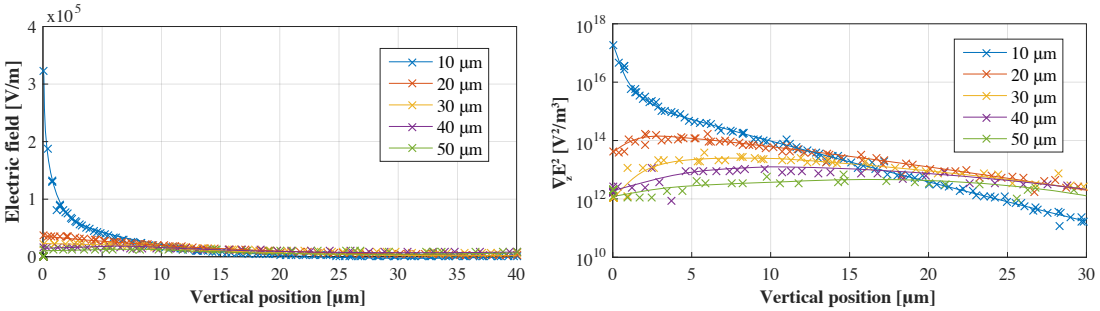

FIGURE 2.11: Dependence of the electric field (left) and vertical component of the ∇E^2 (right) on the size of the gap between ID electrodes.

half of the 40 μm high microchannel making it easier to occupy only the lower 20 μm section by the DEP-focused cells, which is one of the requirements necessary for proper 2DEP Cytometry function. Hence 10 μm inter-electrode gap was selected as optimal. Values of the ∇E^2 can be further increased by increasing the electric potential difference between electrodes.

2.5.1.1 Summary of the electrode optimization

The results of the electrode optimization show strong DEP dependence on specific electrode configuration. Hence, electrode optimization and corresponding electrode design are essential in live cell DEP. A 10-micron gap was identified as optimal for efficient live cell DEP as it increases the values of $K(\omega)$ at frequencies where values of $K(\omega)$ are low, and limit the working distance of DEP to the intended lower vertical half of the microchannel, which is suitable for 2DEP Cytometry (see Chapter 4).

2.5.2 DE models of biological cells

All living organisms in nature consist of elementary units, biological cells. Different cell types are suitable to perform different tasks. Each of the cells possesses unique properties and the physiology of the cells differs. In this section, process of biological cell model design for the purpose of simulation of the behavior of cell in the presence of non-uniform electric field is described.

Model of biological cell and its properties are defined on several levels. Obviously, cells differ in aspects such as the cell size, sphericity, motility. Detailed investigation of cell structure reveals several constitutional layers. Every biological cell, in fact, consists of a shell encapsulating the interior space, the cytoplasm. On the molecular scale, the cells are built up of countless number of molecules, such as proteins, lipids, polysaccharides

and other building blocks. Properties of the building blocks and their arrangement define the behavior of the cell in specific environment under certain conditions.

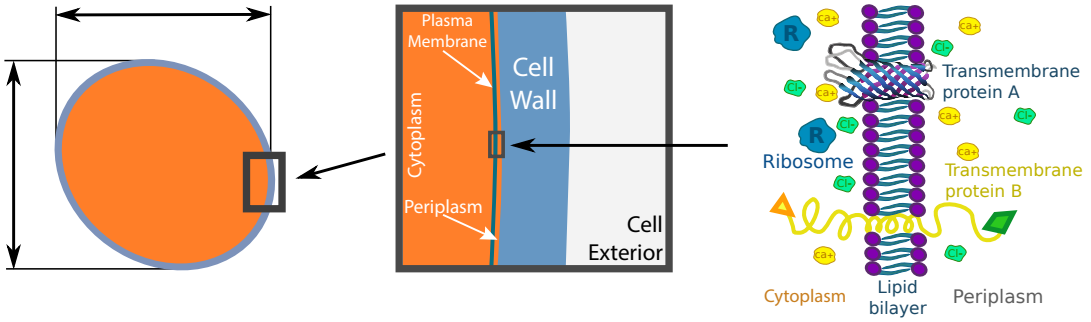

FIGURE 2.12: Model of biological cell and its description on different levels.

Properties like sphericity and cell size dictate the cell dynamics in a microfluidic system, such as the Stokes drag, migration and sedimentation velocity, while the electrical permittivity and conductivity of the cell building blocks and their relative arrangement dictate the DEP response of the cell.

2.5.3 Cell model and simulation complexity

Numerical simulation based on analytical solutions is often less time consuming and does not require excessive computing power. On the other hand, considerable simplifications are made. Each of these simplifications introduces an evaluation error. For instance, when deriving the effective dipole moment described in Section 2.4.1.1, only the electric field in the center of the geometry is considered. This error increases with the ratio of the cell diameter to the size of the variation of the electric field.

But even with FEM, the molecular structure of cell must be simplified into several homogenous layers due to the complexity and computational limitations. Fortunately models of live cells are often spherical or ellipsoidal, and an axial symmetry can be applied to them. Figure 2.13 illustrates simple examples of live cell models. In case of simulation based on analytical solution, the cell structure simplification described in 2.4.2 is required in order to obtain the cell DEP response.

2.5.3.1 DE model of *S. cerevisiae* cell

S. cerevisiae cells are one of the best-studied experimental organisms. Selection of *S. cerevisiae* as model organism increases experiment reliability, reproducibility and robustness. Unlike the mammalian cells, genetic manipulation in *S. cerevisiae* is relatively easy and cheap. Hence *S. cerevisiae* cells are often used to study mammalian

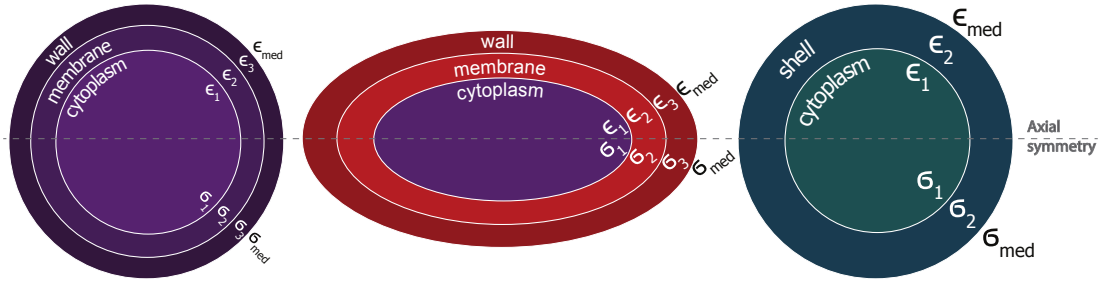

FIGURE 2.13: Three examples of live cell models. A simplified *S. cerevisiae* cell (left), an *Escherichia coli* bacterium (middle), a model of mammalian cell or simplified model of more complex cell (right). The individual models and the layers they consist of are not in scale.

homologs [12]. The simplicity of *S. cerevisiae* cell culture, cultivation, and engineering turned *S. cerevisiae* to useful model organism for eukaryotic and synthetic biology.

A four-shelled model of *S. cerevisiae* cell was developed and used in order to model *S. cerevisiae* DEP response. Similar model was previously used in *S. cerevisiae* ER studies [90]. DE properties of the *S. cerevisiae* cells presented in literature sources are usually in agreement [21,40,70,108]. The values are presented in Table 2.14. These values agree with expectations based on the knowledge of the physiology of the *S. cerevisiae* cells. For instance, the low conductivity of the plasma membrane as it controls the transmembrane transport (even transport of ions); high conductivity of the cytoplasm due to the high concentration of ions in it; or the middle value of cell wall conductivity which usually uses only passive mechanisms of transport and all the required materials must be able to pass through.

	Relative permittivity	Electrical conductivity	Radius	Thickness
Cell wall	60	0.01-1 [S/m]	-	100-200 [nm]
Periplasm	50-120	2.5-3.2 [S/m]	-	35-45 [Å]
Plasma membrane	2-10	0.01-100 [μS/m]	-	7 [nm]
Cytoplasm	50-120	1-10 [S/m]	2.5-5[μm]	-

FIGURE 2.14: Dielectric properties of the building blocks of *S. cerevisiae* cells.

The model is axially symmetric and consists of individual layers representing inner and outer cell wall, periplasmic space, plasma membrane and the cytoplasm. This model is used in simulations based on the analytical solution, simulation of the effect of *S. cerevisiae* budding cycle on its DEP response presented in Section 3.2, hybrid stochastic simulations of DEP-induced cell levitation described in Section 4.3.1, and the 2DEP Cytometry sensitivity analysis described in Section 4.3.2. The model is illustrated in Figure 2.15. DE properties of the individual cell layers are provided in Table 2.16.

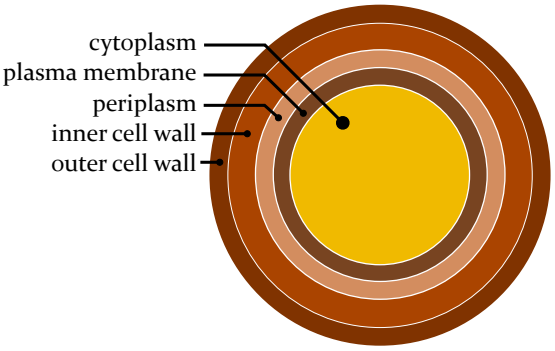

FIGURE 2.15: Illustration of *S. cerevisiae* cell model.

	Relative permittivity	Electrical conductivity	Radius	Thickness
Outer cell wall	5.9	20 mS/m	-	50 nm
Inner cell wall	60	5 mS/m	-	110 nm
Periplasm	14.4	1 S/m	-	4 nm
Plasma membrane	6	3 $\mu S/m$	-	7 nm
Cytoplasm	51	1 S/m	3 μm	-

FIGURE 2.16: *S. cerevisiae* model properties and their values.

Numerical simulation based on analytical solution of DEP was used to analyze the DEP response of *S. cerevisiae*, to optimize medium electrical conductivity and to select the frequency range of interest. In order to be able to use the analytical solution of DEP, the cell multilayered structure was simplified and the effective complex permittivity was evaluated using the cell structure simplification process described in Section 2.4.2. Dependence of the real and imaginary parts of the $K(\omega)$ on the frequency of the electric field is illustrated in Figure 2.17.

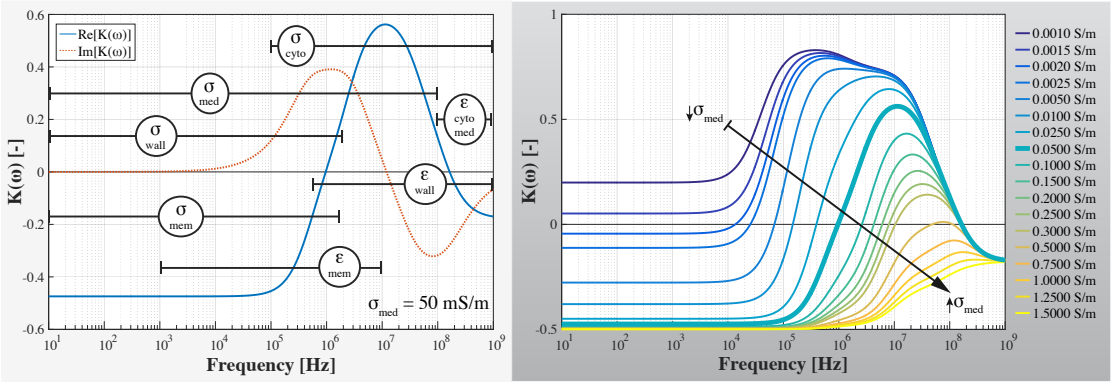

FIGURE 2.17: Real and imaginary parts of the $K(\omega)$ of *S. cerevisiae* cell in a frequency spectrum for one fixed value of medium electrical conductivity $\sigma_{med} = 50$ mS/m (left). The real part is responsible for DEP, the imaginary part is linked to ER. Dependence of the real part of the $K(\omega)$ on the electrical conductivity of the medium (right).

Frequency ranges and the individual DE properties that affect DEP in these frequency ranges are highlighted. There are two crossover frequencies in the DEP response of

S. cerevisiae cell causing the frequency range division in two frequency intervals showing N-DEP and one frequency interval showing P-DEP. The range below the first crossover frequency is driven by molecular composition and DE properties of most of the cell parts of interest (e.g., plasma membrane DE properties and cytoplasm conductivity); while in the highest frequency range, DEP is dominated by the difference between cytoplasm and medium electrical permittivity. The medium electrical conductivity 50 mS/m was identified as optimal for DEP-based *S. cerevisiae* analysis, because it comprises both N-DEP and P-DEP of reasonably large magnitudes, while larger values of medium electrical conductivity result in diminishing P-DEP, and lower values of medium electrical conductivity result in diminishing N-DEP.

2.5.3.2 DE model of K562 cell

K562 cells line was the first established human immortalised myelogenous leukemia line. As well as other mammalian cells, they are formed by cytoplasmic space surrounded by plasma membrane. Hence, unlike *S. cerevisiae* cell model, the K562 cell model is simpler, lacking the periplasmic space, and the cell wall layers. Size of the cells about 15 microns in diameter on average and was confirmed by optical microscopy. The simple structure of a K562 cell model is shown in Figure 2.18.

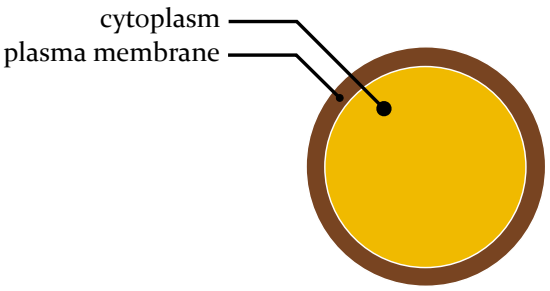

FIGURE 2.18: Illustration of K562 cell model.

Although DE properties of K562 cell line were not studied as deeply as the DE properties of *S. cerevisiae*, the values published in literature sources are usually in agreement [9,19, 34]. These values were obtained by ER and DEP. Values of the model parameters are provided in Table 2.19.

	Relative permittivity	Electrical conductivity	Radius	Thickness
Plasma membrane	12	6.9 $\mu S/m$	-	7.5 nm
Cytoplasm	51	0.5 S/m	7 μm	-

FIGURE 2.19: K562 model properties and their values.

Using analytical solution of DEP, cell multilayered structure was simplified and the effective complex permittivity was evaluated. Dependence of the real and imaginary parts of the $K(\omega)$ on the frequency of the electric field is illustrated in Figure 2.20.

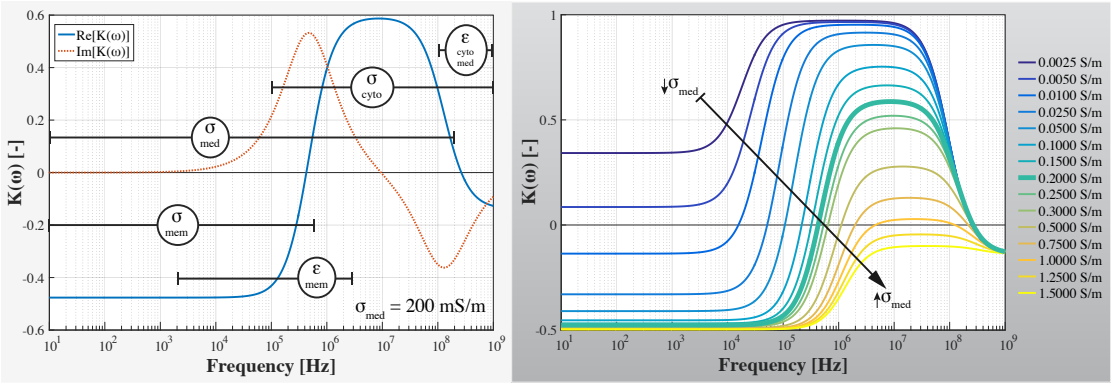

FIGURE 2.20: Real and imaginary parts of the $K(\omega)$ of K562 cell in a frequency spectrum for one fixed value of medium electrical conductivity $\sigma_{med} = 200$ mS/m (left). The real part is responsible for DEP, the imaginary part is linked to ER. Dependence of the $K(\omega)$ on the electrical conductivity of medium (right).

The frequency ranges and the individual DE properties that affect DEP in these frequency ranges are highlighted. Similarly to *S. cerevisiae* DEP spectra, there are two crossover frequencies in the DEP response of K562 cell causing the frequency range division in two frequency intervals showing N-DEP and one frequency interval showing P-DEP. The range below the first crossover frequency is driven by molecular composition and the DE properties of the plasma membrane and the cytoplasm electrical conductivity. In the highest frequency range, DEP is dominated by the difference between the cytoplasm and the medium electrical permittivity. Unlike in the case of *S. cerevisiae*, medium electrical conductivity 200 mS/m was identified as optimal for DEP-based K562 analysis for the same reasons. Larger values of medium electrical conductivity result in diminishing P-DEP, while lower values of medium electrical conductivity result in diminishing N-DEP.

2.6 Integration in microfluidic lab-on-chip devices

Lab-on-chip devices combine microfluidic technologies and integrated analytical methods to decrease the experiment costs by minimization of sample and reagents volumes; and increase in throughput by parallelization, or spatial distribution of the microfluidic channels. Lab-on-chip analytical methods based on DEP measurements take advantage of correlation of DE and structural properties with the cell phenotype and the cell internal state, and enable real-time analysis under relevant conditions. DEP is well suited for integration in microfluidic devices, and lab-on-chip devices with integrated DEP already

showed their potential to identify different cell lines and pathogens, and to characterize their properties [13, 29, 45, 48].

The diffusion processes are slow, and the inertial effects are negligible on micro-scale with low Reynolds number [5]. Hence microfluidics enable complex control of the extracellular micro-environment. In Chapter 4, microfluidic technology is used to establish stable hydrodynamic behavior in terms of parabolic flow profile along the vertical axes inside the microchannel enabling efficient measurement of live cell DE signatures on population level using DEP-induced cell levitation.

2.7 Conclusion

Literature survey shows DEP can be used to probe cells on sub-cellular level. However current DEP-based methods are often custom tailored for a given application. No general DEP-based platform exists that enable continuous measurement of probabilistic distribution of live cell DE properties on an entire cell populations. Instead, general population statistics providing robustness and versatility is still missing, and DEP-based techniques are not yet considered as general identification and sorting tools in biotechnology, although it may increase throughput or improve sensitivity in comparison to more standard methods (e.g., flow cytometry and Dielectric Spectroscopy (DS)).

A mathematical background including analytical solution of DEP and cell structure simplification was provided, and an introduction to live cell DEP modelling based on the analytical solution was presented as well as detailed description of *S. cerevisiae* and K562 cell models. The simulation results show how individual cell and medium DE properties affect DEP in specific frequency ranges. This model-based approach helps to understand the role of individual cell layers and their DE properties, and to identify values of key experimental parameters (e.g., medium electrical conductivity). FEM-based electrode optimization was presented and it was shown that it is a necessary step required to increase the efficiency of DEP in frequency ranges where values of $K(\omega)$ are small, and it may be used to focus the DEP active region to micro-channel section of interest.

Chapter 3

Improvements of DEP cytometry through fabrication

3.1 Introduction

The limiting factor of live cell sorting devices based on Dielectrophoresis (DEP) is lower sorting efficiency and output sample purity [86]. The most sensitive state of the art force equilibrium designs of Dielectrophoretic (DEP) cytometry discussed in Section 2.3.2 require attaining high precision during the fabrication process. However attaining such high precision is difficult with fast prototyping fabrication processes, such as the Poly(dimethylsiloxane) (PDMS) soft lithography. Instead, it requires complex and expensive clean room fabrication processes to be employed, as the sensitivity of DEP sorting in microfluidics relies on precisely complied design parameters. In this chapter, it is shown that the sorting efficiency and the output sample purity can be significantly improved if precise alignment of micro-channel above electrode structures is achieved.

Recently, soft lithography processes have been viewed favorably for their low cost and fast prototyping of microfluidic devices [39]. However, the rough alignment of the PDMS microstructures with the underlying electrode structures makes it difficult to use in applications requiring sensitive DEP. Hence, complex and expensive fabrication methods using Silicon (Si) or glass substrates to construct microfluidic devices are still used for prototyping of high precision devices. Standard fabrication methods using silicon or glass substrates to construct microfluidic devices offer perfect relative alignment of individual device layers and good chip-to-chip reproducibility. However such fabrication processes are complex, time consuming, and expensive [67]. Fabrication of microfluidic devices using PDMS decreases the process complexity, shortens the fabrication times, and decreases the overall costs. The straightforward and inexpensive fabrication makes soft

lithography particularly advantageous in the initial stage of research. For these reasons, PDMS became one of the most exploited polymers for fabrication of microfluidic device prototypes [72]. In addition, PDMS is widely used for its optical properties, flexibility, and gas permeability. These properties make PDMS an outstanding material to use in aqueous media applications. On the other hand, the shrinkage of PDMS during curing, and the manual alignment of the PDMS with the underlying substrate make it impossible to construct high precision designs [30, 66]. Standard techniques are therefore still used for prototyping if high precision is required.

Bad reproducibility, decreased efficiency, or even a device failure was reported with soft lithography combined with integrated DEP [92]. An alternative solution to PDMS based soft lithography is described by [38]. Standard sputtering and photolithography processes were used to pattern microelectrodes and SU-8 microchannels on a glass substrate. Oxygen plasma activated flat sheet of PDMS was used to seal the device. However, direct bonding of SU-8 to PDMS is not trivial and results in reversible bond providing unstable fluidic isolation for several hours only. Herein, direct bonding of PDMS to SU-8 surface was achieved by efficient wet chemical silanization combined with oxygen plasma treatment of the contact surface providing strong irreversible bond between PDMS and SU-8.

The importance of precise alignment of microchannels above microelectrode structures has not been formulated or analyzed in detail. Importance of alignment was briefly mentioned in DEP-assisted concentration of micro-particles and their rapid quantitation [47], pairing of two particles of different size by DEP [17], and DEP-driven precise cell trapping [111]. However the detailed characterisation of misalignment is missing.

In this chapter, the importance of precise alignment is formulated. A benchmark problem of DEP-driven cell sorting in microfluidics is defined. The problem focuses on sorting of *Saccharomyces cerevisiae* (*S. cerevisiae*) cells according to their life cycle phase in a specific microfluidic topology. Parameters describing electrode structures were numerically optimized. A simplified model of a budding *S. cerevisiae* cell is presented and experimentally validated.

The benchmark problem is characterised numerically to show that high sorting efficiencies can be achieved only with precise alignment. Alignment of the microchannel above the electrode structures must be in the order of the sorted cell size in order to achieve meaningful sorting efficiencies. Hence, the standard soft lithography fabrication process comprising a manual alignment stage is not suitable.

Finally, a novel fabrication process enabling rapid prototyping of microfluidic devices with integrated electrodes and with high precision alignment is presented in detail. The process enables faster development of DEP-based microfluidic technology achieving higher efficiencies and fully utilizing its real potential. The fabrication process was developed in ENS Cachan, Laboratory of Systems & Applications of Information & Energy Technologies (SATIE).

3.2 Benchmark problem

The following benchmark problem is defined to allow quantitative characterisation of misalignment in microfluidic devices with integrated DEP. The benchmark problem includes the microfluidic topology, the electrode structure, the sorted particle including its mathematical representation, and the corresponding performance measure.

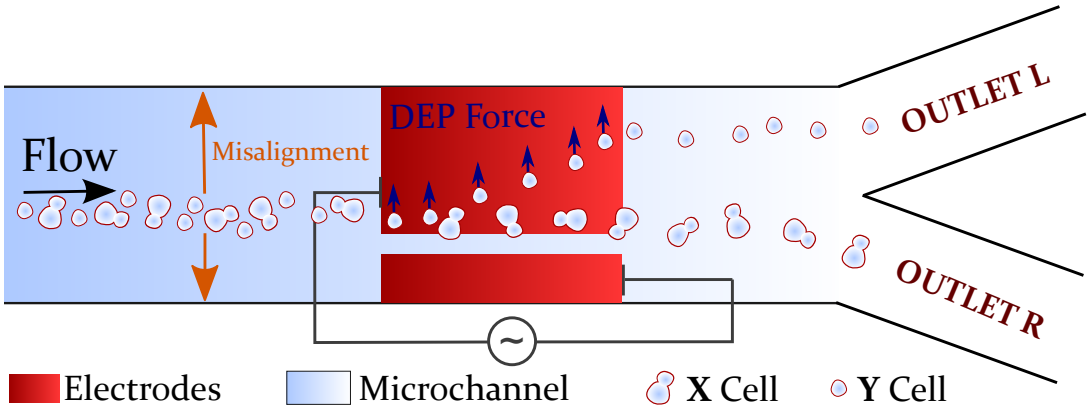

FIGURE 3.1: A benchmark cell sorting device. DEP sorting stage in a microfluidic device illustrates separation of *S. cerevisiae* cells in G1 phase cells from *S. cerevisiae* cells in G2 phase (top view). Frequency and intensity of the electric field is chosen so that cells in G1 phase are sorted to the left outlet by N-DEP, while cells in G2 phase are sorted to the right outlet. The frequency of the electric field is located in specific frequency range where forces acting on dividing *S. cerevisiae* cells are negligible.

The system underlying the benchmark problem is illustrated in Figure 3.1. The microfluidic topology includes single inlet and two outlets to spatially separate the sorted cells. This represents the canonical topology for continuous spatial cell sorting and allows easy evaluation of sorting efficiency. Cells of two types at equal concentrations enter the left end focused to a 10-micron wide stream of cells. The cell focusing is achieved for instance by hydrodynamic flow focusing [64] or by N-DEP [28]. It is assumed that cells enter the sorting stage in well defined position relative to the sorting electrodes (as this presents the best case scenario). In the second stage, cells are sorted by DEP along 100 microns long sorting electrodes to one of the outgoing channels. The electrode topology was taken from [16]. Extensions of this benchmark study to other topologies represents

future work. Relatively small 10-micron inter-electrode gap was identified as optimal at low voltages (below 10 V_{p-p}) by numerical simulations based on analytical solution of DEP combined with a Finite Element Method (FEM) model-based approach simulated in Comsol Multiphysics with LiveLink^{TM} for Matlab. Correct placement of electrodes in microchannel and their relative position to microchannel define the flow trajectories by which cells move through the electric field. Misalignment of the microchannel (also pictured in Figure 3.1) and the microelectrode structures causes the cells to be moved to different positions above sorting electrodes, where the gradient of the electric field is lower. Therefore the effect of DEP is significantly decreased. The effect of misalignment of the microchannel on the efficiency of the sorting is studied in detail in Section 3.3.

Electrode structures were optimized for sorting. Relatively small 10-micron gap was chosen in order to increase the DEP-induced Distance Of Separation (DOS) of cells passing through the 100 microns long sorting stage. The average cell velocity is 100 $\mu m/s$. The height of the microchannel is approximately 20 microns. Medium conductivity was chosen 0.051 S/m to increase the differences between DEP response of cells in different life cycle phases. A sine wave with an amplitude of 3 V and frequency 530 kHz is applied to sorting electrodes.

The benchmark problem is to discriminate *S. cerevisiae* cells in the G1 phase from cells in the G2 phase. The discrimination between these two cell types roughly corresponds to discrimination between 4-micron and 7-micron diameter cells. The corresponding mathematical model of *S. cerevisiae* cells is derived below. The size-based cell sorting was selected as it is often used in numerous general cell sorting applications [11, 54, 59].

The performance measure of the benchmark problem was defined as follows. Two types of cells are sorted, the *S. cerevisiae* cells in G1 phase and the *S. cerevisiae* cells in G2 phase, X and Y respectively. The X cells sorted to the L and R channels are denoted X_L and X_R respectively. The sorted Y cells are denoted similarly. The sorting performance measure ξ is given by the geometric mean of the sorting efficiencies of the two outgoing channels. In other words,

$$\xi = \sqrt{\frac{X_L}{X_L + Y_L} \frac{Y_R}{Y_R + X_R}}. \tag{3.1}$$

Perfect sorting is achieved when all X cells are sorted to the right channel, and all Y cells are sorted to the left channel, giving a performance measure ξ equal to 1.

A four-shelled model of *S. cerevisiae* cell presented in Section 2.5.3.1 was used and extended in order to model *S. cerevisiae* cells and their DEP response variation through their budding cycle. In the cell division cycle, the total volume of the budding *S. cerevisiae* cell increases. Herein, the budding *S. cerevisiae* is therefore approximated by spherical

S. cerevisiae cell of larger diameter (see Figure 3.2) keeping the axial symmetry of the cell model. Such approach facilitates the use of analytical tools to solve the DEP response.

Although merely proportional dependence of DEP on cell size was predicted in various literature resources [101], detailed simulation results show the consequences of the heterogeneity of the cell structure lead to variation of the Clausius-Mossotti Factor ($K(\omega)$). The size dependence of the $K(\omega)$ is obvious from the formula for the effective permittivity (see Section 2.4.2).

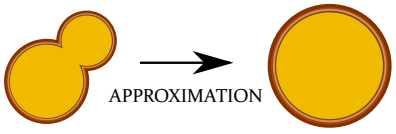

FIGURE 3.2: Approximation of a budding *S. cerevisiae* cell by a larger spherical non-dividing *S. cerevisiae* cell.

Numerical simulations were performed in Matlab using the analytical axial symmetry solution of DEP for multi-shelled particles in the non-uniform electric field described in 2.4.1. The simulation results show swing of the first crossover frequency in the DEP response of the *S. cerevisiae* cell over large frequency range making it easily detectable by DEP. Numerical simulation results showing the $K(\omega)$ for different *S. cerevisiae* cell diameters are shown in Figure 3.3. The simulation data show decrease of the 1^{st} crossover frequency from 1.5 MHz to 520 kHz as *S. cerevisiae* cell grows from 4 microns to 7 microns in diameter. The value of electrical conductivity of the surrounding medium was chosen carefully to increase the DEP variations in the frequency range of interest.

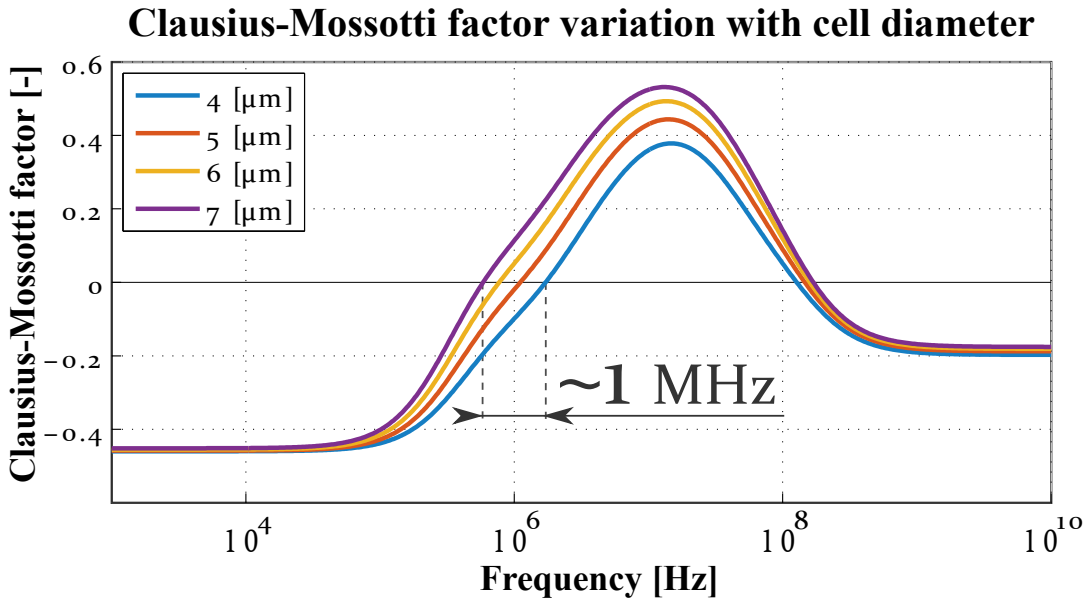

FIGURE 3.3: Numerical simulation results showing the $K(\omega)$ for different *S. cerevisiae* cell diameters.

The simulation results were validated in microfluidic experiments where cells in the G1 phase were discriminated from cells in the G2 phase using DEP (see Figure 3.4 for experimental results). The data are in good agreement with numerical simulation of the developed budding *S. cerevisiae* model. The experimentally measured cross-over frequency equals 900 $kHz \pm 150\ kHz$, which is precisely the range of cross-over frequencies predicted by the approximate model.

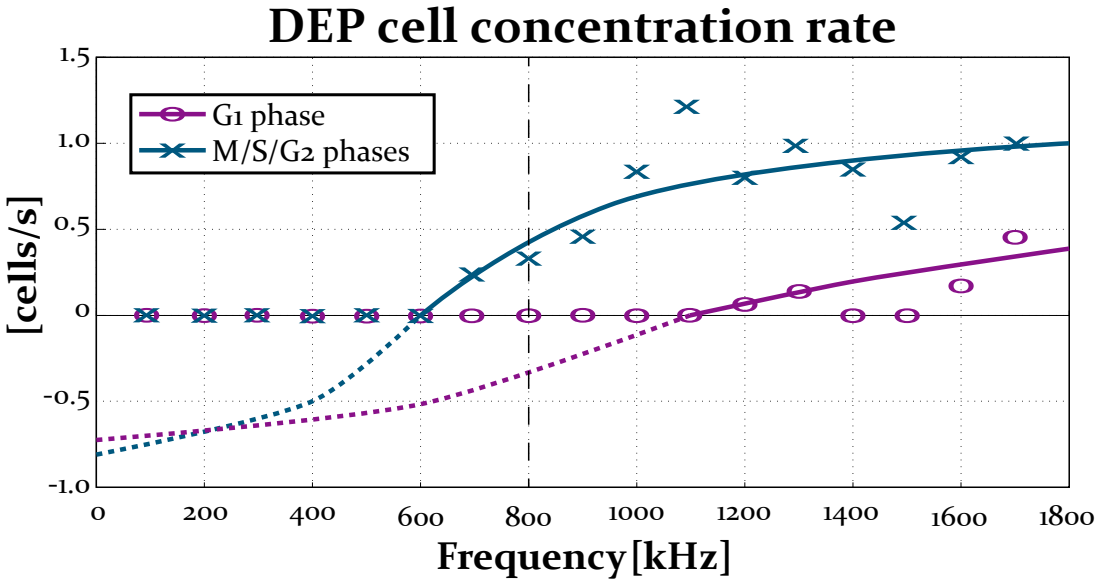

FIGURE 3.4: Preliminary results on the DEP response of the *S. cerevisiae* cells.

3.3 Effects of alignment on live cell DEP

The benchmark microfluidic device for *S. cerevisiae* cell sorting with integrated DEP presented in Section 3.2 was simulated to study the effect of misalignment of microchannels above electrode structures on efficiency of the *S. cerevisiae* cell sorting according to their life cycle phase. The results show that the sorting efficiency is high only if the alignment of microchannels above electrode structures is precise.

Numerical simulation results showing distribution of cells within a microchannel after the sorting stage for different values of misalignment are shown in Figure 3.5. The effect of misalignment on the efficiency of the DEP sorting evaluated by Equation 3.1 are shown in Figure 3.6. The results show that perfect alignment corresponds to above 99% sorting efficiency, while with increasing misalignment the sorting efficiency decreases rapidly. Hence, the alignment of the microchannel above the electrode structures must be on the order of the sorted cell size to achieve meaningful sorting efficiencies. However, attaining such high precision using standard soft lithography can be difficult due to additional requirements of an alignment stage and its associated tight timing limits. In the next

section, an alternative fabrication process enabling rapid prototyping of high precision microfluidic devices with integrated microelectrode topologies is presented and verified.

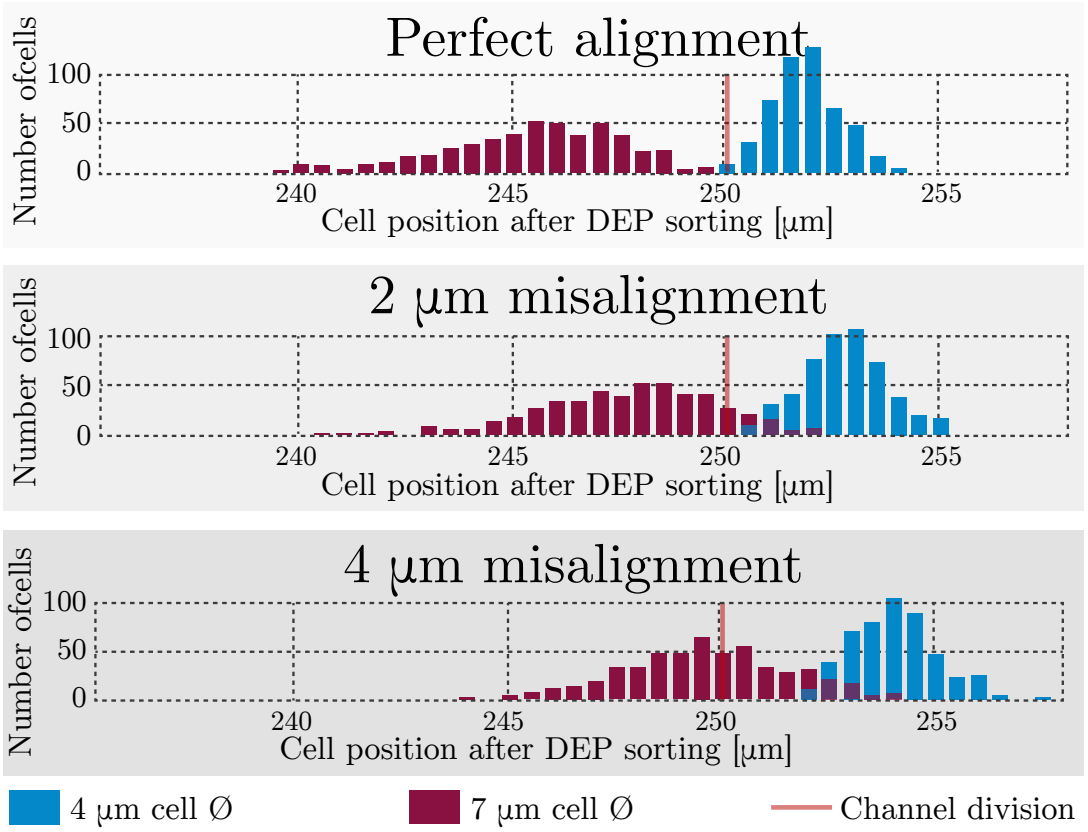

FIGURE 3.5: Distribution of cells within microchannel after the sorting step.

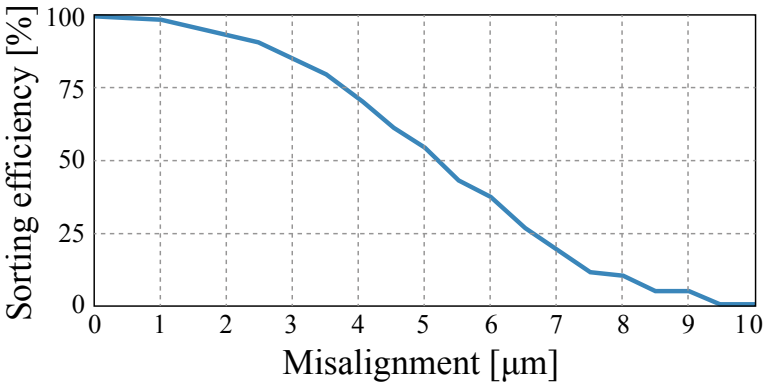

FIGURE 3.6: Efficiency of DEP sorting in microfluidic device and its dependence on misalignment.

3.4 Highly precise fabrication

3.4.1 Fabrication protocol

Microfluidic devices were designed and fabricated to discriminate between *S. cerevisiae* cells in the G1 phase cells from cells in the G2 phase. The fabrication process was proposed to achieve precise alignment in prototyping of highly sensitive DEP cell sorting devices.

Microelectrode structures were patterned on glass using standard photolithography processes. A 50 nm thick layer of Ti/W, and 500 nm thick layer of gold were deposited by sputter-coating. The layer of Ti/W was deposited first to improve the adhesion and stability of the deposited gold layer. After the metal deposition, a 1.1 μm thick layer of PFR7790 (JSR Micro) photoresist was spin-coated and patterned. The gold and Ti/W were etched by wet etching in the areas not covered by photoresist. The remaining photoresist was removed.

FIGURE 3.7: Fabrication of the SU-8 microfluidic channel structures.

A 30 microns thick layer of SU-8 was spin-coated on top of the glass substrate to serve as a carrier of the microfluidic channel structures. The SU-8 photoresist was pre-baked immediately after spin-coating, exposed to UV light through a photomask, followed by post-exposure bake. The SU-8 development revealed the designed microstructures. Finally the wafer was hard-baked to increase thermal, chemical and physical stability of the developed resist structures. Fabrication process is schematically shown in Figure 3.7.

Simple flat sheets of PDMS were fabricated to seal the microfluidic devices. Two-part silicone elastomer Sylgard 184 from Dow Corning was used to produce the PDMS sheets. The base part was mixed with sufficient amount of curing agent (10:1 ratio) and stirred well in a disposable plastic cup. The mixture was placed in a desiccator to remove the air bubbles introduced by mixing. PDMS mixture was poured into a plastic petri dish to form homogenous approximately 5 mm thick layer. The petri dish containing the mixture was then placed into an oven, for 2 hours at 80 °C. Perfect horizontal position was required to assure good planarity. The PDMS edges were cut off with a sharp tool and the PDMS sheet was gently peeled off the petri dish. The released PDMS sheet was cut into pieces equal in size to the individual microfluidic devices. Inlets and outlets were drilled carefully by sharp needle of the appropriate diameter at the desired locations. A

paper template with the preprinted pattern may serve well for easier localisation of the inlets and outlets.

Short oxygen plasma treatment of the SU-8 surface and subsequent chemical silanization process was performed to enable direct irreversible bonding of the SU-8 structures to the PDMS [50]. First, the oxygen plasma treatment allowed binding of silanes to the SU-8 surface through opening of the epoxy rings at the SU-8 surface. Subsequently, SU-8 structures were immersed into (3-Aminopropyl)trimethoxysilane (APTMS) solution diluted with methanol to 9% by mass. The samples were dried at 110 °C for 30 minutes. Silanization process is illustrated in Figure 3.8.

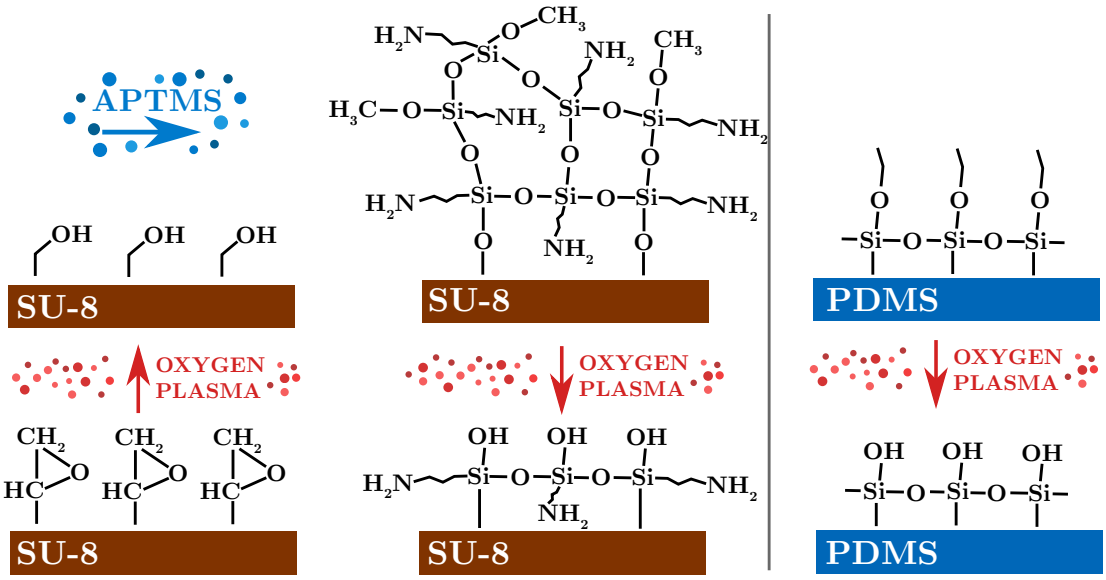

FIGURE 3.8: Illustration of the silanization process and the final oxygen plasma activation of the SU-8 (left). Oxygen plasma activation of the PDMS (right).

The microfluidic devices were sealed with prepared flat sheets of PDMS. Individual flat sheets of PDMS were cleaned properly with adhesive tape. The PDMS and SU-8 surface was treated by oxygen plasma for 20 seconds. The oxygen plasma affects the PDMS backbone and forms reactive silanol functional groups (Si-OH) enabling formation of permanent irreversible bond of the PDMS to the silanized SU-8 surface [106]. The oxygen plasma activation is illustrated in Figure 3.8.

Note that the PDMS treatment with oxygen plasma is also beneficial as it avoids non-specific adsorption, decreases cell clogging and turns the PDMS to hydrophilic, that facilitates the future microchannel wetting [61]. Immediately after the oxygen plasma treatment, small droplet of methanol was poured over the SU-8 surface to avoid instantaneous bonding of the activated PDMS to the SU-8. The methanol between the SU-8 and the PDMS increased the time necessary for alignment of the PDMS microstructures above the SU-8 microstructures to approximately one minute. Alternatively, methanol

may be replaced by less dangerous isopropyl alcohol. The alignment of the flat PDMS sheets was performed manually. The bonded devices were placed in the oven at 80 °C for 5 minutes. Finally, the devices were placed at room temperature covered with a petri dish to avoid contamination. All inlets and outlets were sealed by adhesive tape after 24 hours. The bonding of the flat PDMS sheet to the SU-8 layer is illustrated in Figure 3.9.

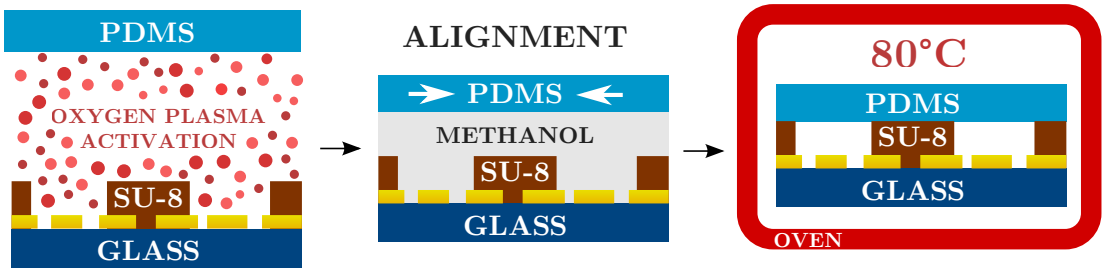

FIGURE 3.9: Bonding of PDMS to SU-8.

If the given guidelines are followed, the fabrication process is simple and reproducible. Identical devices were fabricated using standard PDMS soft lithography processes.

3.4.2 Verification

The fabricated microfluidic devices were tested under experimental conditions and the correct alignment was verified by optical microscopy. The devices fabricated with the SU-8 formed microchannels showed perfect alignment of the microchannel structures with the electrodes, as well as perfect adjoining of the SU-8 layer to the glass substrate with patterned electrodes. No noticeable PDMS delamination or microchannel shrinkage was observed. Delamination of the PDMS above electrode structures and the imprecise alignment common for soft lithography fabricated devices are shown in Figure 3.10. The shrinkage of the PDMS dimensions was estimated to be approximately 2%. The misalignment of the microchannel structures using the PDMS soft lithography ranged from 10 to 50 microns. The benchmark problem was used to characterise sorting efficiencies for different misalignment errors. This suggests the alignment achievable using the standard PDMS procedure is well outside the range required for reasonable cell sorting. The presented process is only limited by the precision of the mask aligner, hence near optimal efficiency is possible.

3.4.3 Prerequisites and comparison to soft lithography

Microfluidic devices exploiting interactions of live cells with electric field require electrodes to be patterned on a substrate. However, it is difficult to obtain perfect alignment

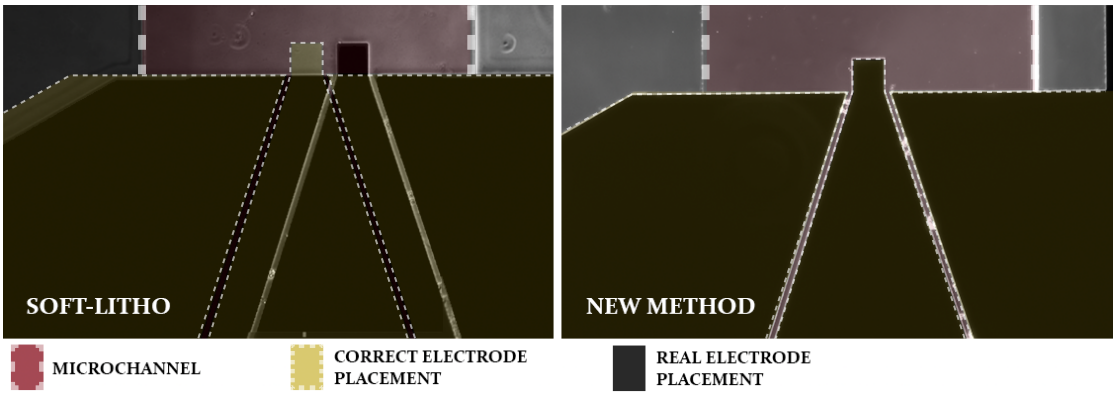

FIGURE 3.10: Bottom view of the device fabricated with standard soft lithography showing misalignment and delamination above cell focusing electrode structures (left), and the device with SU-8 formed microchannels (right). The color overlay illustrates the correct alignment of microchannels above microelectrodes.

with standard soft lithography due to the manual alignment. Here a mask aligning system is utilized to perform a high precision alignment prior to the UV exposure of the SU-8 layer.

The presented method requires patterning of the microfluidic channels to be performed for each set of microfluidic devices. On the other hand, the soft lithography process requires single fabrication of the Si (or SU-8) master necessary for PDMS mold replication. These additional replications do not require a mask aligner, a spin processor or a UV exposure system.

In terms of time requirements the two methods are roughly the same with the exception of the electrode to channel alignment. While the standard PDMS requires each device to be aligned separately, the method presented herein involves single alignment stage per wafer (containing up to tens of devices).

PDMS material is generally considered as bio-compatible. However, the use of PDMS with sensitive cell lines may not always be so straightforward [69, 96]. After curing of PDMS, there is up to 5% of the weight of the PDMS in the form of un-crosslinked oligomers. These oligomers may be released, contaminate the culture medium, and suppress the growth and proliferation of present cells, e.g. primary neurons [112]. The un-crosslinked PDMS oligomers can be decreased or avoided by extraction of the oligomers with highly soluble solvents [65].

Unlike PDMS, SU-8 shows perfect biocompatibility without any additional processing. Photo-thermal activation of SU-8 results in high degree of cross-linking as each of the constituent SU-8 monomers contains eight reactive epoxy sites [27]. No problems have been reported in conjunction to the release of insufficiently cross-linked SU-8 products. SU-8 has been widely used in applications ranging between cell encapsulation [62] and

neuronal probes [20]. Several deep analysis were performed *in vitro* and even *in vivo* to prove the biocompatibility. The SU-8 showed no influence on cell growth and proliferation in *in vitro* experiments with various mammalian cell cultures [10,20,78,102]. No viability issues were observed during our experiments in connection with the silanization process. This is in agreement with a prior study wherein surface biocompatibility was confirmed by measuring viability of the HT29 human cell line (colon cancer) following a 2.5 h incubation period on silanized surface [60].

3.5 Conclusion

In this chapter, an innovative fabrication process for rapid prototyping of microfluidic devices providing high precision alignment of microchannels to underlying electrode structures was presented. The effect of misalignment of a microchannel above electrode topologies on live cell DEP was characterised through a proposed benchmark problem. The main results of this characterisation indicated that alignment precision must be on the order of the cell size in order to achieve meaningful sorting efficiencies. For this purpose, the standard PDMS soft lithography fabrication process comprising a manual alignment stage is not suitable. Devices fabricated by the presented method showed close to perfect alignment of the microchannels above electrode topologies, higher reliability and resistance to pressure. One of the main contributions was showing that permanent bonding of SU-8 to PDMS can be achieved by simple and efficient wet chemical silanization step in combination with oxygen plasma treatment. The presented method is easily reproducible and enables simple, low cost, fast prototyping of microfluidic devices suitable for live cell handling.

Chapter 4

Distributed Dielectrophoretic Cytometry (2DEP Cytometry)

4.1 Introduction

Dielectrophoretic (DEP) cytometry designs in which differences in Dielectric (DE) properties of cells manifest themselves through lateral separation, and the complex state of the art force equilibrium DEP cytometry methods require attaining high precision during the fabrication processes (see Chapters 2 and 3 for more details). On the other hand, methods based on vertical separation, such as Dielectrophoresis Field Flow Fractionation (DEP-FFF) are less sensitive to misalignment of micro-channel structures to electrode topologies. Hence fast, simple and relatively cheap prototyping fabrication processes, such as the Poly(dimethylsiloxane) (PDMS) soft lithography, may be used.

In this chapter, a novel force equilibrium method called Distributed Dielectrophoretic Cytometry (2DEP Cytometry) was developed. It uses a DEP-induced vertical translation of live cells in conjunction with Particle Image Velocimetry (PIV) in order to measure probabilistic distribution of live cell DE signatures on an entire cell population. The method is integrated in a micro-fluidic device. It is less sensitive to misalignment of microchannel to electrode topologies enabling PDMS soft lithography to be used for the device fabrication. The bottom of the micro-fluidic channel is lined with an Interdigitated (ID) electrode array. Cells passing through the micro-channel are acted on by sedimentation forces, while DEP forces either oppose sedimentation, support sedimentation, or neither, depending on the DE signatures of the cells. The heights at which cells stabilize correspond to their DE signature and are measured indirectly using PIV. The presented method is similar to all-electric DEP cytometry [80], however it is based on PIV analysis, which enables simultaneous and high-throughput collection of hundreds of

single-cell responses in a single frame. In addition, PIV may be further integrated with fluorescence measurements yielding correlations between DE signatures and intracellular processes.

A stochastic model of 2DEP Cytometry was developed and used to estimate probability distributions of the DEP-induced cell levitation heights by allowing for random variation in cell structural and DE properties, and to validate the values of experimental parameters, such as the flow rate and the frequency range of interest. Resolution of the 2DEP Cytometry due to technological parameters (e.g., camera resolution and height of the microchannel) was estimated, and sensitivity of 2DEP Cytometry to variation of the individual live cell DE properties was evaluated using numerical simulation of Dielectrophoresis (DEP) based on live cell models presented in Section 2.5.2.

Custom electric signal generator based on Direct Digital Synthesis (DDS) was designed and fabricated. The frequency, the amplitude and the Direct Current (DC) offset of the individual output channels are controlled from Personal Computer (PC) via Graphical User Interface (GUI). Complex signal profiles may be designed and implemented. The output peak-to-peak voltage range meets the 10 V requirements. DC offset ±10 V may be applied. The generator was successfully tested up to 50 MHz. An interface platform providing necessary mechanical support, and electrical and fluidic interconnections, enabling full encapsulation for precise control of the Carbon Dioxide (CO_2) and humidity levels was developed.

Experimental data quantify the DE signature of a *Saccharomyces cerevisiae* (*S. cerevisiae*) population and Human Immortalised Myelogenous Leukemia (K562) cell line. In addition, a comparative study was performed on genetically modified *S. cerevisiae* cell populations, and stressed K562 cell lines. It shows that DEP-induced cell translation along the parabolic velocity profile can be measured by PIV with sub-micron precision, enabling identification of individual cell DE signatures. It was possible to analyse more than 5 thousand cells within 1 minute with the actual experimental setup. The high-throughput enabled measurement of DE signatures at 20 different frequencies in almost real-time. The experimental results are consistent with other studies [68, 100].

4.2 Principles of operation

In 2DEP Cytometry, DEP forces are measured by measuring the levitation heights above ID electrodes. Continuous collection of data is achieved by allowing the cells continuously flow through the channel and measure cell levitation by measuring the cell velocity.

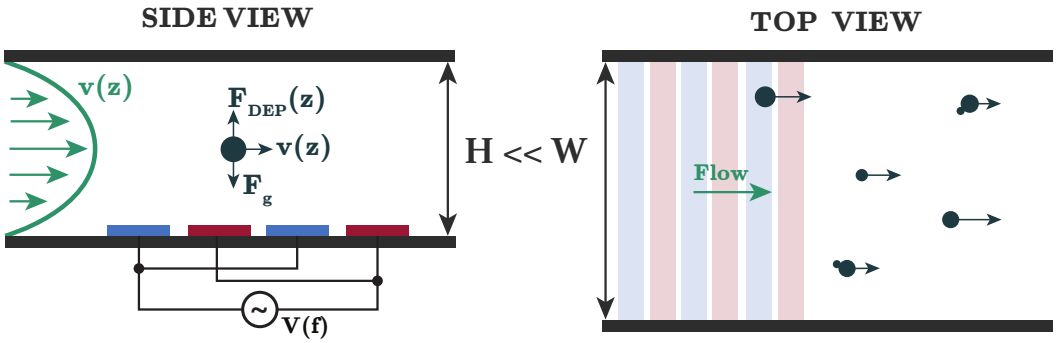

FIGURE 4.1: DEP-induced cell levitation in parabolic flow profile

Important to this concept is the parabolic velocity profile in the vertical direction. Because the flow is laminar and the horizontal dimensions are much larger than the vertical dimension of the microchannel, the flow profile in the vertical dimension is parabolic (the boundary micro-channel sections are omitted). Hence the levitation height is obtained from cell velocity by solving the following expression of the parabolic flow profile:

$$v = \frac{1}{2\mu}\frac{\partial p}{\partial x}(z^2 - \frac{h^2}{4}) \tag{4.1}$$

where v stands for the velocity, μ stands for the dynamic viscosity of the medium, $\frac{\partial p}{\partial x}$ stands for the pressure gradient, z stands for the vertical position within the channel, and h stands for the height of the channel.

PIV is used to measure the cell velocities. In other words, two images are taken in a short well defined time interval, the cells in the consecutive images are paired, and the velocity measurements are obtained from their distance of separation. In result, the process is easy to automate, and yields the DEP force measurements of 5 thousand cells every one minute. In addition, the PIV is based on imaging, and the DE measurements can be further correlated with other fluorescence and optical data.

Figure 4.2 illustrates the process flow involving two cell types. Each cell type enters the channel at the same rate, uniformly distributed in the channel. Cells travel some distance while they sediment near the channel floor. They pass across the ID electrode array, and levitate to their respective heights due to DEP. One cell type may levitate lower, while the other cell type may levitate higher. The cell velocities are then measured through PIV measurements at the end of the channel. The content of one PIV measurement is highlighted by the blue rectangle. Even though each cell type enters the channel at the same rate, the PIV image over-represents the slowly travelling cell types. In order to achieve probabilistic measurements of DEP forces, the bias must be accounted for by normalization of the data by cell velocity (see Equation 4.2).

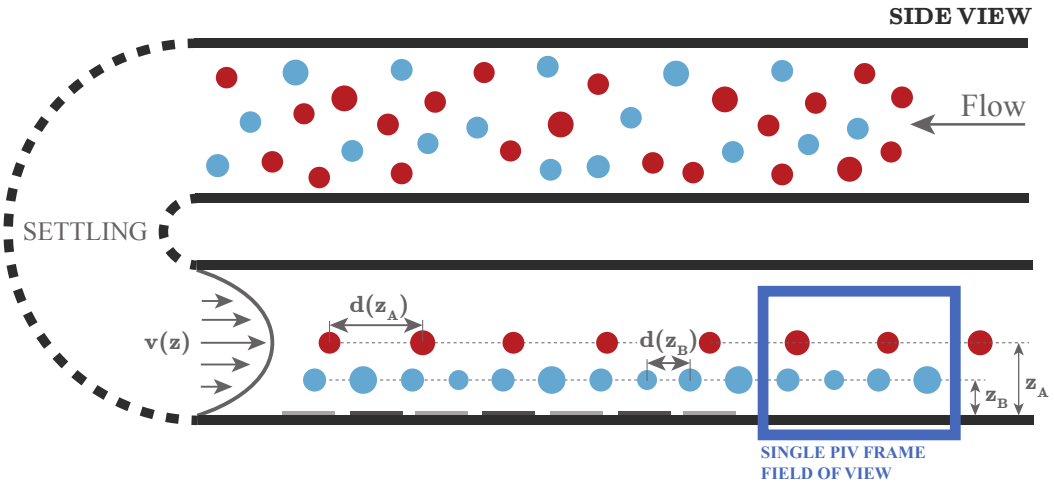

FIGURE 4.2: Schematic of distributed DEP cytometry

$$p(z_A) = \frac{N(z_A).v(z_a)}{N_T.v_{MAX}} \tag{4.2}$$

In the equation $p(z_A)$ stands for probability of cells travelling at levitation height z_A, N_T is the total number of cells, $N(z_A)$ is the number of cells travelling at z_A, $v(z_A)$ is the velocity at z_A, and v_{MAX} stands for the maximum achievable velocity in the specific parabolic flow profile.

4.3 *In silico* 2DEP Cytometry

4.3.1 Stochastic modelling

A stochastic model of 2DEP Cytometry was developed and used to estimate probability distributions of the DEP-induced cell levitation heights by allowing for random variation in multiple inputs (e.g., cell structural and DE properties) and to validate the values of experimental parameters (e.g., flow rate and the frequency range of interest). The electric field distribution was obtained by Finite Element Method (FEM) using Comsol Multiphysics, and then post-processed in Matlab in order to determine spatial distribution of the Gradient of the Square of the Electric Field (∇E^2). *S. cerevisiae* and K562 cell models described in Sections 2.5.3.1 and 2.5.3.2 respectively, were extended and used to model DEP-induced cell levitation in electric field within the 2DEP Cytometry microfluidic device described in Section 4.4.1.

The numerical simulation of 2DEP Cytometry is performed as follows. N cells is introduced to microfluidic device through the inlet. The cells are distributed randomly in the

vertical direction by uniform distribution. Cells are dragged through the microchannel by velocity v, which is defined by the flow-rate and the levitation height. The cell velocity at specific height can be obtained from Equation 4.1 for parabolic flow profile. As cells pass through the microchannel, they tend to sediment near the channel floor. On the other hand as they pass above the electrode array, Negative Dielectrophoresis (N-DEP) may push them to certain levitation height according to the frequency of the electric field and the cell DE signature. Eventually, cells may be attracted towards the channel floor more significantly in case of Positive Dielectrophoresis (P-DEP). Cell velocities and levitation heights are quantified behind the electrode array. Although DE signatures of cells of the same phenotype are similar, every cell has its own DE signature that is unique. Hence a randomly generated set of DE properties is assigned to each of the N cells to simulate the cell diversity in cell population. Every set of DE properties is generated randomly around the central values provided in Sections 2.5.3.1 and 2.5.3.2, in Tables 2.16 and 2.19. The DE properties are distributed randomly within all cells by gaussian distribution with 10% variation. Cell trajectories are evaluated independently for each of the frequencies in the frequency range of interest. The Clausius-Mossotti Factor ($K(\omega)$) is calculated according to the unique set of cell DE properties based on the analytical solution of DEP and the cell structure simplification process presented in Section 2.4. The actual DEP force acting on cell is determined by the combination of the real part of the $K(\omega)$, relative permittivity of the medium, cell size, and the ∇E^2 at the specific location. Cell vertical and lateral movement is given by combination of the drag, sedimentation, and DEP force. Vertical position and cell velocity of each of the cells is quantified at the end of the microchannel, behind the electrode array, where PIV analysis is performed. The intermediate outputs of the simulation are the mean real part of the $K(\omega)$ and its dependence on frequency, the mean final cell velocity and its dependence on frequency, the final cell vertical positions within microchannel, and the final cell velocities. The modelled final mean vertical positions of cells within a microchannel are shown in Figure 4.3.

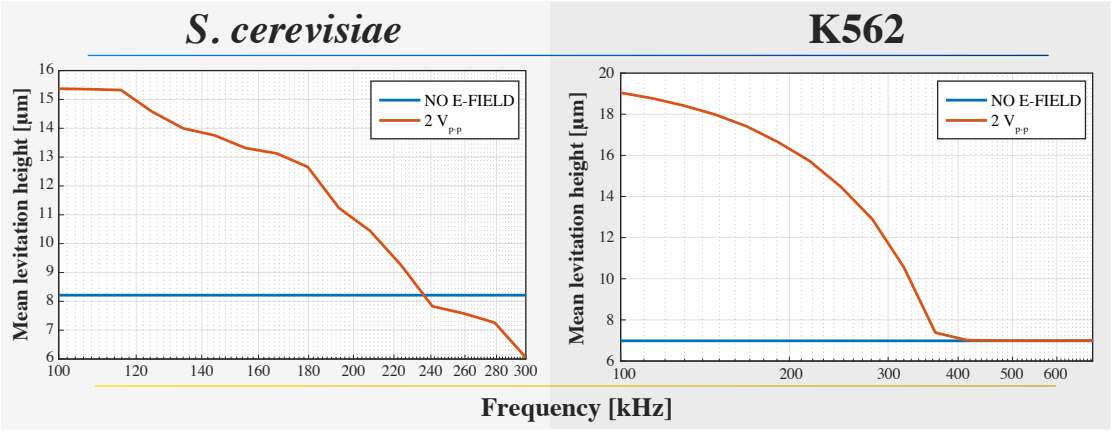

FIGURE 4.3: Simulated 2DEP Cytometry results showing the final mean vertical position of *S. cerevisiae* cells (left) and K562 cells (right) within a microchannel.

Finally, the simulation results are illustrated in terms of cell enrichment in specific microchannel sections due to DEP. Figure 4.4 illustrates the channel section in which the cell enrichment is quantified.

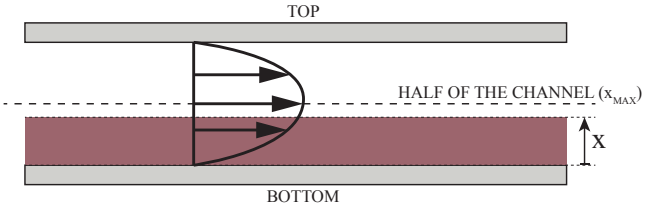

FIGURE 4.4: Illustration of the vertical channel section in which the enrichment due to DEP is quantified. The channel section is highlighted by the brown color.

Figure 4.5 presents an ensemble of simulation results for *S. cerevisiae* cells (left), and K562 cells (right). The various graphs correspond to different frequencies as indicated by the blue to yellow color map. Height above electrodes is plotted on the x-axes. It goes from zero to half the height of the microchannel (20 μm). On the y-axes the enrichment due to DEP in the sector below the corresponding height is plotted.

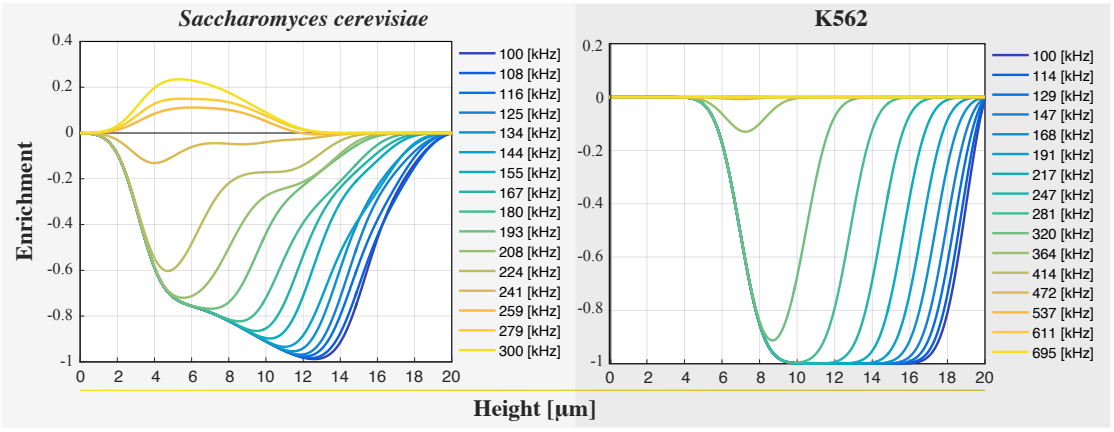

FIGURE 4.5: Simulated 2DEP Cytometry results showing enrichment of vertical channel sections due to DEP of *S. cerevisiae* cells (left), and K562 cells (right).

At the low frequencies (those are the blue lines, going from 100 kHz), purely N-DEP was observed, which is illustrated by negative enrichment at all the sectors below the center line. At the high frequencies (the yellow lines, rising up to 300 kHz in case of *S. cerevisiae* cells, and up to 695 kHz in case of K562 cells), purely P-DEP was observed, which is marked by the positive enrichment at all the sectors below the center line. At higher frequencies, the distribution remain unchanged suggesting only N-DEP, and P-DEP in very close proximity to the crossover frequency can be measured.

4.3.2 Resolution and sensitivity analysis

4.3.2.1 Introduction

The sensitivity of 2DEP Cytometry is given mainly by two factors. First, technological parameters define the z-resolution, which is given by the smallest measurable levitation height variation dz_{min}. The resolution vary with height of the microchannel and flow-rate, because they determine the parabolic flow profile, as well as with camera resolution, field of view, and time interval between two PIV images, which define the resolution with which the cell velocity can be measured. Second factor defines how the individual DE properties manifest themselves through the DEP-induced levitation height variation d_z. Herein, sensitivity of the 2DEP Cytometry to certain parameter is given by the change in levitation height dz linked to variation of the parameter dx. It is introduced as a sensitivity factor s and is given by Equation 4.3.

$$s(x_0, dx) = \frac{\mid z(f, x_0 + dx) - z(f, x_0) \mid}{dz_{min}}, \tag{4.3}$$

where f is the frequency of the electric field that results in the highest s, x_0 is the default value of the selected parameter, dx is the change of the parameter, z is the levitation height, and dz_{min} is the minimum measurable dz. Changes in x that result in values of sensitivity parameter s above 1 are measurable. The larger the sensitivity parameter s, the larger the variation of the levitation height in response to the change of the parameter x, and the more accurate results.

In this section, first the effect of two technological parameters (height of the microchannel, camera resolution) on the resolution dz_{min} is explored independently. Subsequently, sensitivity of the 2DEP Cytometry to variation of the individual DE parameters is investigated and the sensitivity limits are determined.

4.3.2.2 Resolution due to technological parameters

The z-resolution of 2DEP Cytometry due to the technological parameters (height of the microchannel and camera resolution) is illustrated in Figure 4.6. The left part of

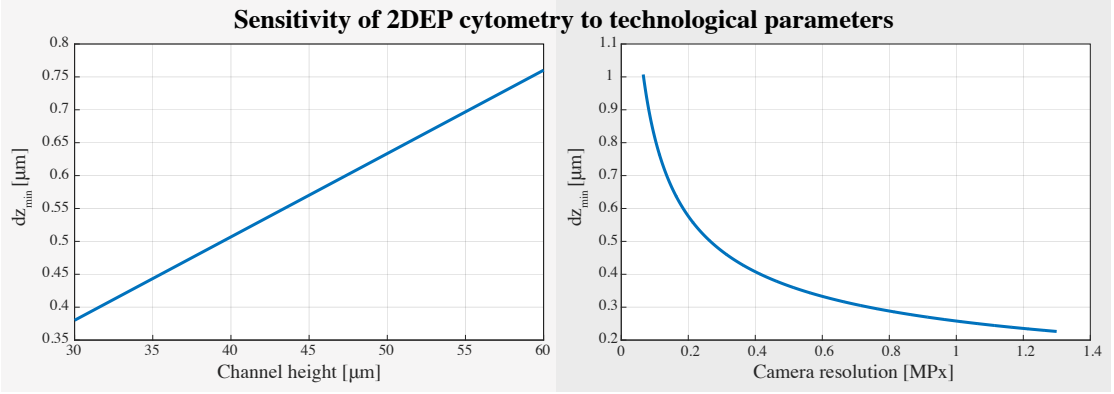

FIGURE 4.6: Sensitivity of the 2DEP Cytometry z-resolution to height of the channel (left); and sensitivity of the 2DEP Cytometry z-resolution to camera resolution (right).

figure shows sensitivity of 2DEP Cytometry to height of the microchannel, while camera resolution is kept constant (approximately 0.26 MPx for 671 x 897 μm field of view), while the right part of figure shows sensitivity of 2DEP Cytometry to camera resolution, while height of microchannel is kept constant at 40 μm, and the field of view remains 671 x 897 μm. The simulation results suggest that even with low camera resolution, sub-micron z-resolution can be achieved.

4.3.2.3 Sensitivity to variations of live cell DE properties

In order to determine sensitivity of the 2DEP Cytometry to changes of DE properties of cells, DEP-induced cell levitation was numerically simulated and its dependence on

the DE properties of individual cell parts was illustrated in terms of sensitivity factor s presented by Equation 4.3.

The DE models of a *S. cerevisiae* cell, and K562 cell described in Section 2.5.2, respectively, were used to quantify the DEP-induced cell levitation in an electric field, and its variation with changing DE properties of the individual cell parts (e.g., plasma membrane and cytoplasm). The sensitivity analysis includes the electric field distribution above micro-electrode array used in the 2DEP Cytometry device, the DE model of the corresponding cell, and the sedimentation forces. The z-resolution given by dz_{min} is calculated based on the technological parameter values (height of the microchannel, flowrate, camera resolution and field of view). The considered camera resolution was approximately 0.26 MPx (which corresponds to 696x372 px large image), the height of the microchannel was 40 μm, the field of view was 671 x 897 μm, and the flowrate was 5 nl/s, which were the values used during the experiments discussed in 4.5. The DE properties were then varied independently, the variation of the DEP-induced levitation height due to the changes in the DE properties was calculated, and the sensitivity factor s was quantified in the selected frequency range.

Sensitivity to variations of *S. cerevisiae* DE properties

Sensitivity of 2DEP Cytometry to changes of *S. cerevisiae* DE properties of the cytoplasm, the plasma membrane, the periplasmic space, the inner and outer cell wall, was quantified in the lower frequency range, where cells exhibit N-DEP, which is the most suitable frequency range for 2DEP Cytometry analysis. The detection limit of 2DEP Cytometry is illustrated by dashed line, highlighting the $s = 1$ level. The DE property changes are measurable when $s \geq 1$. The DE properties of *S. cerevisiae* cells were varied around their central values defined in Section 2.5.3.1, provided in Table 2.16.

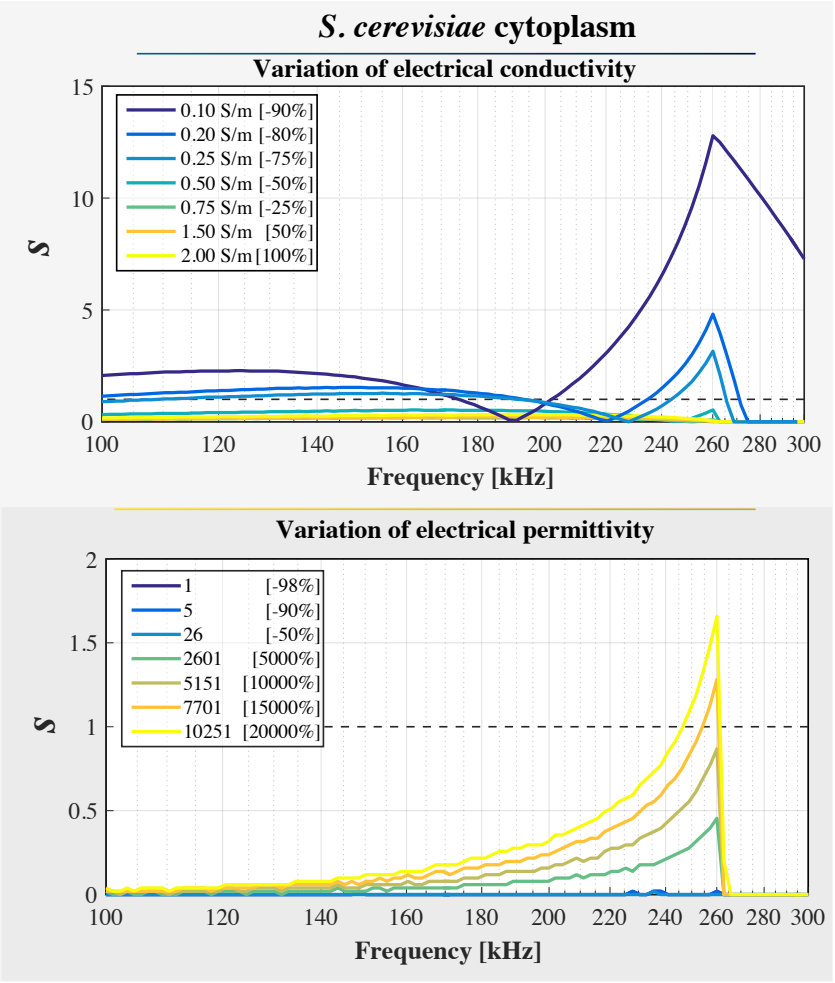

FIGURE 4.7: Sensitivity of the 2DEP Cytometry to variation of the *S. cerevisiae* cytoplasm DE properties.

Figure 4.7 shows that change of *S. cerevisiae* cytoplasm electrical conductivity is measurable only if the cytoplasm electrical conductivity decreases. The change is measurable in the frequency range, which is closer to the 1^{st} crossover frequency of the *S. cerevisiae* DEP response, and the electrical conductivity must drop from the default 1 S/m to almost 0.25 S/m in order to be detectable by 2DEP Cytometry. On the other hand, the change of cytoplasm electric permittivity is not detectable in this frequency range.

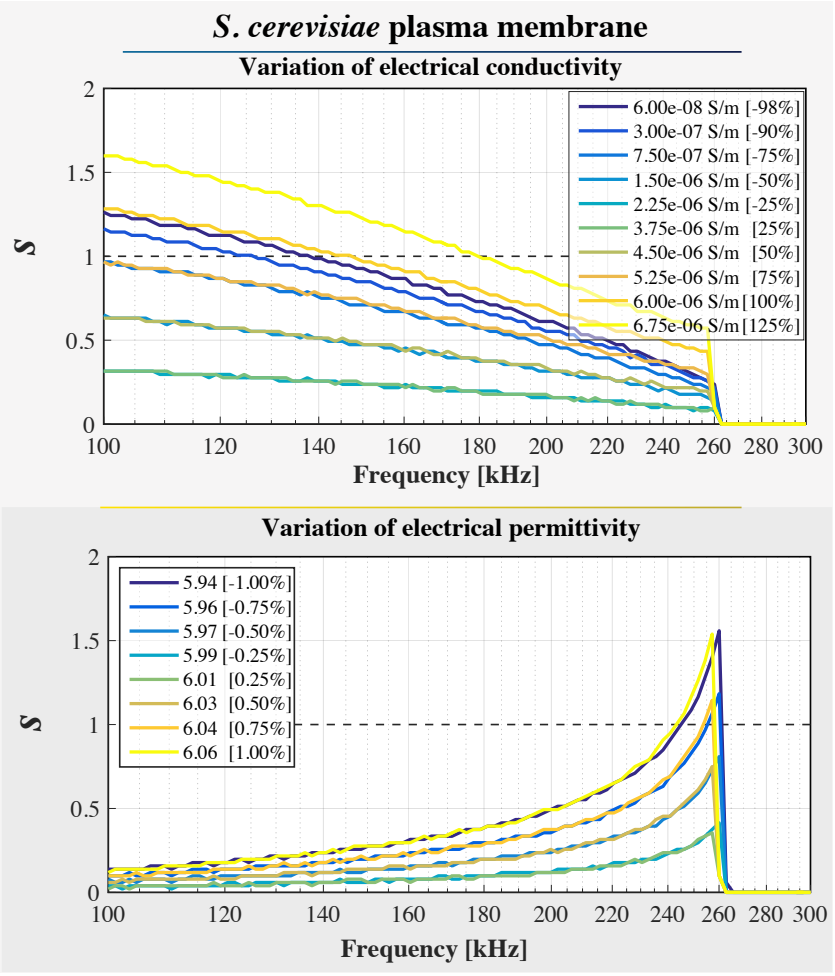

FIGURE 4.8: Sensitivity of the 2DEP Cytometry to variation of the *S. cerevisiae* plasma membrane DE properties.

On the other hand, sensitivity analysis shows high sensitivity of 2DEP Cytometry to changes of *S. cerevisiae* plasma membrane DE properties. The corresponding sensitivity factor values are presented in Figure 4.8. Changes as small as 0.04 in the *S. cerevisiae* plasma membrane relative permittivity are measurable, as well as plasma membrane electrical conductivity changes larger than 2.25 $\mu S/m$.

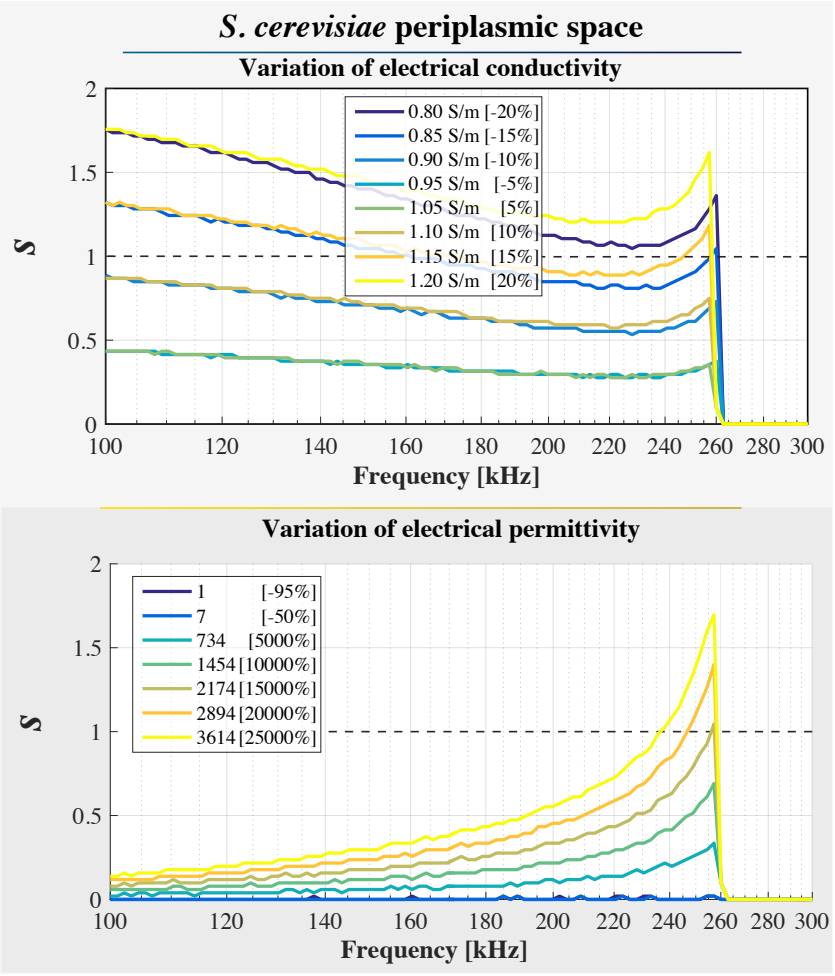

FIGURE 4.9: Sensitivity of the 2DEP Cytometry to variation of the *S. cerevisiae* periplasmic space DE properties.

According to the sensitivity analysis, changes of electrical conductivity of *S. cerevisiae* periplasmic space can be detected on the order of 10%. The corresponding sensitivity factor values are illustrated in Figure 4.9. Changes in electrical permittivity of periplasmic space are not detectable.

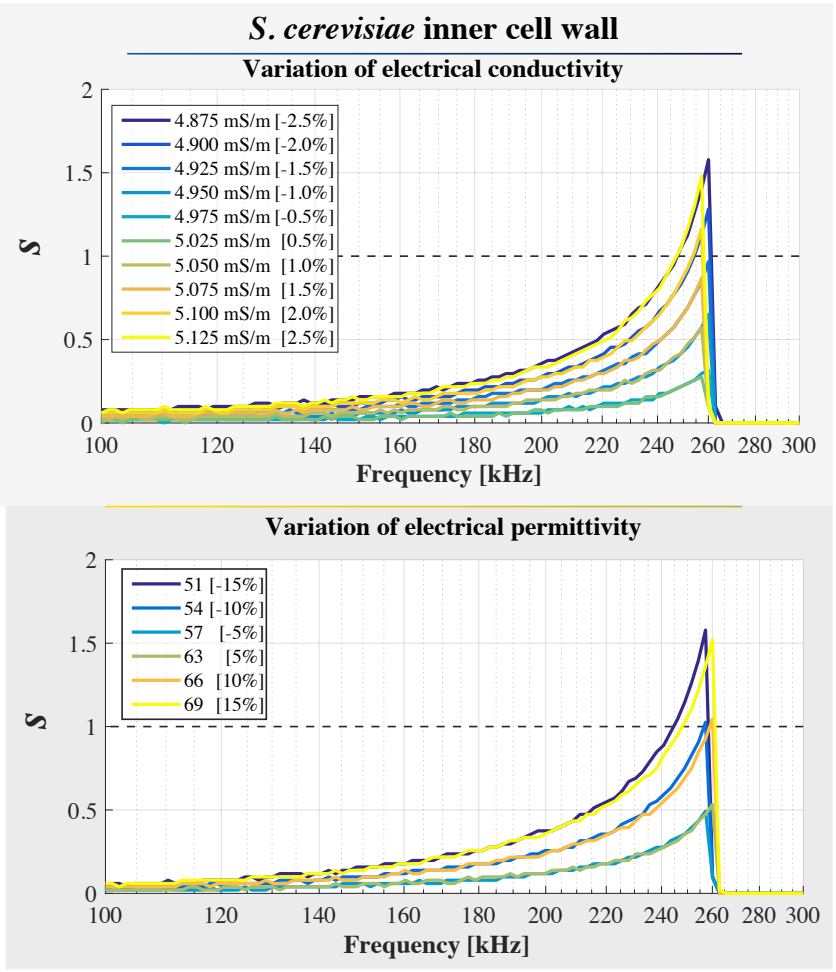

FIGURE 4.10: Sensitivity of the 2DEP Cytometry to variation of the *S. cerevisiae* inner cell wall DE properties.

Figure 4.10 shows the sensitivity factor values corresponding to changes of *S. cerevisiae* inner cell wall DE properties. The data suggest 2DEP Cytometry is sensitive to changes of its electrical conductivity as well as the electrical permittivity. 2DEP Cytometry is most sensitive to *S. cerevisiae* plasma membrane and periplasmic space electrical conductivity changes in the lower frequency range, while in the higher frequency range it is more sensitive to electrical permittivity changes.

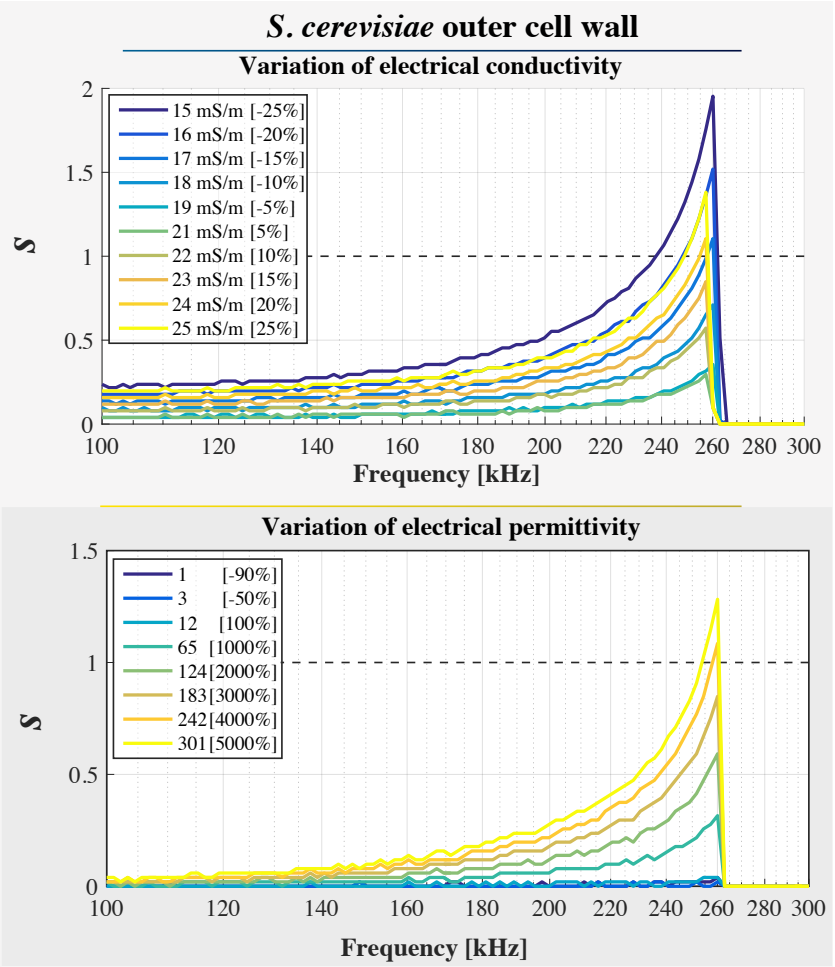

FIGURE 4.11: Sensitivity of the 2DEP Cytometry to variation of the *S. cerevisiae* outer cell wall DE properties.

Finally, Figure 4.11 shows the sensitivity factor values corresponding to changes of *S. cerevisiae* outer cell wall DE properties. While 2DEP Cytometry is sensitive to changes of its electrical conductivity, changes in the electrical permittivity of the outer cell wall are not measurable. Both, the inner and outer wall DE properties are measurable in the frequency range close to the 1^{st} crossover frequency in the DEP response of *S. cerevisiae* cell.

Sensitivity to variations of K562 DE properties

Sensitivity of 2DEP Cytometry was quantified to changes of K562 DE properties of the cytoplasm, and the plasma membrane. The DE properties of K562 cells were varied around their central values defined in Section 2.5.3.2, provided in Table 2.19. Sensitivity of the 2DEP Cytometry to changes of DE properties of the cytoplasm is shown in Figure 4.12, and to changes of DE properties of the plasma membrane is shown in Figure 4.13.

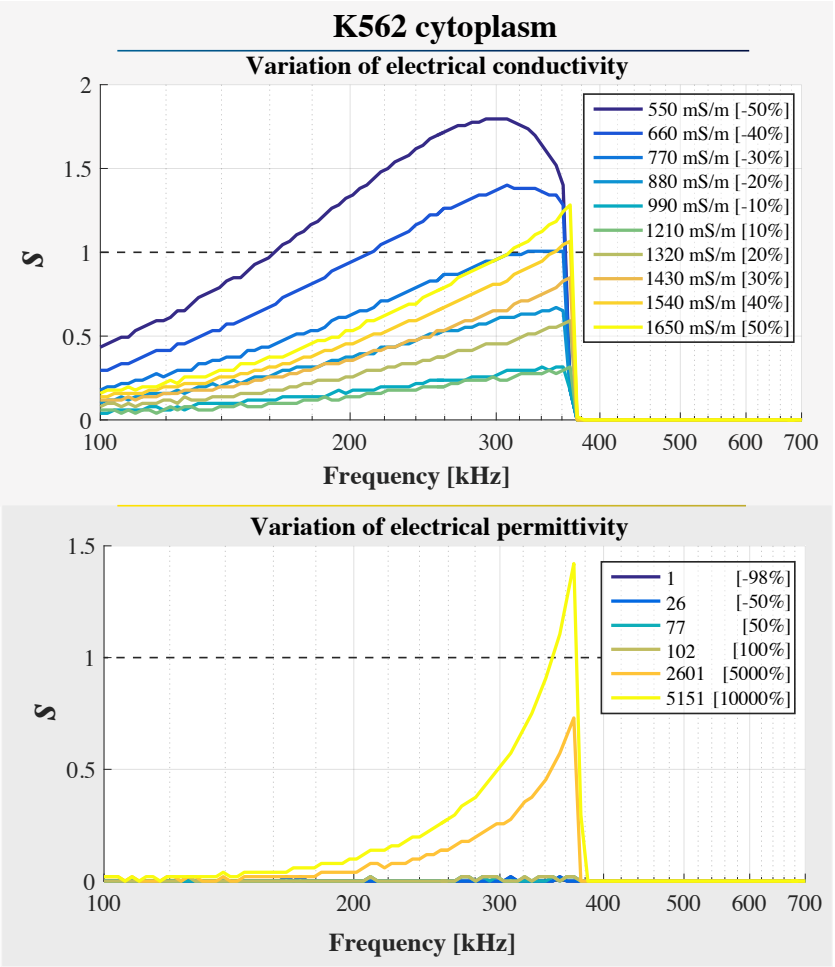

FIGURE 4.12: Sensitivity of the 2DEP Cytometry z-resolution to variation of the K562 cytoplasm DE properties.

Figure 4.12 shows fine sensitivity of 2DEP Cytometry to changes of the K562 cytoplasm electrical conductivity in both directions. On the other hand, it reveals 2DEP Cytometry is insensitive to changes of its electrical permittivity in this frequency range.

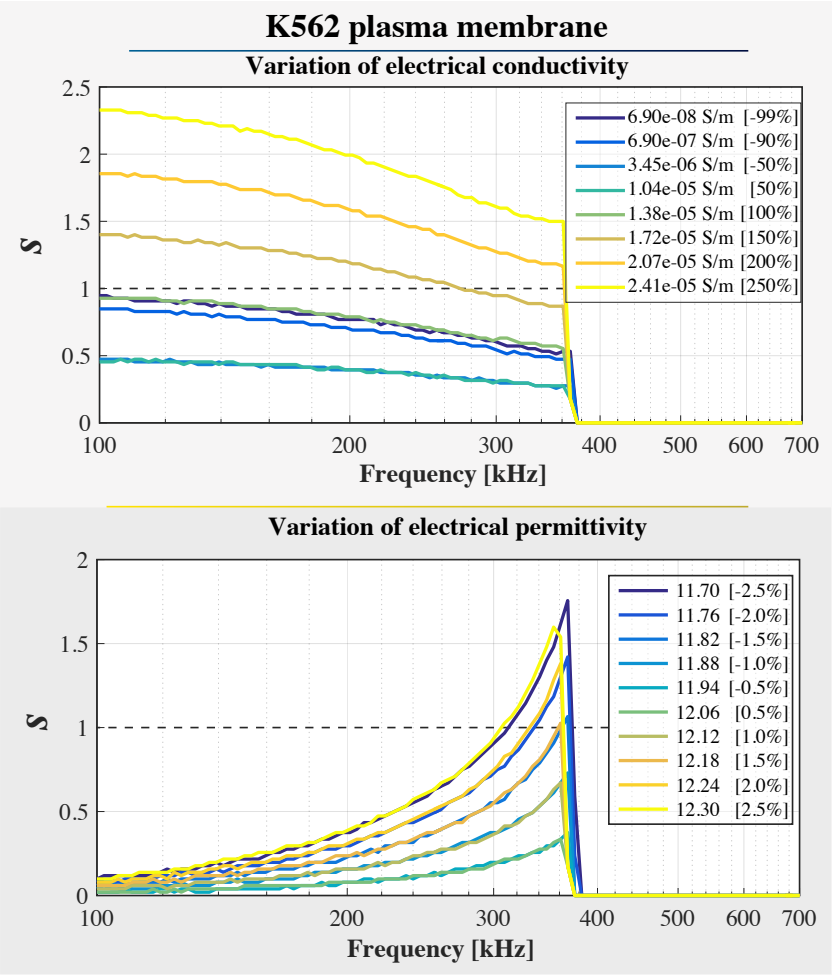

FIGURE 4.13: Sensitivity of the 2DEP Cytometry z-resolution to variation of the K562 plasma membrane DE properties.

Figure 4.13 shows that 2DEP Cytometry is highly sensitive to both, changes of K562 plasma membrane electrical conductivity, and even very fine changes of its electrical permittivity.

4.3.2.4 Summary

Table 4.1 summarizes the sensitivity of 2DEP Cytometry to changes of DE properties of *S. cerevisiae* and K562. The values are linked to the specific technological parameter values, such as the height of the microchannel and the camera resolution. In this particular example, the camera resolution is the main parameter limiting the 2DEP Cytometry sensitivity limits. The camera resolution value corresponds to a CCD camera used in the experiments discussed in 4.5. Using faster CMOS camera instead of CCD, the image resolution could be increased easily by factor of ten resulting in much finer z-resolution, and much finer 2DEP Cytometry sensitivity. In addition, sensitivity to DE parameters

TABLE 4.1: Sensitivity of 2DEP Cytometry to changes of DE properties of *S. cerevisiae* and K562 cells.

Cell	**Cell part**	**DE property**	**Default value**	**Measurable change**	**Direction**
S. cerevisiae	Cytoplasm	σ	1 S/m	<0.75 S/m	$\downarrow$
S. cerevisiae	Cytoplasm	ϵ_r	51	-	-
S. cerevisiae	Plasma membrane	σ	3 $\mu S/m$	>2.25 $\mu S/m$	$\updownarrow$
S. cerevisiae	Plasma membrane	ϵ_r	6	<0.04	$\updownarrow$
S. cerevisiae	Periplasm	σ	1 S/m	>0.12 S/m	$\updownarrow$
S. cerevisiae	Periplasm	ϵ_r	14.4	-	-
S. cerevisiae	Inner cell wall	σ	5 mS/m	>75 $\mu S/m$	$\updownarrow$
S. cerevisiae	Inner cell wall	ϵ_r	60	>6	$\updownarrow$
S. cerevisiae	Outer cell wall	σ	20 mS/m	>3 mS/m	$\updownarrow$
S. cerevisiae	Outer cell wall	ϵ_r	5.9	-	-
K562	Cytoplasm	σ	1.1 S/m	>30 mS/m	$\updownarrow$
K562	Cytoplasm	ϵ_r	51	-	-
K562	Plasma membrane	σ	6.9 $\mu S/m$	>6.9 $\mu S/m$	$\updownarrow$
K562	Plasma membrane	ϵ_r	12	>0.18	$\updownarrow$

that are not measurable in the selected frequency range (e.g., cytoplasm permittivity) might be explored above the 2^{nd} crossover frequency of the corresponding cell DEP response. These parameters may potentially be mapped in the higher frequency range and the information would be complementary to the data measured around the 1^{st} crossover frequency of the cell DEP response.

From table 4.1 it can be concluded that sensitivity of 2DEP Cytometry to *S. cerevisiae* cell DE properties is similar to the sensitivity to DE properties of K562 cells, although, few differences are present. For instance, measurement of *S. cerevisiae* cytoplasm DE properties is limited to decreasing electrical conductivity. In case of K562 cytoplasm DE properties, both, decrease and increase of the electrical conductivity can be detected. In addition, sensitivity to changes of K562 cytoplasm electrical conductivity is much greater, which is due to the lack of the additional cell envelope layers in case of K562 cell (mammalian cells do not synthesize walls).

4.4 HW platform

The 2DEP Cytometry HW platform is a set of equipment required for the 2DEP Cytometry cell analysis. In general, it consists of the image acquisition system, the fluid current or pressure source, the electric field stimuli generator, and the 2DEP Cytometry microfluidic chip. The specific equipment used for the 2DEP Cytometry experiments performed throughout this PhD project are the Olympus IX83 inverted microscope system;

the CCD QImaging Exi-Blue camera optimised for fluorescence microscopy and high-resolution imaging of live cells used for image acquisition; the custom designed frequency stable electric signal generator enabling easy definition and automation of the required frequency sweeps over the frequency range of interest; the Cetoni neMESYS pulsation free, highly precise and nanoliter accurate high-end syringe pumps; the 2DEP Cytometry microfluidic chip; and the custom designed interface platform providing mechanical support, and fluidic and electric interconnections between the microfluidic chip, the electric field generator and the syringe pumps. In this section, design and fabrication process of the custom designed parts are described.

4.4.1 Microfluidic device design

The 2DEP Cytometry microfluidic device consists of three main parts defined in three layers. The first part is the flat glass substrate which forms the bottom of the microfluidic channel and provides the mechanical support for the whole microfluidic chip. The second part is the ID electrode array, which generates the non-uniform electric field inside the microchannel. And the third part is the PDMS layer forming the microfluidic channel, which determines the hydrodynamic behavior. The 2DEP Cytometry microfluidic device design is illustrated in Figure 4.14. The design parameters including electrode and microchannel geometries were selected carefully using model-based approach. Herein, the selected parameters are presented. Selection of the specific parameter values is based on numerical simulation and optimization results previously discussed in Section 2.5 and 4.3.2.

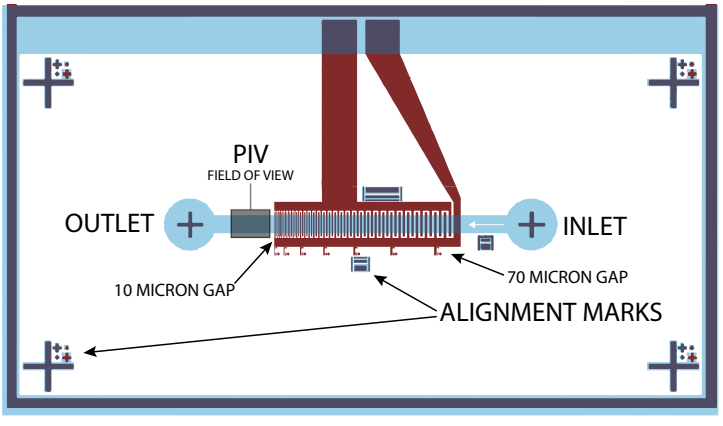

FIGURE 4.14: Top view illustration of the 2DEP Cytometry microfluidic device design. Dark brown are the metallic structures. Microchannel structures are illustrated by the blue shade.

The chip total size is 20 x 12 mm, the channel width is 500 μm, the channel height is 40 μm, and the channel length before the PIV field of view is approximately 7.5 mm

from the inlet. The electrode array goes from right to left, and the electrode width and the gap between electrodes changes progressively from 70 μm to 10 μm. The progressive design ensures the cells being first focused by weaker electric field resulting in lower trans-membrane voltages, decreases the danger of dielectric breakdown of the cell plasma membrane, and decreases potential increase of the fluid temperature in case of higher voltage requirements. Two 1 x 1 mm metallic pads providing connection to the ID electrode array are located at the top edge of the device. The pads are not covered by PDMS. Connections are made with spring-loaded contacts for fast and easy manipulation. The electrical and fluidic interface is further discussed in Section 4.4.4 presenting an interface platform, which was custom designed for 2DEP Cytometry.

Microfluidic device with integrated DEP was designed using Glade GDS, a freeware IC layer editor from Peardrop Design Systems. Glade is extendable using Python scripting, allowing the design to be generated fully from a parametrized Python script.

4.4.2 Microfluidic device fabrication

2DEP Cytometry microfluidic devices were fabricated by combination of standard photolithography and PDMS soft lithography. The electrode and channel design was generated with python script and GDS files were in exported via GladeGDS. Fabrication of the photomasks was outsourced.

4.4.2.1 Fabrication of micro-electrodes

Microelectrode structures were patterned on glass using standard photolithography processes. Approximately 100 nm thick layer of Chromium or Tungsten, was sputtered on a glass wafer to assure good adhesion of gold to the glass substrate. Subsequently, 500 nm thick layer of gold was sputtered on top of the adhesion layer. Layer of photoresist was spin-coated. The photoresist was exposed to UV light through photomask to transfer the pattern to it. The photoresist was developed and electrode structures were wet etched. First, KI solution was used to etch the layer of gold. The chromium layer was etched in a solution of perchloric acid ($HClO_4$), and ceric ammonium nitrate $(NH_4)_2[Ce(NO_3)_6]$. Eventually, the tungsten layer was etched in hydrogen peroxide (H_2O_2). Finally, the remaining photoresist was removed. The microelectrode patterning process is illustrated in Figure 4.15.

FIGURE 4.15: Schematic of the fabrication process of the glass substrate with electrodes

4.4.2.2 PDMS soft lithography fabrication process

Recently, PDMS soft lithography processes have been favorable for its low cost and fast prototyping of microfluidic devices [39]. To transfer the patterns to the PDMS, Silicon (Si) master was fabricated. PDMS was poured over the Si master and peeled off after curing. The PDMS sheets containing the microchannels were bonded to glass substrates with patterned electrodes after short exposure to air plasma.

Silicon master fabrication

First, layer of photoresist was spin coated on top of Si wafer. The photoresist was exposed to UV light through photomask to transfer the pattern to the photoresist. Subsequently, the photoresist was developed. The high aspect ratio structures were obtained by Deep Reactive Ion Etching (DRIE). Height of the structures was approximately 40 microns. Immediately after the DRIE process, several nanometers thick layer of teflon was deposited. Thin layer of teflon covering the silicon wafer disables the PDMS to stick heavily to the wafer. Hence, it facilitates the later release of the PDMS replica from the Si master.

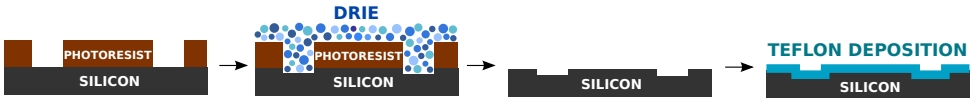

FIGURE 4.16: Schematic of the silicon master fabrication process

PDMS

Two part silicone elastomer Sylgard 184 was used to produce PDMS. The base part was mixed with sufficient amount of curing agent (10:1 ratio) and stirred well in a disposable plastic cup. The mixture was placed in dessicator to remove the air bubbles introduced by the mixing. The Si master was placed in a petri dish and the mixture was poured over. The remaining air bubbles were removed from the PDMS by sharp tip of a needle. The poured PDMS was maintained in perfect horizontal position to assure good planarity, and was cured in an oven, for 1 hour at 80°C. The PDMS edges were cut off with sharp tool and the PDMS was peeled off the Si master. The PDMS mold was sliced into

sections containing individual devices. Inlets and outlets were drilled carefully by biopsy punch of the appropriate diameter at the desired locations of the PDMS replica.

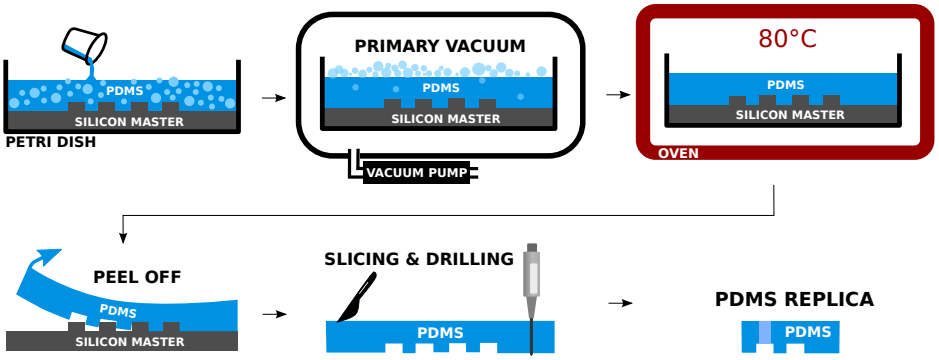

FIGURE 4.17: Schematic of the PDMS mould fabrication process

Bonding of PDMS to the glass substrate

Prepared PDMS replicas with imprinted microstructures were cleaned properly with scotch tape. The PDMS and glass substrate were treated by air plasma for 150 seconds. The air plasma affects the PDMS backbone and forms reactive silanol functional groups (Si-OH) enabling formation of permanent irreversible covalent bond of the PDMS to the glass substrate [106]. In addition, the PDMS treatment with air plasma is beneficial as it avoids nonspecific adsorption, decreases cell clogging and turns the PDMS to hydrophilic. The hydrophilicity of PDMS facilitates the future microchannel wetting [61]. Immediately after the air plasma treatment, 15 μl of Isopropyl Alcohol (IPA) was poured over the glass substrate to avoid instantaneous bonding of the activated PDMS to the glass substrate. The IPA between the glass and the PDMS increases the time necessary for alignment of the PDMS microstructures above the patterned microelectrode topologies. The alignment was performed manually under binocular. The glass substrate bonded to PDMS was placed in the oven, for 5 minutes at 80°C. The bonded devices were placed in a room temperature covered with a petri dish to avoid contamination. All inlets and outlets were sealed by scotch tape after 24 hours.

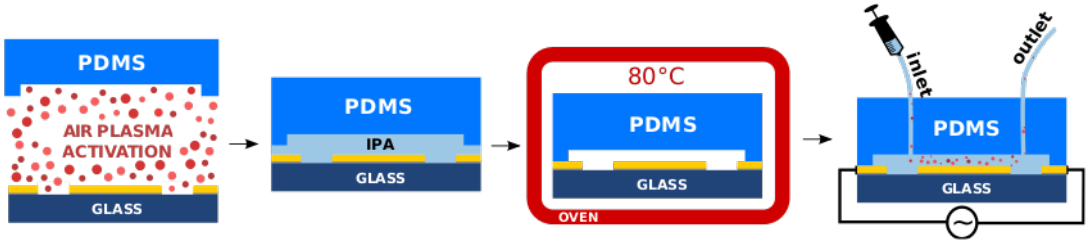

FIGURE 4.18: Schematic of the bonding process

The air plasma treatment that is used in order to seal the microfluidic devices results in reliable bond. However with the specified timing of the plasma treatment presented above, the devices may be disassembled when required (by tearing the PDMS from glass substrate by sufficient force), cleaned, and resealed with new PDMS replica several times prolonging the lifespan of the 2DEP Cytometry device.

4.4.3 Design of customized electric field stimuli generator

The response of cells to the non-uniform electric field is sensitive to the amplitude and the frequency of the electric field. Signals of specific frequency and amplitude are required for standard cell handling in microfluidics, while different signals are required for DEP cytometry analysis and cell sorting. In applications, such as Traveling Wave Dielectrophoresis (twDEP) or Electrorotation (ER), precise setting of mutual phase offset of several signals is necessary. DDS has been selected as optimal solution for generation of frequency-stable AC signal. It also enables implementation of solution that allows generation of multiple output signals maintaining constant mutual phase offset.

Direct digital synthesiser is a frequency synthesiser with specific waveform at the output, such as the sine wave. One stable fixed-frequency reference clock is required for the DDS. In addition, the DDS consists of the digitally controlled oscillator, Digital-to-Analog Converter (DAC), comparator, several functional registers, reconstruction output low pass filter, and other optional blocks. A simplified block diagram is illustrated in Figure 4.19.

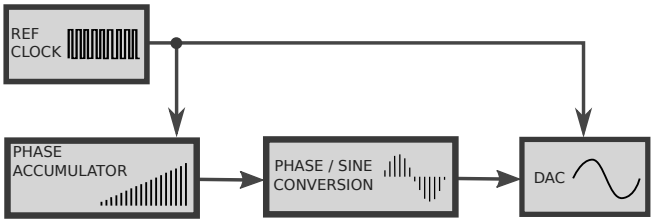

FIGURE 4.19: Principle of the direct digital synthesis

4.4.3.1 Requirements on signal generator specification

Several basic requirements on the design of the signal generator have been defined. The specification of these requirements is noted in the following list:

- Frequency stable DDS based sine wave output
- Frequency range 100 kHz - 10 MHz

- Amplitude range 0 - 10 V (peak-to-peak)
- Eight independent output channels
- Maximum current rating of single channel up to 500mA
- Configurable DC offset (±5 V)

The designed system is controlled from PC via GUI. A single master microcontroller is responsible for communication between the PC and the output modules (slave modules). Among other things, the master module broadcasts the necessary synchronization symbols to enable synchronized starts/stops of multiple slave modules at one moment. Simple block diagram representing the corresponding configuration is illustrated in Figure 4.20.

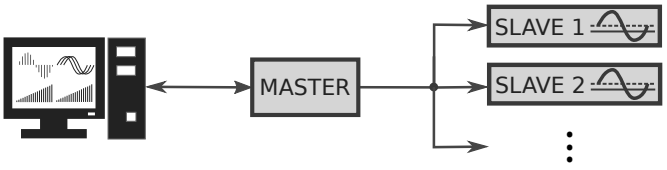

FIGURE 4.20: Block schema of the signal generator

Each of the slave modules contains a microcontroller which controls overall function of the module. It stores the information about the configuration of the module and its sub-parts. The module sub-parts are the DDS unit, which generates the frequency-stable sine wave; the DAC, which enables the DC offset; the high-speed amplifier, which sums and amplifies the outputs of the DDS, the DAC, and at the same time is connected as low pass reconstruction output filter. A block schema representing a slave module is illustrated in Figure 4.21.

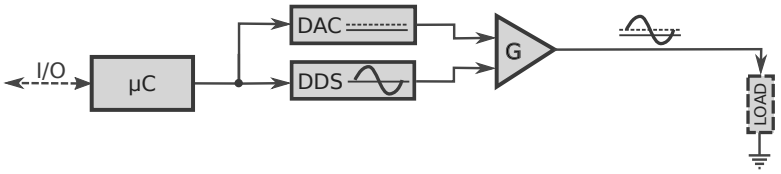

FIGURE 4.21: Block schema of the slave module

The signal generator was designed according to the Figures 4.20 and 4.21 to provide up to 20 independent sine wave outputs. A 40MHz quartz crystal oscillator is used to generate stable reference clock and is fed to all DDS units. Each of the channels is equipped with the 32-bit Microchip microcontroller PIC32MX575F256H, the Analog Devices AD9954 direct digital synthesizer, the Analog Devices AD667 digital-to-analog converter, and the Texas Instruments THS3001 high-speed amplifier. In theory, every channel is capable of an independent sine wave generation in a frequency range up to 160 MHz with a 0.01

Hz frequency resolution. The system is controlled via custom designed GUI. Universal Serial Bus (USB) interface provides the communication channel between the PC and the signal generator. The USB interface is operated by single master 32-bit Microchip microcontroller PIC32MX575F256H. The master microcontroller controls the individual modules, detects their presence in the system and provides communication channel between them and the user interface. The GUI allows to define complex dynamic electric signal profiles, frequency and amplitude steps and sweeps, synchronized or individual starts/stops of the modules and other features.

4.4.3.2 Communication protocol

Communication between the PC and the signal generator is provided via USB. The USB interface makes it easy to connect embedded devices to a computer. A USB Communication Device Class (CDC) was implemented to provide the features of the USB interface among with the simplicity of serial port communication. The theoretical max data throughput is 1,216,000 bytes/s. The communication packets are of variable length and structure. All packets start with the destination address. Eventually, 0x55 byte represents a broadcast message reaching all slave units. A message of 1B length containing the module ID is used to reveal the presence and the eventual configuration of the corresponding module. Alternatively, the address byte is followed by the instruction byte. If the packet contains an instruction intending to transfer a specific value (e.g. the value of the DC offset), the value decomposed to individual bytes follows the address byte. A list of instruction bytes and their description is provided in Table 4.2. The CR (Carrier Return, 0x0A) and NL (New Line, 0x0D) bytes are inserted at the end of each packet. A structure of the frame transmitted via USB/CDC is illustrated in Figure 4.22.

A Serial Peripheral Interface (SPI) communication was implemented between the master and slave modules providing reliable on-board communication. The master/slave SPI communication packets are fixed length (64 bytes). The structure of the communication packet differs according to the content, and is defined by the content of the first two bytes. The first byte of the packet stands for the destination address. The destination address is given by slave unit unique ID. The unique ID is hardcoded in the Flash memory of the specific slave microprocessor. Eventually, 0x55 byte represents a broadcast message addressed to all slave units. The destination address byte is followed by instruction byte. Instruction byte may require a start/stop of the unit, a read/write cycle from/to the DDS unit control or functional registers, or other configuration setting. The remaining

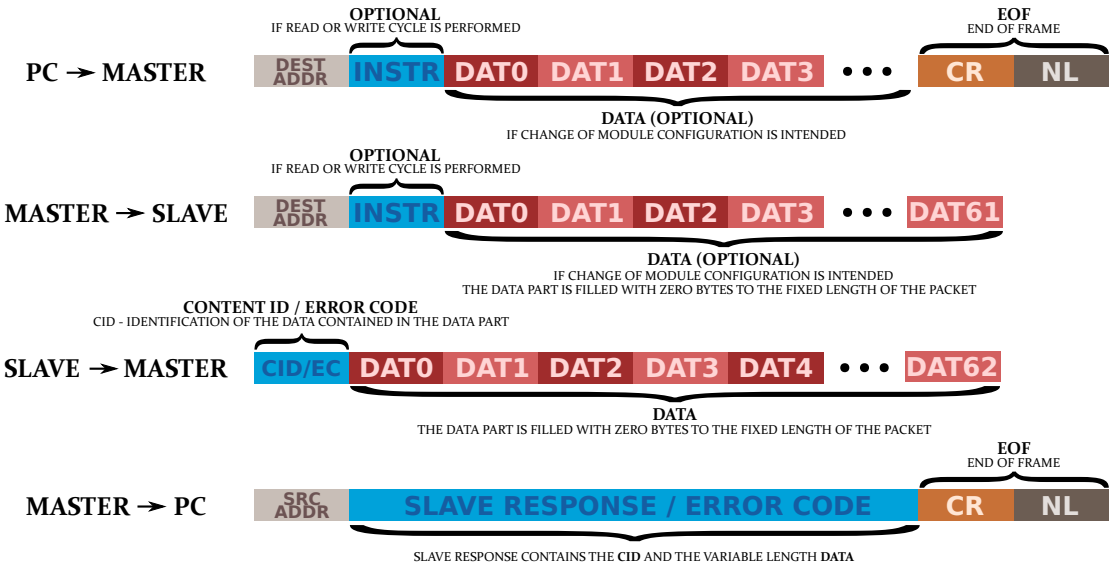

FIGURE 4.22: Illustration of the communication flow and the structure of the frames transmitted via USB/CDC and the SPI interface.

Instruction (Hex)	Description
0x00	Read/Write the CFR1 register of the DDS
0x01	Read/Write the CFR2 register of the DDS
0x02	Read/Write the ASF register of the DDS
0x03	Read/Write the ARR register of the DDS
0x04	Read/Write the FTW0 register of the DDS
0x05	Read/Write the POW register of the DDS
0x06	Read/Write the FTW1 register of the DDS
0x07	Read/Write the NLSCW register of the DDS
0x08	Read/Write the PLSCW register of the DDS
0x0A	Read/Write the DC offset value (DAC)
0xA1	Check the presence of a module and reveal the module configuration
0x0E	Enable module
0x0D	Disable module
0xEA	Enable all modules
0xDA	Disable all modules
0xE1	Start timer and set the DC offset (modules enabled)
0xD1	Stop timer and reset the DC offset (modules disabled)
0xCC	Clear all control points defining the dynamic mode signal profile and enable dynamic mode
0xCD	Disable dynamic mode (switch to static mode)

TABLE 4.2: A list of instruction bytes and their description.

part of the packet is defined by the instruction byte, as well as the delay, length and structure of the expected response. Broadcast messages addressed to all units do not require any response. Otherwise, the response is pulled by master after sufficient time to allow the slave micro-controller to read/write data from/to the DDS or the DAC. A structure of the frame transmitted via SPI between the master and the slave units is

illustrated in Figure 4.22.

Another SPI channels are implemented between each slave micro-controller and the corresponding DDS units. These SPI channels are enhanced by IOSYNC and IO_UPDATE signals. The IOSYNC signal is controlled by the slave unit and serves as an asynchronous active high reset of the DDS serial port controller. The rising edge of the IO_UPDATE signal transfers the contents of the DDS internal buffer memory to the DDS I/O registers. Unlike the IOSYNC, the IO_UPDATE signal is controlled by the master unit, which enables precise synchronous starts and stops of multiple DDS units.

The AD667 DAC is controlled via parallel interface. Internally, the DB0-DB11 bits are divided into three four-bit registers. Value stored in the registers represent the output voltage value of the DAC. The DB input pins share four wires connected to four I/O pins at the slave micro-controller unit. The selection of the specific register is made via the address bits A0-A3.

A simple communication schema of the systems is illustrated in Figure 4.23.

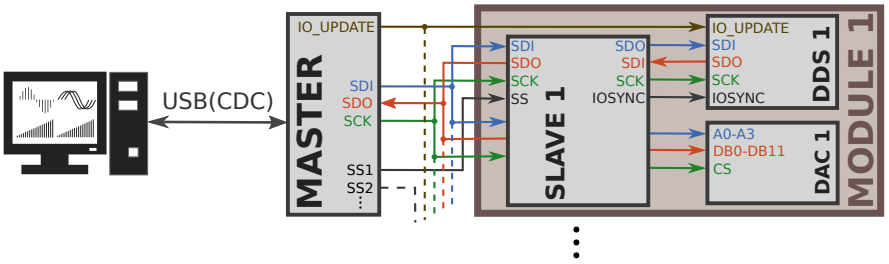

FIGURE 4.23: Illustration of the communication solution of the designed signal generator.

4.4.3.3 Modes of operation

The signal generator is capable of running in static or dynamic mode of operation. In the static mode of operation, single frequency, amplitude, DC and phase offset is configured. In the dynamic mode of operation, definition of complex signal profiles is possible. The complex dynamic signal profile is time-varying, and contains step or sweep transitions in frequency, amplitude, DC and phase offset. Signal profile is defined in GUI and the information is then transferred to the corresponding slave unit and stored in its Flash memory. The slave micro-controller employs the internal timer peripheral to manage the progress of the signal based on the signal profile definition. The dynamic mode of operation is one of the prerequisites to 2DEP Cytometry automation enabling autonomous collection of the live cell DE signatures in the whole frequency spectrum of interest.

4.4.3.4 PCB design

A four-layer Printed Circuit Board (PCB) was designed in Altium Designer. The inner layers serve as ground and power planes. The outer layers are the signal layers used for signal routing. A 40-pin, 2.54mm pitch connector was selected to provide the output to the outer world. The maximum specified current rating of a single pin is approximately 3A, which is sufficient. The interconnection is made of wide flat ribbon cable, arranged for high speed signal transfer in G-S-G configuration. Insulated flat ribbon cables are commonly used in systems with typical speeds up to 1 Ghz. Impedance matching was not performed, but its implementation is taken into account if necessary. The modularity of the system is accomplished by vertical stacking of identical modules, each of the module containing four DDS units. One of the modules must contain the master microcontroller. Selection of the master DDS unit is defined via corresponding jumpers as well as routing of the output signals to the output connector and routing of the SPI slave select signals.

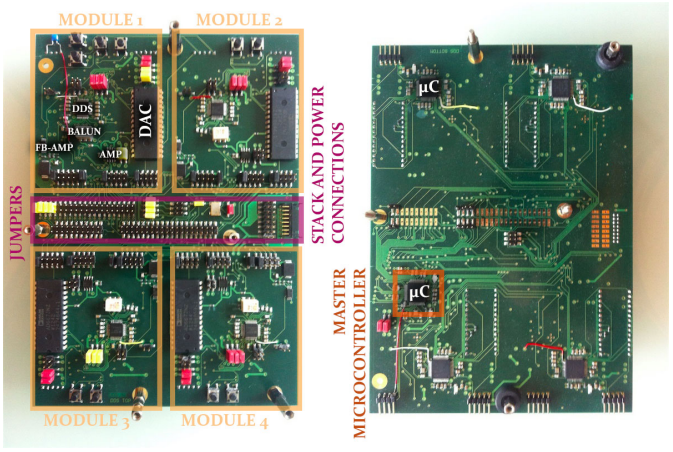

FIGURE 4.24: Photo of the DDS main board containing 4 independent channels and the master controller. Side A (left), side B (right).

4.4.3.5 Firmware development

Firmware for the master and slave micro-controllers was developed in MPLAB IDE and consequently loaded to the units via PICkit 3 In-Circuit debugger/programmer. SPI interface was selected to provide the communication channel between the master and slave micro-controllers. CDC was implemented in the master micro-controller to open a virtual serial port between the PC and the master micro-controller via USB. The CDC implementation preserves the easy connection, performance and reliability of the USB interface and the simplicity of the serial communication. The firmware of the slave units is identical. Each of the slave micro-controller has a unique ID stored in a flash memory. The actual state of the module is stored in the memory to provide the information in case of re-initialization after an unintended reset of the device.

4.4.3.6 Control software and GUI development

A GUI was designed and developed in Microsoft Visual Studio 2012 (C#). The application automatically detects the connected signal generator, opens the communication channel, and scans for the active modules and their actual configuration. The application window is structured into four main parts organised in individual tabs. The *DDS control* tab illustrated in Figure 4.25 contains a list of modules detected.

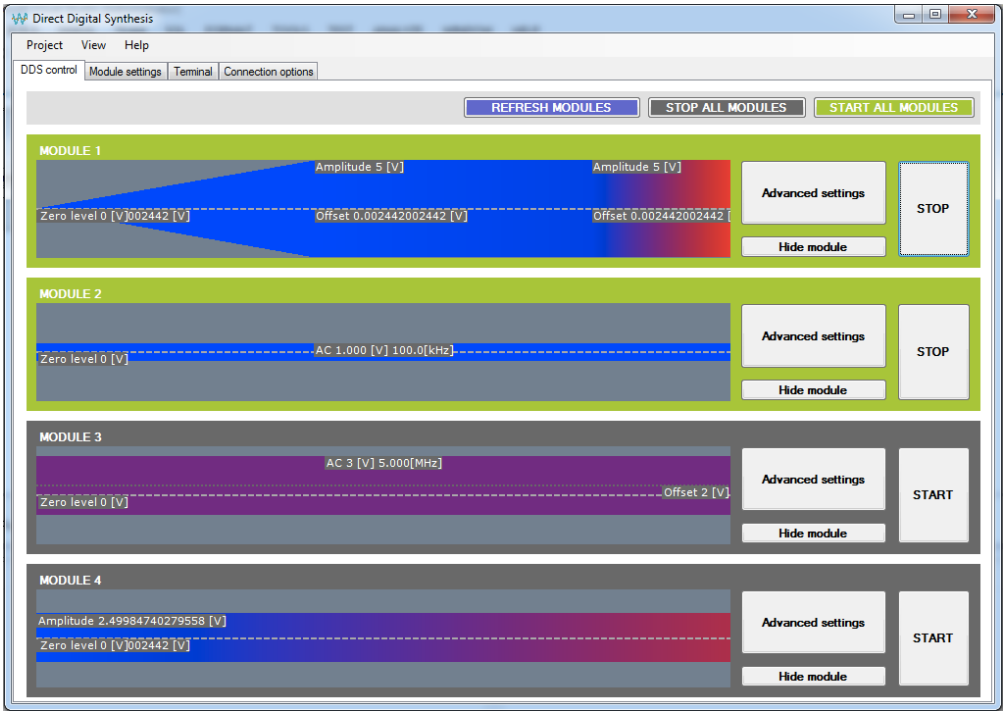

FIGURE 4.25: Printscreen of the GUI controlling the signal generator showing list of the connected modules and the corresponding control elements.

The interface allows the user to start/stop the modules individually, as well as start/stop the modules at once. The *Refresh modules* button scans for the connected modules and their actual configuration. The green frame of a module signifies a running module (the output is enabled). The dark gray frame of a module signified disabled module (the output is disabled). The *Advanced settings* button shows a complete setting of a module and allows the user to modify the module parameters. Each module frame contains an illustration of the configured signal profile. The *Hide module* button hides the module from the interface if the module is redundant or if it is not intended to modify the parameters of the module. It is possible to show the hidden modules via top *View* menu at any moment. The modules may be started or stopped individually. Eventually, all modules can be started or stopped at one moment. Each module can be configured individually under the *Module settings* tab. Static mode or dynamic complex control mode is possible. The options of the static mode configuration are shown in Figure 4.26. In static mode, single frequency, amplitude, DC and phase offset of the signal is set. The

changes will be effected immediately after change of the specific value and confirmation by hitting the *Enter* key.

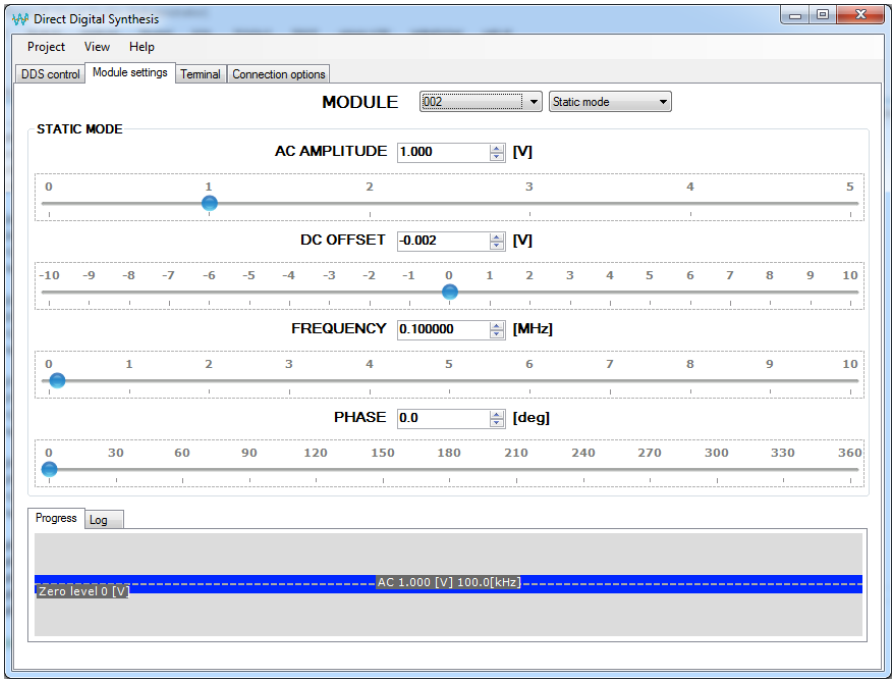

FIGURE 4.26: Printscreen of the GUI controlling the signal generator showing custom settings of individual module in static mode.

Dynamic control configuration is shown in Figure 4.27. In dynamic complex control mode, frequency, amplitude, DC and phase offset steps or sweeps can be configured. First, individual control points must be set at specific time. When the dynamic profile is configured, it can be transferred to the module by hitting the *Upload to module* button. The interface allows the user to save the currently designed dynamic profile, or to load one of the previously designed and saved dynamic profiles. The dynamic profiles can be configured to run repeatedly for a specific number of repetitions, to run in loop infinitely, or to run an infinite time keeping the last specified value at the output.

The *Module settings* tab contains an illustration of the configured signal profile and a communication log of the corresponding module. It is possible to save the custom settings of the environment, the individual modules and their configuration into a project file. The project file can be later loaded allowing fast configuration of complex experiment control. The *Terminal* tab allows user to follow the communication between the computer and the signal generator and the corresponding modules. The application translates the transmitted and received messages to hexadecimal format, and assigns an explanation to the specific messages if possible. The interface allows the user to sent messages to the signal generator in hexadecimal and text format for debugging purposes. The communication interface and the configuration of the communication channel is shown in Figure 4.28.

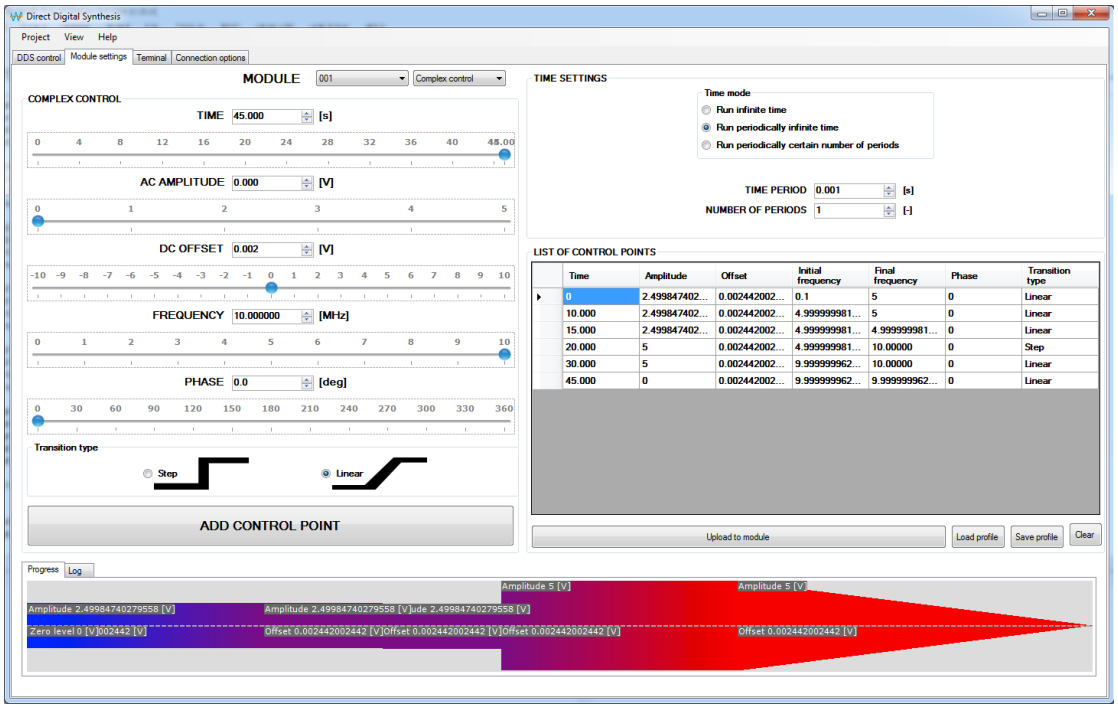

FIGURE 4.27: Printscreen of the GUI controlling the signal generator showing custom settings of individual module in dynamic complex control mode.

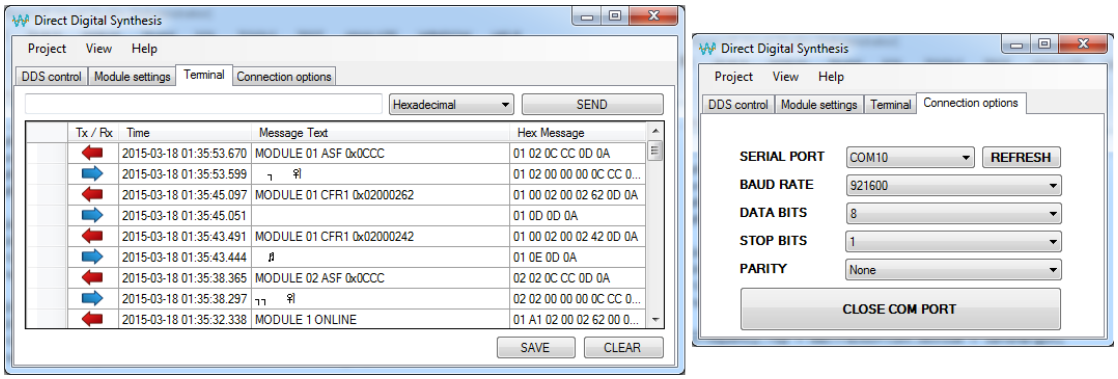

FIGURE 4.28: Printscreen of the GUI showing the interactive communication console (left); and printscreen of the graphical user interface showing settings of the communication channel (right)

4.4.3.7 DDS results and discussion

DDS based signal generator was developed. It is controlled via computer interface. The communication is well established. The individual channels are capable of generation of the output sine waves with the optional DC offset. The sine wave generation works reliably and was tested up to 50 MHz at this moment. Further increase in frequency is planned in future, as well as impedance matching and synchronization of multiple units to provide output signals with precise mutual phase offset. All modules are capable of individual or synchronized starts/stops. Output of the signal generator measured by oscilloscope is shown in Figure 4.29.

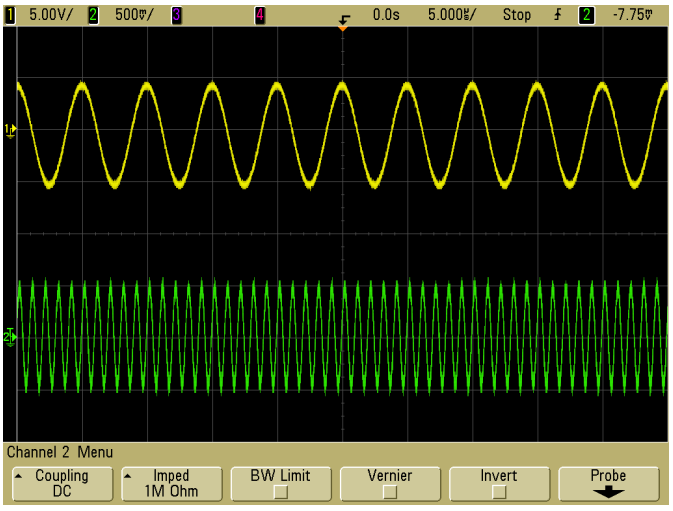

FIGURE 4.29: Output of an oscilloscope showing sine wave outputs of two independent output channels of the developed signal generator.

4.4.4 Interface and experimental platform

Customized interface platform was developed to provide mechanical support, electrical interconnection between the electric field generator and the metal pads at the side of the microfluidic device, and the fluidic interconnections between the syringe pumps and the microfluidic device. The interface platform consists of incubation chamber allowing complete encapsulation of the microfluidic device in controlled environment. Precise control of CO_2 and humidity levels is achieved by connection of the platform to the OKO lab CO2 and humidity controller. The size and shape of the interface platform is compatible with the Olympus IX83 microscopy station used in the 2DEP Cytometry experiments. The image acquisition is provided by CCD QImaging Exi-Blue camera optimised for fluorescence microscopy and high-resolution imaging of live cells.

A connector with spring-loaded contacts was selected to provide electrical interconnections to the microfluidic device. Microfluidic devices may be easily and quickly replaced in the interface platform. It does not require wire bonding and fixing of the devices is reversible. A transparent glass observation window is present at the top and the bottom of the platform. The PCB with connector with spring-loaded contacts contains small breadboard for signal routing, and a wire-to-board connector compatible with the electric signal generator presented in Section 4.4.3. Openings are present in the incubation chamber walls for the fluidic and electrical interconnects.

The incubation chamber may be used with all bacterial and *S. cerevisiae* cultures, or mammalian cell lines. The whole platform is easily disassembled and autoclaved maintaining sterility and avoiding potential cross-experimental contamination.

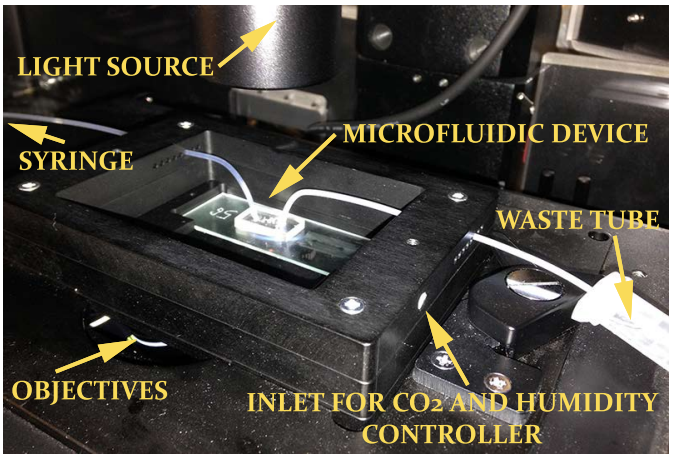

FIGURE 4.30: Photo of the developed interface platform

4.5 Experimental results

Preliminary experimental data quantifies the DE signature of a *S. cerevisiae* population and K562 cell line. For each of these cell types, a model-based approach was used to separately tune the experimental conditions, in terms of medium electrical conductivity, frequency range, flow-rate, and voltage amplitude.

4.5.1 DE signature of *S. cerevisiae* cell population

In this section, DE signature of a *S. cerevisiae* population quantified by the 2DEP Cytometry is presented and discussed in detail. It is showed that DEP-induced cell translation along the parabolic velocity profile can be measured by PIV with high enough precision, enabling identification of individual cell DE signatures. It was possible to analyse more than 5 thousand cells within 1 minute with the actual experimental setup. Such high-throughput enabled measurement of DE signatures at 20 different frequencies in almost real-time.

4.5.1.1 Cell preparations

S. cerevisiae 6194 MATx cells were obtained from Duncan laboratory. Culture was inoculated into YPD medium from deep frozen aliquots and incubated under air atmosphere at 30 $°C$. The culture was transferred on agar plate the following day, and left at 30 $°C$ for another two days. Liquid culture was then inoculated from a single colony in the plated culture and left to grow over night. It was refreshed in the morning and left to grow up to OD 0.35. Cells were centrifuged and perfused twice in an isotonic Low Conductivity (LC) medium. Medium conductivity was adjusted to 50 mS/m to increase

accuracy of the measured DE signatures. The LC medium was prepared in advance by mixing deionized water with sucrose (8.5% w/v) and dextrose (0.3% w/v). Conductivity of the medium was increased to 50 mS/m by adding small amount of PBS.

4.5.1.2 DEP measurements

DE signature of *S. cerevisiae* cell population was measured using the 2DEP Cytometry. Cells were introduced to microfluidic device in an isotonic LC medium at concentrations 15,000 cells/μL suitable for PIV measurements, assuring high enough throughput, while avoiding cell-cell interactions. Cell-cell interactions, otherwise known as dipole-dipole interactions, may result in clustering of cells with different DE signatures and eventually cell trapping at the electrode array that would not occur otherwise [73]. However, the fundamental requirements of the PIV analysis define the spacing between the cells to be larger than the cell displacement of cells between two consecutive images, which satisfies the requirement of at least 3 cell diameter spacing for avoiding the cell-cell interaction [44]. Cells then travelled through 500 μm wide and 40 μm high microchannel above ID electrodes at 5 nl/s flow-rate. At the end of the microchannel, cells levitate at heights according to the electric field distribution, frequency of the electric field, their DE signatures and the DE properties of the medium. The levitation heights were measured indirectly by PIV. Sinusoidal 2 V_{p-p} signal was applied to electrodes. DE signatures were mapped in frequency ranging between 100 kHz and 1,771 kHz. The voltage was generated using custom-built sinusoidal signal generator described in Section 4.4.3. Each frequency was applied for 60 seconds, while two images separated by 60 milliseconds were taken every one second for the PIV analysis. Processing of the collected images, including image recognition, PIV, and data processing, was performed offline in custom-designed software.

4.5.1.3 Results and discussion

The measured data are illustrated in terms of enrichment of microchannel sections due to DEP, similar to results of numerical modelling of 2DEP Cytometry described in Section 4.3.1. Therein, the channel section in which the cell enrichment is quantified is illustrated in Figure 4.4. Figure 4.31 presents an ensemble of results for *S. cerevisiae* cells in log phase. The various graphs correspond to different frequencies as indicated by the blue to yellow color map. On the x-axes we plot the height above the electrodes, which goes from zero to half the height of the microchannel. On the y-axes we plot the enrichment due to DEP in the sector below the corresponding height.

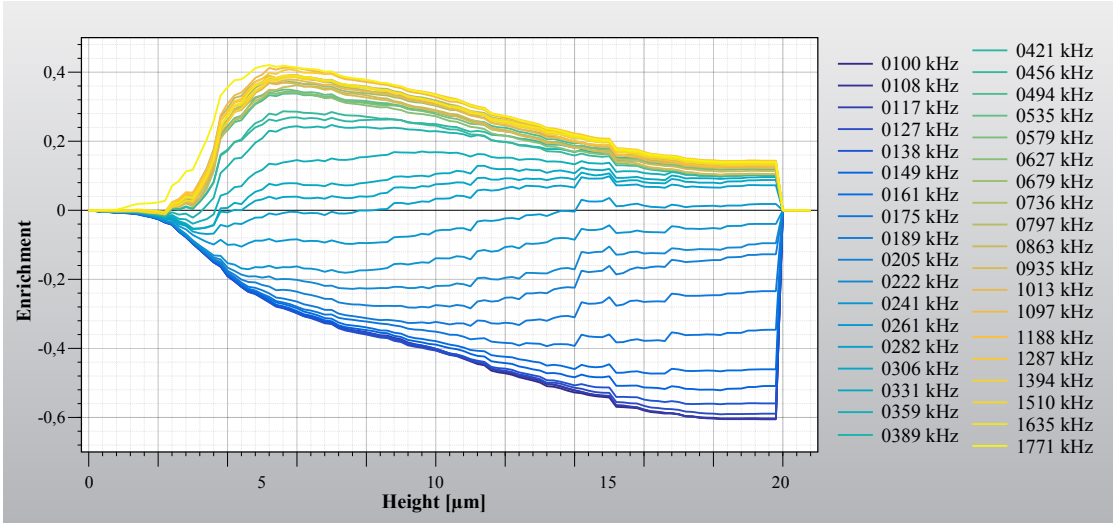

FIGURE 4.31: Measured DE signature of *S. cerevisiae* cell population.

At the low frequencies (those are the blue lines, going from 100 kHz), purely N-DEP was observed, which is illustrated by negative enrichment at all the sectors below the center line. At the high frequencies (the yellow lines, rising up to 1.7 MHz), purely P-DEP was observed, which is marked by the positive enrichment at all the sectors below the center line. The characteristic shape of the graphs is typical for all experiments. For N-DEP, the graph is monotone decreasing until it reaches its minimum, and then sharply returns to zero. For P-DEP, it is the mirrored image.

More subtle graphs near the zero line correspond to close to zero enrichment and provide the information regarding behavior near the crossover frequencies. Instead of giving a single value for the crossover frequency, a frequency range for the entire population is obtained. This is especially important in applications where high enrichment is required. A closer look at a graph corresponding to frequency within this range provides information about heterogeneity of the population. The number of extrema roughly indicates the number of subpopulations with unique DE properties. Detailed look at Figure 4.31 reveals two subpopulations, where the first of them experiences N-DEP, while the second one experiences P-DEP.

The left part of Figure 4.32 illustrates probability of cells being present in a lower 10 μm sector of the micro-channel relative to the case when no electric field applied. In addition, variety of additional operations can be done on the experimental data, including simple statistics, such as illustrating the mean cell velocity shown in the right part of Figure 4.32. There is frequency of the electric field on the horizontal axis, and mean cell velocity relative to the reference cell velocity measured when no electric field is applied on the vertical axis. At low frequencies, cells are pushed strongly by N-DEP to higher levitation heights, and thus the cells travel faster through the micro-channel. With

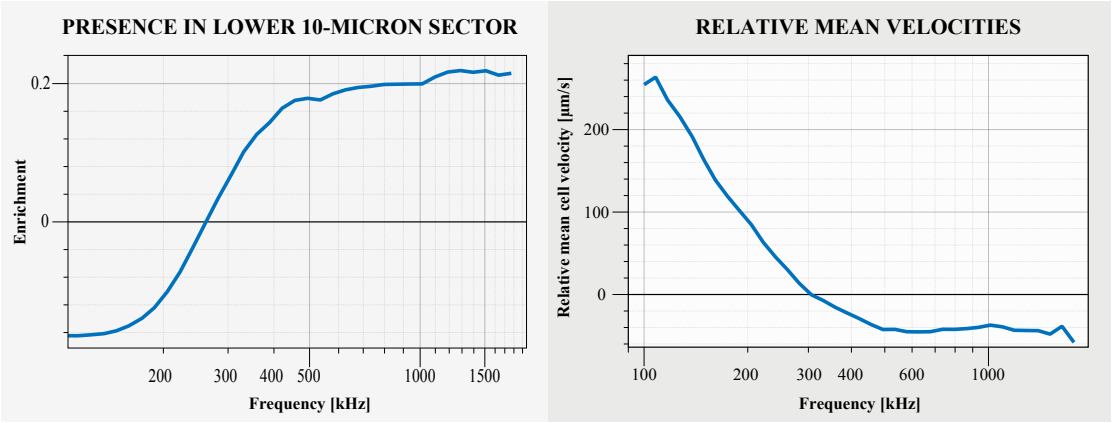

FIGURE 4.32: Enrichment of the lower 10 μm sector of the micro-channel and its dependence on the frequency of the electric field relative to the case when no electric field is applied (left); and mean *S. cerevisiae* cell velocities relative to reference measured cell velocity values with no electric field applied.

increasing frequency, the force magnitude decreases as well as the mean cell velocity, until it reaches the point, where it changes to P-DEP. The frequency at which the relative mean cell velocity crosses the zero line roughly corresponds to the 1^{st} crossover frequency in the cells DEP response.

Unlike the simulation results discussed in 4.3.1, the experimental results show that significant P-DEP frequency range above the 1^{st} crossover frequency in the *S. cerevisiae* DEP response can be explored with 2DEP Cytometry resulting in even more informative results and more precise quantification of the crossover frequency range.

4.5.2 DE signature of K562 cell line

2DEP Cytometry is not limited to *S. cerevisiae* cells. Instead, it can be used with numerous types of cells. To prove that it is suitable for mammalian cell lines, it was tested on measurement of DE signatures of the K562 cell line. Because mammalian cells are encapsulated by plasma membrane only, in comparison to *S. cerevisiae* cells that posses of additional cell wall layer, the DE signature differs significantly and medium of different electrical conductivity is required. The specific value of medium electrical conductivity (200 mS/m) was estimated by model-based approach and was discussed in detail in Section 2.5.3.2.

4.5.2.1 Cell preparations

The K562 cell line was provided by Faculty hospital in Pilsen, department of hematology and oncology. The cells were cultured in RPMI 1640, glutamax supplemented with

10% FCS and 1% antibiotic-antimycotic (100 units/ml of Streptomycin, 100 units/ml of Penicillin, 0,25 ug/ml Amphotericin B) in vented plastic flask under 5% CO2-95% air in a humidified incubator at 37 $°C$. Cell proliferation was checked on regular basis and adjusted to maintain the cell concentration between 0.1 and 1 million cells/ml. Before experiment, cells were centrifuged and perfused twice in LC medium of conductivity 200 mS/m to increase accuracy of the measured DE signature of the cell line. The LC medium was prepared in advance by mixing deionized water with sucrose (8.5% w/v) and dextrose (0.3% w/v). Conductivity of the medium was increased to 200 mS/m by adding small amount of Phosphate Buffered Saline (PBS).

4.5.2.2 DEP measurements

DE signature of K562 cell line was measured using 2DEP Cytometry. Cells were introduced to microfluidic device in an isotonic LC medium at concentrations 15,000 cells/μL suitable for PIV measurements, assuring high enough throughput, and avoiding cell-cell interactions. Cells were let pass through 500 μm wide and 40 μm high microchannel above ID electrodes at 5 nl/s flowrate. At the end of the microchannel, cells levitate at heights according to the electric field distribution, frequency of the electric field, their DE signatures and the DE properties of the medium. The levitation heights were measured indirectly by PIV. Sinusoidal 2 V_{p-p} signal was applied to electrodes. DE signatures were mapped in frequency ranging between 100 kHz and 700 kHz. The voltage was generated using the custom-built sinusoidal signal generator described in 4.4.3. Each frequency was applied for 60 seconds, while two images separated by 60 milliseconds were take every one second for the PIV analysis. Processing of the collected images, including image recognition, PIV, and data processing, was performed offline in custom-designed software.

4.5.2.3 Results and discussion

Figure 4.33 presents an ensemble of results for K562 cell line. Similar to the DE signature of *S. cerevisiae* cells, the various graphs correspond to different frequencies as indicated by the blue to yellow color map.

Unlike the simulation results discussed in 4.3.1, the experimental results show that significant P-DEP frequency range above the 1^{st} crossover frequency in the K562 DEP response can be explored with 2DEP Cytometry resulting in even more informative results and more precise quantification of the crossover frequency range as in the case of *S. cerevisiae* 2DEP Cytometry.

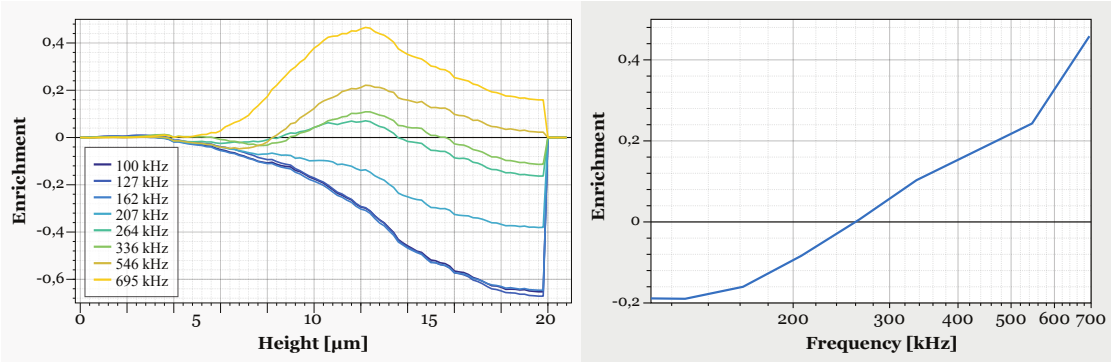

FIGURE 4.33: Measured DE signature of K562 cell line (left); and probability of cells being present in a lower 12 μm sector of the micro-channel and its dependence on the frequency of the electric field relative to reference measurement with no electric field applied (right).

4.5.3 *S. cerevisiae* membrane proteins

A 6194x *S. cerevisiae* strain was genetically modified to over-express certain membrane protein. The measured cell population DE signature was compared to the DE signature of cells expressing a cytoplasmic protein at the same expression rate.

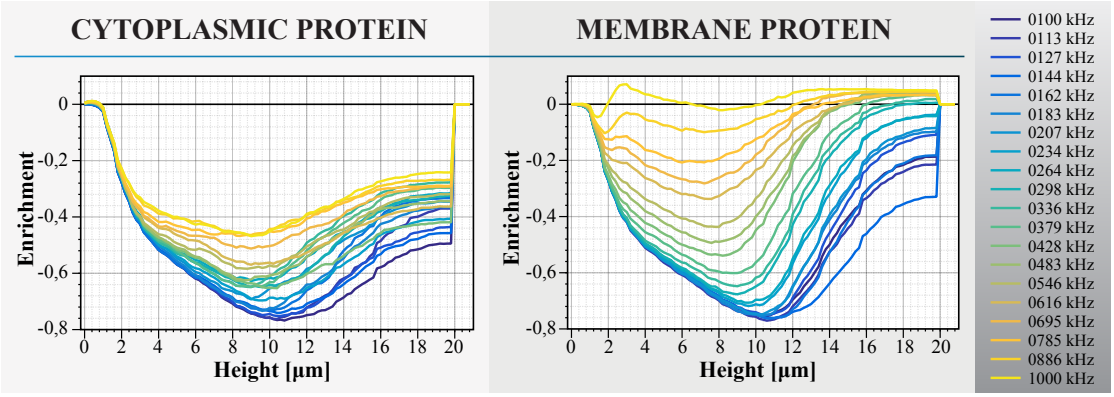

FIGURE 4.34: Measured DE signatures of genetically modified *S. cerevisiae* cell population over-expressing specific cytoplasmic protein (left); and DE signatures of genetically modified *S. cerevisiae* cell population expressing membrane protein at the same rate (right).

At the lower frequencies the responses look similar. But at higher frequencies the membrane protein expressing cells exhibit P-DEP, suggesting membrane protein expression significantly decreases the 1^{st} crossover frequency in *S. cerevisiae* DEP response in comparison to the cytoplasmic protein. Such behavior is consistent with the multi-shell model discussed in Section 2.5.3.1, which predicts a negative shift of the 1^{st} crossover frequency with increasing plasma membrane electrical conductivity (considering over-expression of the membrane protein increases plasma membrane electrical conductivity).

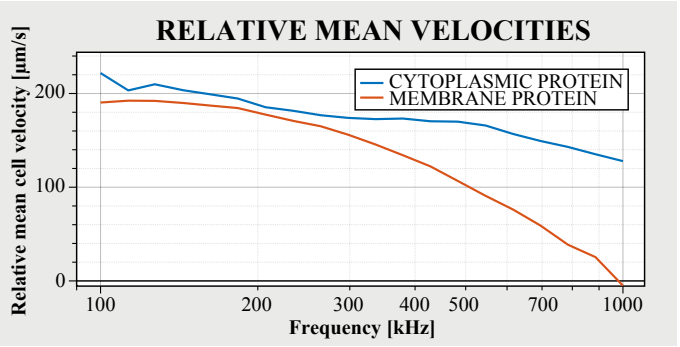

FIGURE 4.35: Measured mean cell velocities (related to reference measurement with no electric field applied) of genetically modified *S. cerevisiae* cell population over-expressing specific membrane protein and *S. cerevisiae* cell population expressing cytoplasmic protein at the same rate.

Figure 4.35 illustrates the relative mean cell velocities (related to reference measurement with no electric field applied) of genetically modified *S. cerevisiae* cell population over-expressing specific membrane protein and *S. cerevisiae* cell population expressing cytoplasmic protein at the same rate.

4.5.4 Stressed K562 cell line

In the next set of experiments, similar comparisons for the K562 cell line under various types of stress induced by medium pH variation and heat shock were performed.

4.5.4.1 Medium pH stress

First, the effect of pH was analyzed. Most mammalian cells grow in medium with pH 7.4. However as long as the cells are cultivated, the medium pH changes with dissolved CO_2 and Bicarbonate (HCO_3-). The medium pH balance throughout longer periods of cultivation is achieved by controlling the atmospheric CO_2 levels (usually between 4% and 10%).

Herein, DE signature of fresh K562 cell line cultivated under 5% CO_2 was measured. Subsequently, DE signature of K562 cell line left for 60 minutes in atmosphere lacking CO_2 level control, and the measured data were analysed. The data are shown in Figure 4.36. There is a clear difference between the measured DE signatures. Although the data are more-less similar in the lower frequency range (illustrated by the blue lines, going from 100 kHz), with increasing frequency more significant differences are obvious. To illustrate the disparity, the enrichment in a single micro-channel sector (lower 10-microns) for various frequencies was quantified and shown in Figure 4.37.

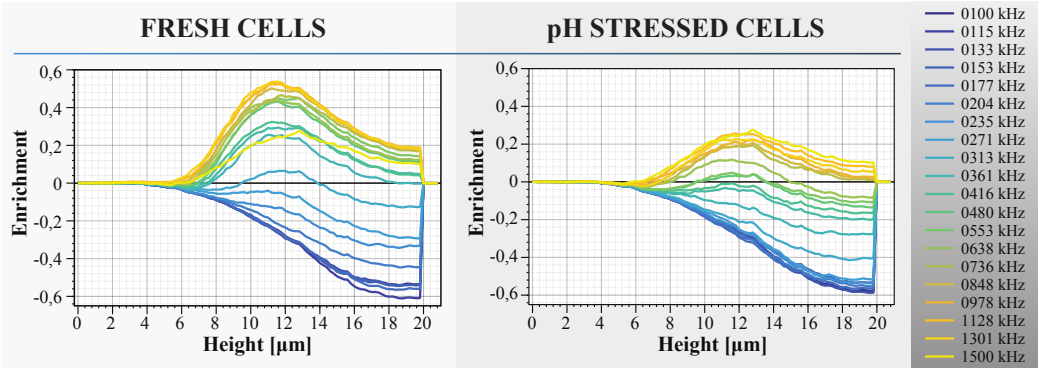

FIGURE 4.36: Measured DE signatures of K562 cell line before (left) and after CO_2 deprivation (right).

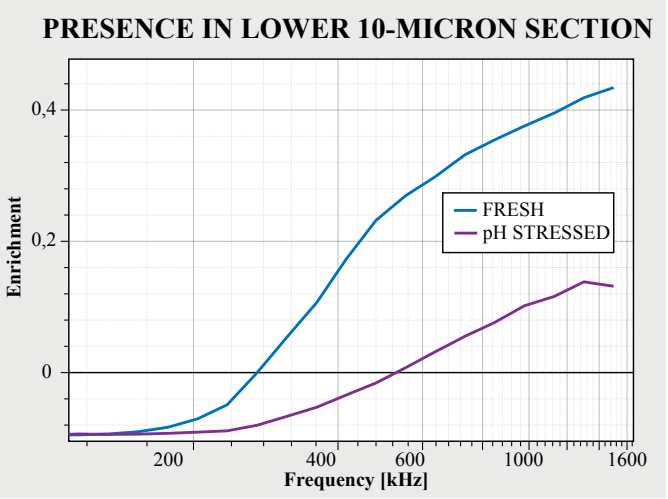

FIGURE 4.37: The enrichment of the lower 10 μm vertical channel section due to DEP.

Focusing on the bottom 25% of the channel, N-DEP resulting negative enrichment at the low frequencies for the both the fresh and the stressed cells was observed. However the crossover frequency of the stressed cells was significantly shifted towards the higher frequency range. Such effect may correspond to decreased electrical conductivity of cytoplasm.

4.5.4.2 Heat shock

The effect of heat shock is known to induce necrosis and apoptosis in cells depending on the temperature and cell phenotype. Here preliminary probabilistic measurements of DEP forces were taken before, after, and 30 minutes after the heat shock. A 60 $°C$ heat shock was applied for 10 minutes. The presented data are less smooth in comparison to the previous experimental results, which may correspond to the fact that cells were sampled later in their cultivation period, meaning that some pH stresses already occurred.

Flow cytometry data with standard viability staining that were collected in parallel show significant increase in dead cells right after the heat shock confirming physiological changes in cell states did occur. The flow cytometry and the 2DEP Cytometry data are shown in Figure 4.38.

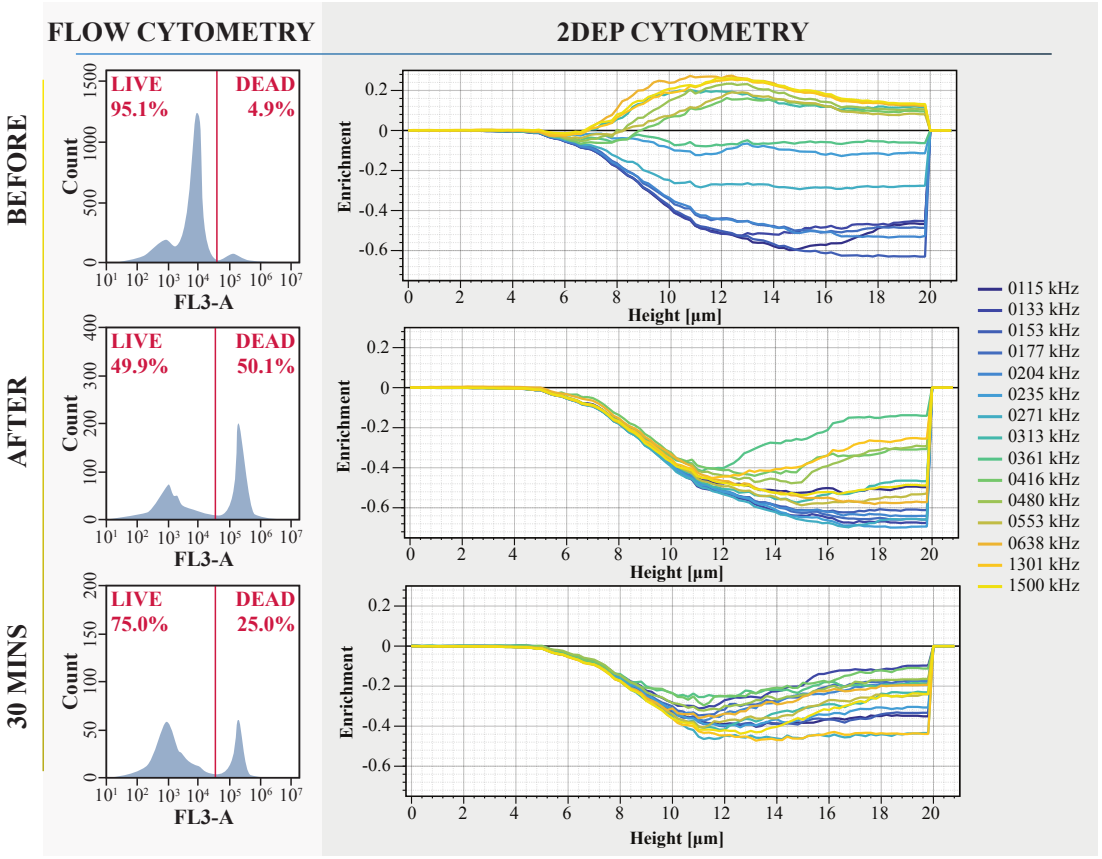

FIGURE 4.38: Flow cytometry data with standard viability staining showing number of live and dead cells in fresh cells sample and heat treated (left); and measured DE signatures of fresh and heat treated K562 cell line (right).

The obvious immediate effect is most probably caused by plasma membrane disruption and subsequent ion leakage causing significant drop in cytoplasmic conductivity. The fact that the cells are driven by N-DEP in even higher frequencies is consistent with K562 cell model described in Section 2.5.3.2, which predicts shift of the 1^{st} crossover frequency to higher frequencies, or eventually N-DEP behavior throughout the whole frequency spectrum lacking any crossover frequency at all due to the decreased electrical conductivity of cytoplasm.

To illustrate the differences between the measured DE signatures, Figure 4.39 presents the relative probability of cells being present in a lower 10 μm sector of the micro-channel, in respect to probability of cells being present in the specific channel section when no electric field is applied.

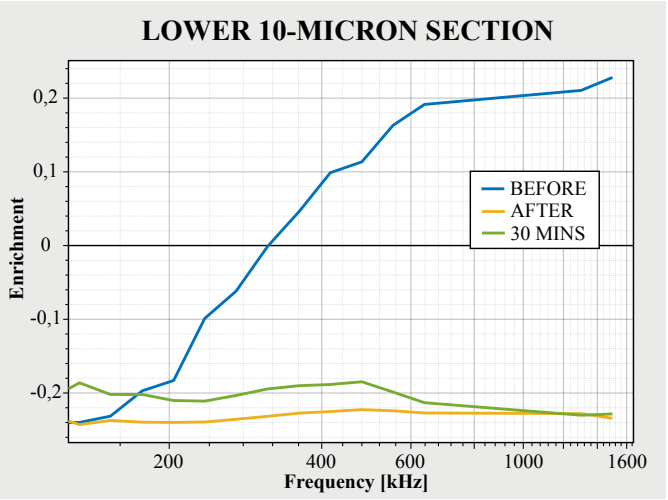

FIGURE 4.39: Probability of cells being present in a lower 10 μm sector of the microchannel and its dependence on the frequency of the electric field in respect to reference measurement with no electric field applied.

4.5.4.3 Apoptosis progression

Cell apoptosis is a programmed cell death. Here preliminary data are presented showing DEP can reveal the effect of chemotherapy on cancer cells by mapping progression of drug-induced apoptosis. The progression of apoptosis was mapped by mapping of the DE signatures of the K562 cell line treated with different concentrations of Imatinib (INN), a tyrosine-kinase inhibitor used in the treatment of multiple cancers. The 2DEP Cytometry data are presented in Figure 4.40. Three different samples, shown in individual rows were analyzed after 24 hours and 48 hours from INN application. First row show DE signature of cells to which no INN was applied. The top left figure can be seen as the DE signature of healthy cell population. The 2^{nd} row, 1^{st} column, presents DE signature of cells treated by 0.1 μM INN measured after 24 hours from INN application. The DE signature is still very similar to healthy cell population. In the 2^{nd} row, 2^{nd} column, more significant changes are already obvious. The higher dose of INN in the 3^{rd} row shows significant changes already after 24 hours from INN application. But mostly after 48 hours, the DE signature of the cell population gets reverted completely upside down illustrating the effect of the treatment.

Flow cytometry viability staining was taken in parallel to 2DEP Cytometry. The flow cytometry data are presented in Figure 4.41. The solid lines correspond to live cells, and the dashed lines correspond to the number of dead cells. In all measurements except the highest doses of INN after 48 hours from INN application, flow cytometry showed very little effect of the treatment, if any, suggesting DEP might be more sensitive to these changes.

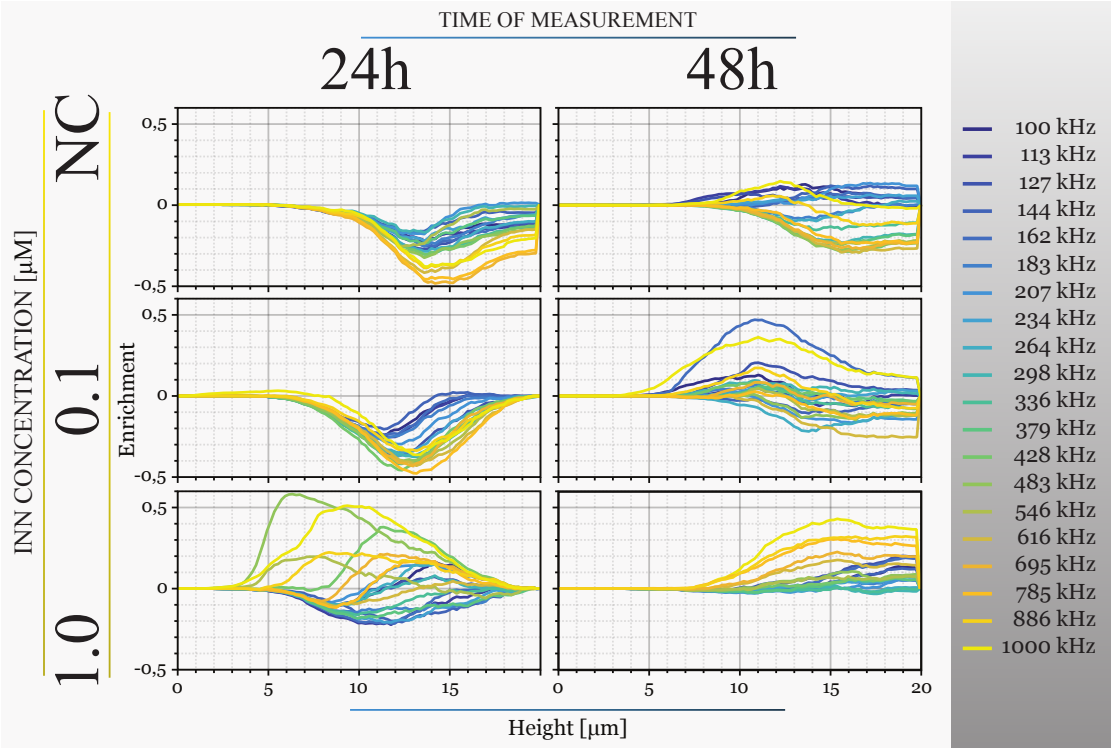

FIGURE 4.40: Measured DE signatures of K562 cell line 24 hours from drug application (left) and 48 hours after drug application (right).

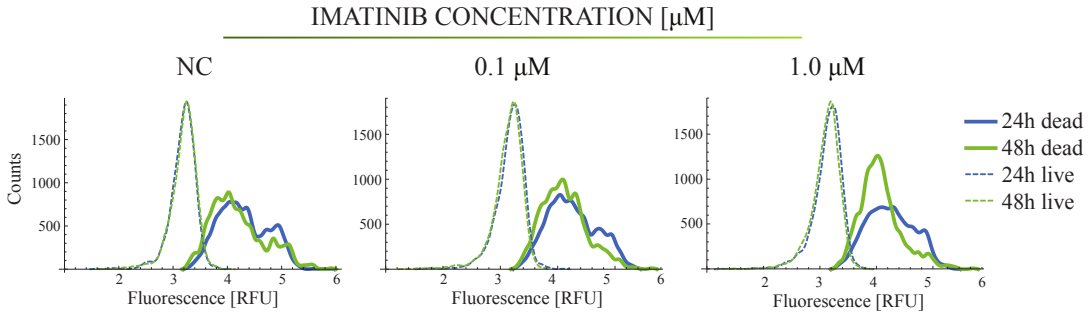

FIGURE 4.41: Flow cytometry data with standard viability staining showing number of live and dead cells after 24 hours from INN application (left); and 48 hours from INN application (right).

4.6 Conclusion

A 2DEP Cytometry was presented as a novel method enabling probabilistic measurements of live cell DE signatures on population level and showed ability to perform comparative study in order to map dynamic changes in certain cell states. Principles of 2DEP Cytometry were discussed, as well as the underlying models and simulations showing 2DEP Cytometry performance and sensitivity. Design of a 2DEP Cytometry microfluidic lab-on-chip device was described, and the parameters obtained via model-based approach were presented. The microfluidic device was fabricated using soft lithography in

combination with air plasma treatment in order to seal the device. The air plasma treatment results in reliable bond, but the devices may be disassembled, cleaned, and resealed with new PDMS replica several times prolonging the lifespan of the 2DEP Cytometry device, which may be beneficial especially in the initial prototyping phase. A custom signal generator based on DDS was developed to provide precise frequency stable sine-wave output to drive the micro-electrode array integrated in the 2DEP Cytometry microfluidic device. The generator is configured via GUI and allows the user to define complex frequency sweeps that may be used for automated 2DEP Cytometry measurements of the live cell DE signature in the whole frequency range of interest without additional user interaction. Finally, 2DEP Cytometry measurement of DE signature distributions in cell populations was demonstrated on *S. cerevisiae* cells and K562 cell line. Unlike the simulation results discussed in Section 4.3.1, it was possible to partially explore the P-DEP frequency range resulting in much more informative data. The presented method does not require any cell labelling, and is non-invasive. In addition, the PIV is based on imaging and the measured DE signatures can be further correlated with other fluorescence and optical data providing deeper insight into each measured single cell properties and cellular processes that govern the cell behavior. Hence, 2DEP Cytometry may be used to identify reliable biomarkers for cell changes, and might be a viable alternative to conventional flow cytometry.

Chapter 5

Statistical analysis of 2DEP Cytometry

5.1 Introduction

The importance of statistical analysis in biology research is indisputable. Weak data analysis may lead to low value or completely invaluable results. Here, statistical analysis on experimental data obtained by Distributed Dielectrophoretic Cytometry (2DEP Cytometry) described in Chapter 4 was performed. Kernel Density Estimation (KDE) was used to overcome to finite nature of the measured data. Special attention was then paid to data analysis in the comparative studies.

The comparative cell studies are often used in cell biology, as they can help the biologists to ascend from the initial exploratory level to a more advanced cell behavior models. The natural variation and disparity between the analyzed cells or cell populations is used to understand the patterns of life on the cellular or even sub-cellular level. Comparative cell studies based on Electrorotation (ER), Dielectric Spectroscopy (DS) and Dielectrophoresis (DEP) already showed that mapping of the frequency dependent Dielectric (DE) properties of the cells can be used in order to measure the progression of cell death [25, 26, 71, 75, 88]. Other comparative study used Dielectrophoresis Field Flow Fractionation (DEP-FFF) to fractionate human leukocyte mixture into individual subpopulations of T- and B-lymphocytes, monocytes, and granulocytes [109]. DEP-based measurements were used to study the dynamic response of budding yeast cells to different concentrations of Lyticase, which stimulates the cells to remove the cell wall and converts them into spheroplasts [95]. Differences in plasma membrane and cytoplasm biophysical properties of apoptotic cells were also revealed using simple static DEP [63]. And numerous other studies show DEP has a great potential in studying dynamic cellular processes

of various kinds [36,43,79,83,84,87]. Although DEP is able to measure certain changes in cell physiology, there is no metric that would enable simple and reliable identification of DE biomarkers for cell changes. Instead the measured Dielectrophoretic (DEP) spectra are compared individually, and the results are interpreted using models that need to be custom tailored for given applications.

Herein, the disparity between DE signatures of cells in different cell states was illustrated by Wasserstein pseudometrics. The KDE and Wasserstein pseudometrics were custom adjusted to include the normalization by velocity step, which is essential for correct interpretation of 2DEP Cytometry data (see Section 4.2 for details). The comparative study with Wasserstein pseudometrics identifies frequencies, where less and more significant differences between the measured DE signatures are observed. Such metric may be used for identification of reliable biomarkers for cell changes.

5.2 Kernel Density Estimation (KDE)

Raw data collected 2DEP Cytometry consist of finite set of cell velocities. The measured distributions are smoothed by KDE to overcome the finite nature of the data. In result, continuous distribution is obtained, as opposed to the set of original discrete scattered values. Commonly used kernel functions include gaussian, triangular, uniform, biweight and others. Herein, gaussian kernel function is used as it is often used in computational biology to identify multiple subpopulations in given dataset. In other words, each of the discrete data points is replaced by gaussian. The effect of KDE on the data is shown in Figure 5.1. The KDE was adjusted so that it includes the normalization by velocity step

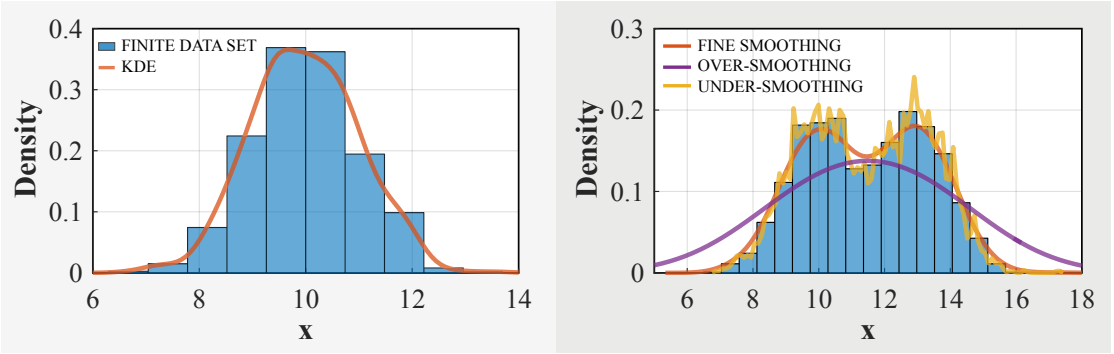

FIGURE 5.1: Left: Effect of KDE on the data. Right: Effect of the bandwidth parameter on the resulting estimate.

to encounter the over-representation of slowly moving cells, which is required for correct interpretation of the 2DEP Cytometry data (see Section 4.2 for details). The custom kernel density estimator is:

$$\hat{f}_h(x) = \frac{\sum_{i=1}^{n} K(x - x_i, v_i)}{\int_{x_{min}}^{x_{max}} \sum_{i=1}^{n} K(x - x_i, v_i)}. \tag{5.1}$$

In this equation x is the variable of interest (e.g. velocity or levitation height), n stands for the number of data samples, K stands for the kernel function, x_i is the position of the corresponding data point, and v_i stands for the measured velocity of the i^{th} data sample. Using the gaussian function as the kernel function, the kernel function including the normalization by velocity step is of the following shape:

$$K(i, x) = v_i.exp(-\frac{(x - x_i)^2}{2\sigma^2}), \tag{5.2}$$

in which σ is the standard deviation, which in KDE has function of smoothing parameter otherwise known as the bandwidth. The resulting estimate is strongly dependent on σ, because large σ values lead to over-smoothing, while low σ values lead to under-smoothing. Both situations are illustrated in the right part of Figure 5.1.

Identification of a suitable σ value is a critical part in the KDE. To identify the correct value, a unifying frequency of the electric field is selected (in this case the 100 kHz). This is a frequency at which all cells in the sample (with all its subpopulations) respond to the electric field in the same manner. At 100 kHz, nearly all cells exert close to the highest DEP force, which focuses the cells towards the vertical center of the microchannel. At this frequency, a minimum KDE σ resulting in distribution with only one subpopulation is identified. That value of σ is then adopted for all distributions at all frequencies. With increasing frequency, individual subpopulations may be discovered and should not get lost by KDE over-smoothing.

The DE signatures measured by 2DEP Cytometry presented in Section 4.5 were analysed and adjusted by the presented custom KDE to overcome the finite length of the data. The resultant continuous distributions of the live cell DE signatures in the frequency spectrum are shown in Figure 5.2 showing DE signature of *S. cerevisiae* cell population; Figure 5.3 showing DE signature of K562 cell line; Figure 5.4 showing DE signatures of the genetically modified *S. cerevisiae* cell populations; Figure 5.6 showing DE signatures of the fresh and heat treated K562 cell lines; Figure 5.5 showing DE signatures of the fresh and pH stressed K562 cell lines; and Figure 5.7 showing DE signatures of cells treated with different concentrations of INN after 24 and 48 hours from drug application K562 cell lines.

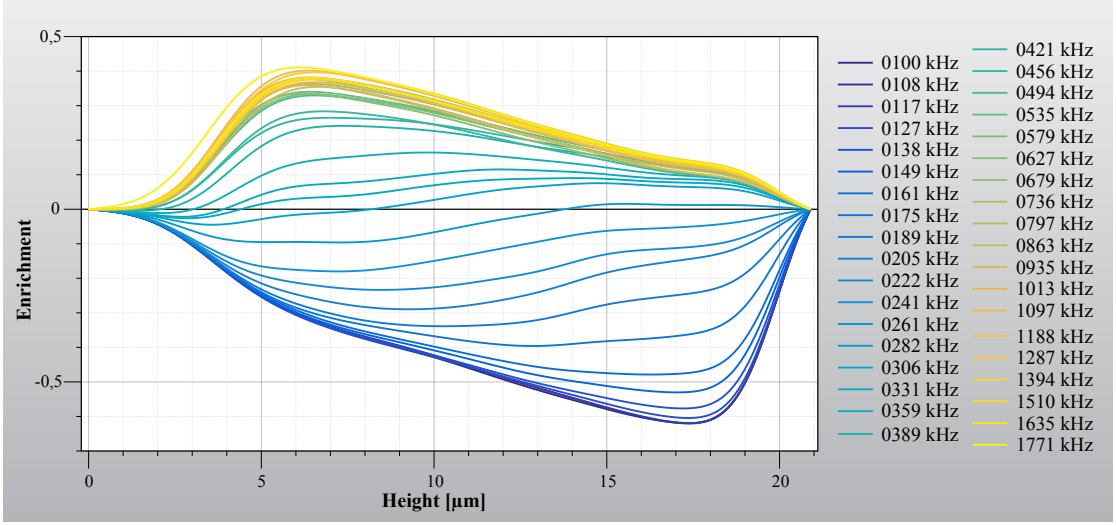

FIGURE 5.2: KDE of the measured DE signature of *S. cerevisiae* cell population. See Figure 4.31 for the raw data.

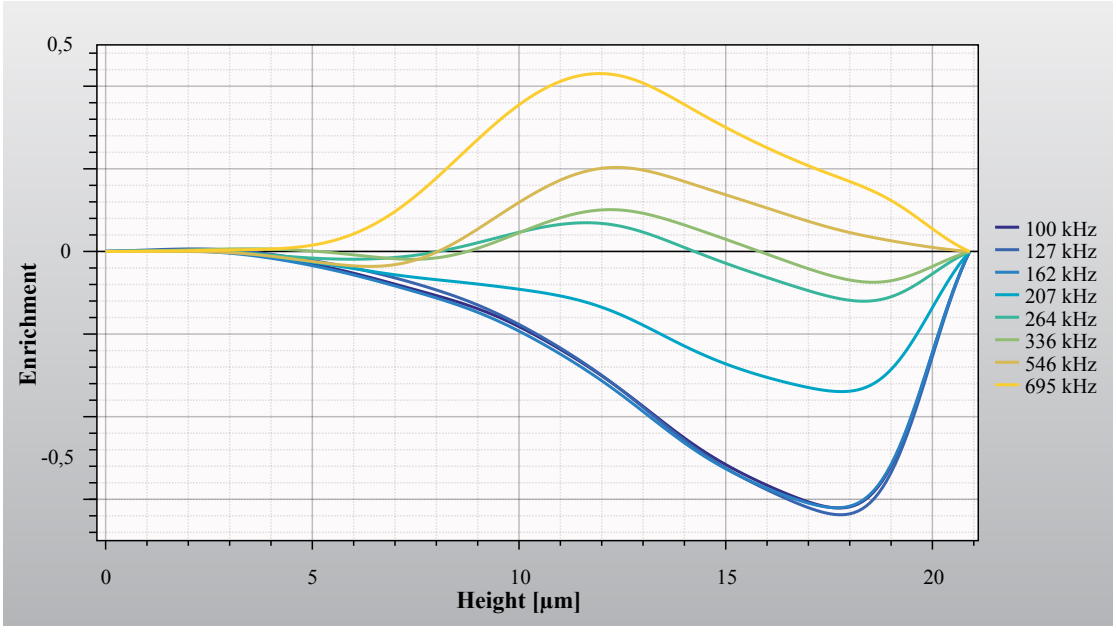

FIGURE 5.3: KDE of the measured DE signature of K562 cell line. See Figure 4.33 for the raw data.

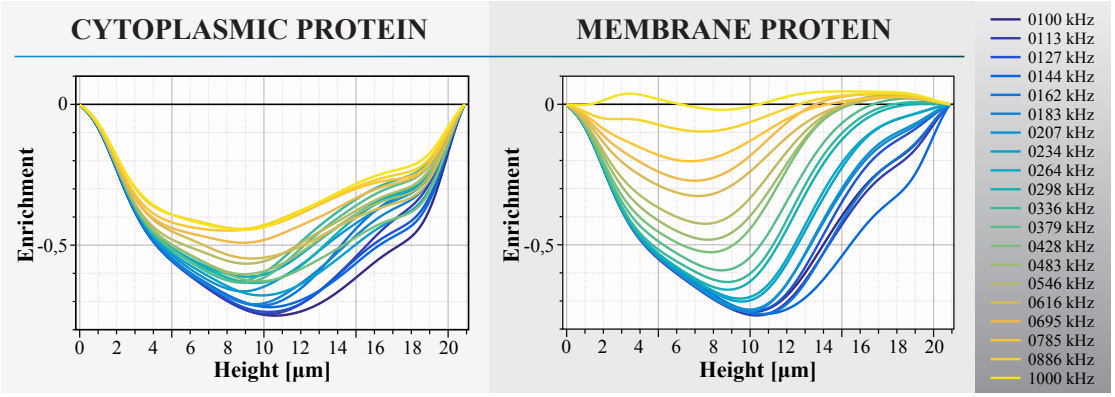

FIGURE 5.4: KDE of the measured DE signatures of genetically modified *S. cerevisiae* cell population over-expressing specific cytoplasmic protein (left) and *S. cerevisiae* cell population expressing membrane protein at the same rate (right). See Figure 4.34 for the raw data.

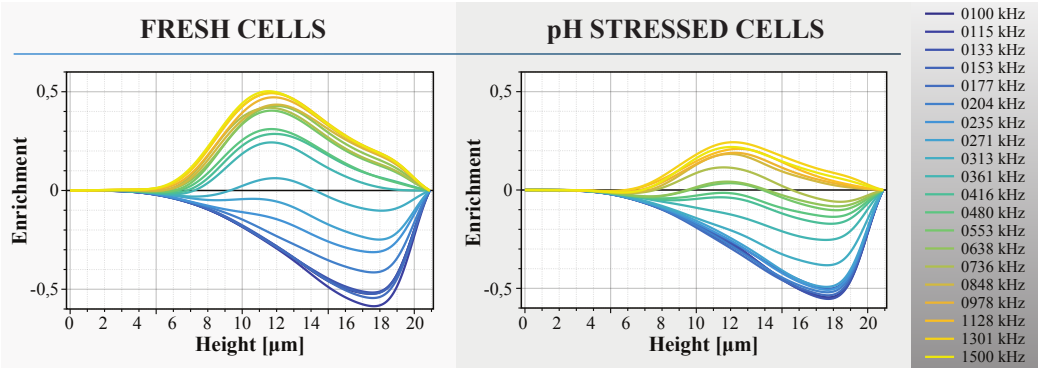

FIGURE 5.5: KDE of the measured DE signatures of K562 cell line before (left) and after CO_2 deprivation (right). See Figure 4.36 for the raw data.

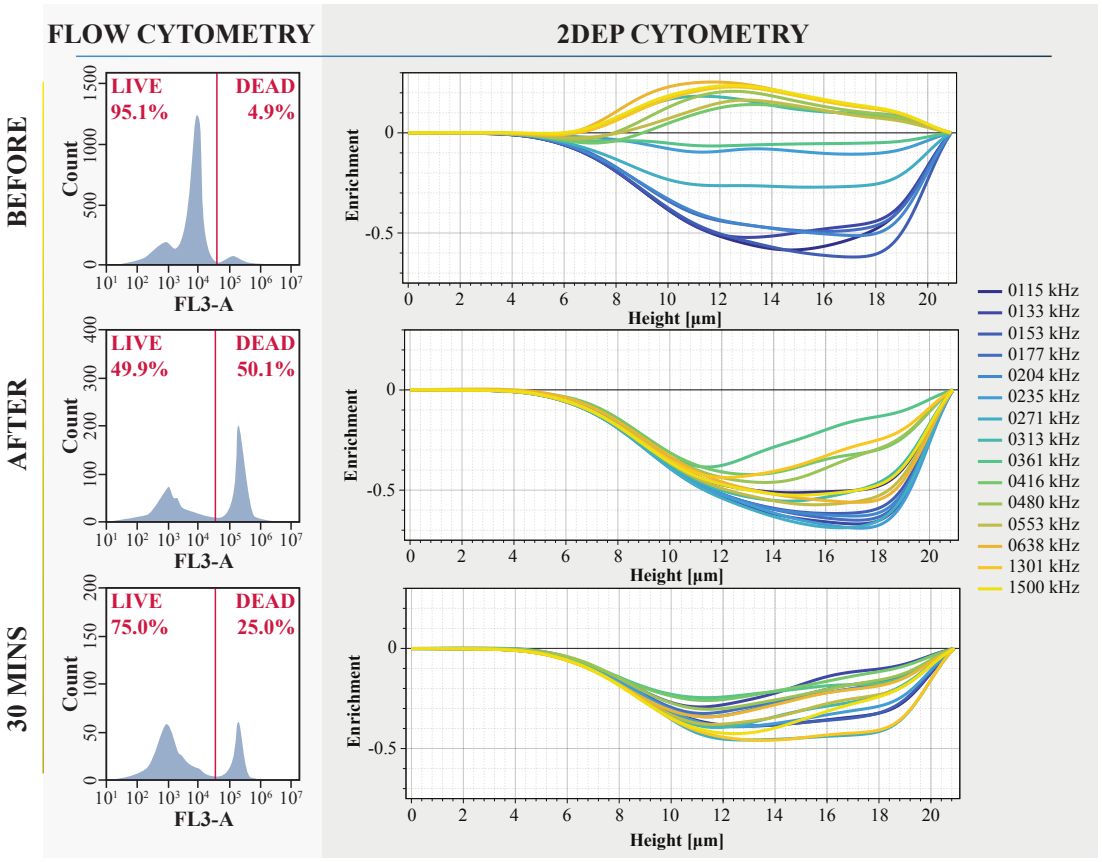

FIGURE 5.6: Flow cytometry data with standard viability staining showing number of live and dead cells in fresh cells sample and heat treated (left); and KDE of the measured DE signatures of fresh and heat treated K562 cell line (right). See Figure 4.38 for the raw data.

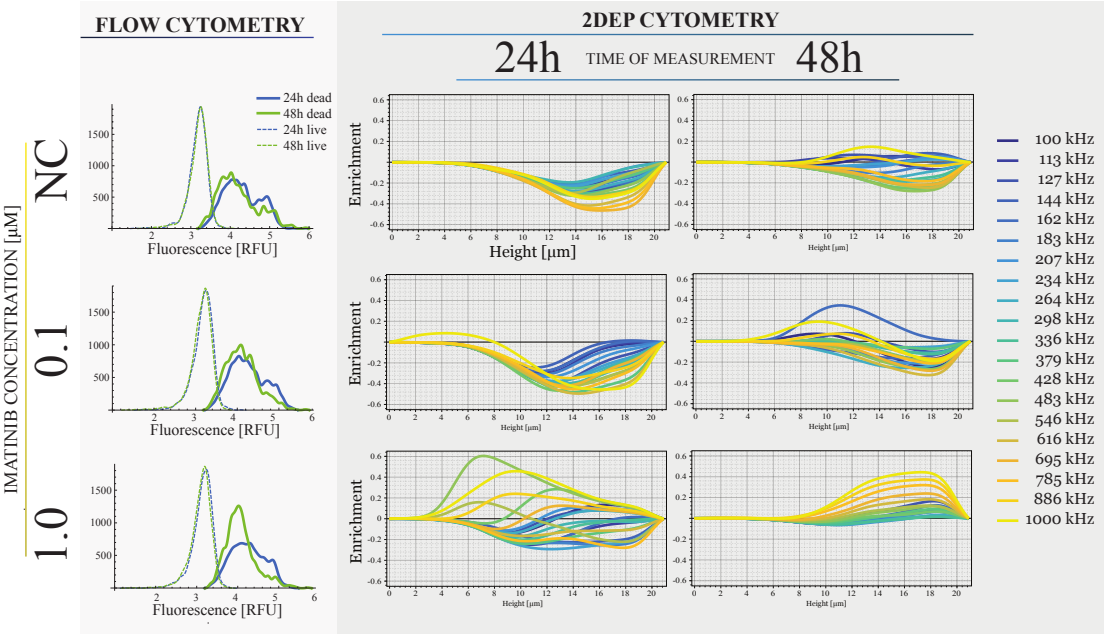

FIGURE 5.7: Flow cytometry data with standard viability staining showing number of live and dead cells in cells treated with different concentrations of INN after 24 and 48 hours from drug application (left); and KDE of the measured DE signatures of cells treated with INN (right). See Figure 4.40 for the raw data.

5.3 Wasserstein pseudometrics

Wasserstein distance is a measure of dissimilarity of two distributions. No model is required which is beneficial as models of the cellular processes are often unknown. Wasserstein pseudometrics from sampled data [97] was adjusted to include the necessary normalization by velocity step and applied directly to measured data samples to analyze the distance between distributions. The Wasserstein pseudometrics identifies frequencies, where less and more significant differences between the measured DE signatures are observed. The quantified dissimilarities between analyzed data sets may be further used to construct or simplify models of the underlying cellular processes that are too complex, difficult to understand, or do not correspond to reality. More importantly, Wasserstein pseudometrics may be used for identification of reliable biomarkers for cell changes. The Wasserstein metric quantification is relatively easy and does not require excessive computational power. The individual Wasserstein distance spectra, denoted as Wasserstein signatures, may be linked to certain cell states and used for later autonomous cell state identification. The degree of similarity between the measured Wasserstein signature and the one that is linked to certain cell state then corresponds to the probability of the cells being in that specific cell state. In addition, 2DEP Cytometry is a unique tool that enables fast and almost autonomous collection of live cell DE signatures for numerous cell phenotypes, and the Wasserstein signatures of cells in individual cell states, enabling construction of large database of the individual cell DE and Wasserstein signatures that may be used as a library of reliable biomarkers for cell state identification.

The Wasserstein distance between two probability measures $\mathcal{P}_1$ and $\mathcal{P}_2$ on sample space Ω with a pseudometric d is defined as:

$$\mathcal{W}_d(\mathcal{P}_1, \mathcal{P}_2) = \inf_{Q \in \mathcal{J}(\mathcal{Z}_1, \mathcal{Z}_2)} E_Q[d(\mathcal{Z}_1, \mathcal{Z}_2)], \tag{5.3}$$

where $\mathcal{Z}_1$ is a random variable of interest with distribution $\mathcal{P}_1$, $\mathcal{Z}_2$ is a random variable of interest with distribution $\mathcal{P}_2$, and $\mathcal{J}(\mathcal{Z}_1, \mathcal{Z}_2)$ is the set of all possible joint distributions of $\mathcal{Z}_1$ and $\mathcal{Z}_2$. Wasserstein pseudometric identifies the infimal cost necessary to transform one distribution to the other one. The pseudo-distance is considered of the form:

$$d(\omega, \eta) = \mid \mathcal{Z}(\omega) - \mathcal{Z}(\eta) \mid, \tag{5.4}$$

where $\mathcal{Z} : \Omega \to \mathbb{R}$ is a characteristic random variable of interest. The characteristic variable relevant to the 2DEP Cytometry may be the identified levitation height or the measured cell velocity.

In order to include the normalization by velocity step required by 2DEP Cytometry, the original Wasserstein pseudometric computation algorithm was adjusted to the following form:

1. Identify $M_1 = \sum_{n=1}^{N} v_i(\omega)$ and $M_2 = \sum_{n=1}^{N} v_i(\eta)$, where v_i stands for the velocity of the i^{th} of N samples in the corresponding distribution.
2. Trim the data set with larger M_i sum, so that when recalculated the M_1 and M_2 sums are as close to each other as possible.
3. Identify $\mathcal{Z}(\omega_i)$ for each ω_i, for $i = 1 \cdots n$.
4. Identify $\mathcal{Z}(\eta_i)$ for each η_i, for $i = 1 \cdots n$.
5. Sort and re-index both data sets in an ascendent nature in respect to the random variable of interest, so that:
   - $\mathcal{Z}(\omega_1) \leq \mathcal{Z}(\omega_2) \leq \cdots \leq \mathcal{Z}(\omega_N)$,
   - $\mathcal{Z}(\eta_1) \leq \mathcal{Z}(\eta_2) \leq \cdots \leq \mathcal{Z}(\eta_N)$.
6. Expand both data sets in respect to the normalization by velocity, as if each of the samples was repeated as many times as is the velocity of the particular sample.
7. Calculate the distances $d_i(\omega, \eta) = \mid \mathcal{Z}_i(\omega) - \mathcal{Z}_i(\eta) \mid$ between the expanded data sets.
8. Calculate the Wasserstein distance between the two compared distributions $\mathcal{W}_d(P_1, P_2) = \frac{1}{M} \sum_{i=1}^{N} d_i(\omega, \eta)$, where M equals the the smaller of the M_1 and M_2.

In result Wasserstein distance is obtained respecting the physical dimensions of the variable of interest. If levitation height in microns is selected as the variable of interest, the resulting Wasserstein distance is given in microns. Step 1 and 2 accounts for different number of samples within the distributions after normalization by velocity, and achieves their as close as possible equalization. The requirement of the normalization of each data sample by its velocity is achieved by the expansion of both distributions, and is performed in step 6.

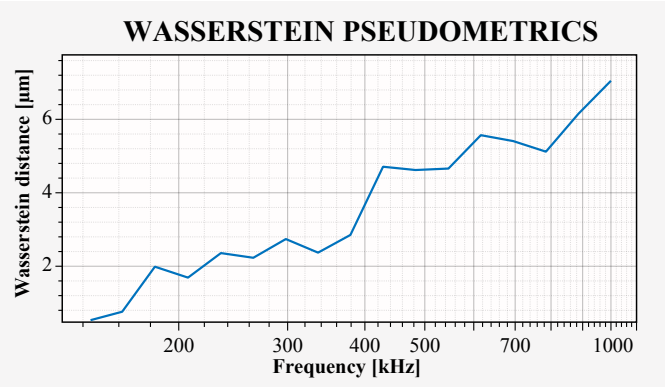

FIGURE 5.8: Estimated Wasserstein distance between genetically modified *S. cerevisiae* cell population over-expressing specific membrane protein and genetically modified *S. cerevisiae* cell population expressing cytoplasmic protein at the same rate.

Figure 5.8 illustrates the Wasserstein distance between the genetically modified *S. cerevisiae* cell population over-expressing specific membrane protein and the genetically modified *S. cerevisiae* cell population expressing cytoplasmic protein at the same rate.

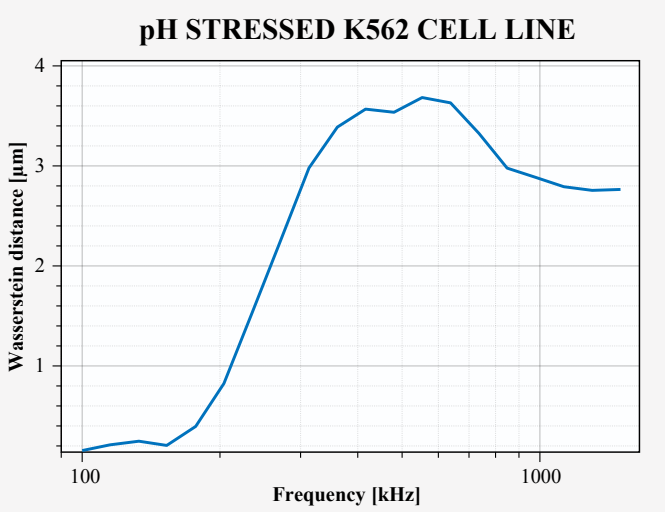

FIGURE 5.9: The estimated Wasserstein distance between fresh and pH stressed K562 cell lines, and its dependence on the frequency of the electric field.

To illustrate the disparity between fresh and pH stressed K562 cell lines, Wasserstein distance between these two distributions was quantified and is shown in Figure 5.9.

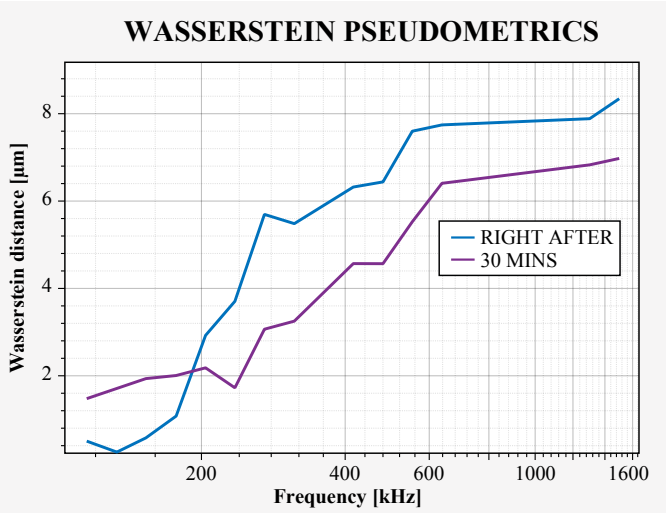

FIGURE 5.10: The estimated Wasserstein distance between the fresh K562 cell line and the K562 cell line heat treated at 60 $°C$, and its dependence on the frequency of the electric field.

Finally, to illustrate the differences between the measured DE signatures of the fresh and the heat treated K562 cell line at 60 $°C$, Figure 5.10 presents the Wasserstein distance between the two distributions.

5.4 Conclusion

KDE was used to overcome to finite nature of the data measured by 2DEP Cytometry. Special attention was then paid to data analysis in the comparative studies by identifying the Wasserstein distance between the measured distributions. Wasserstein pseudometrics was custom adjusted to include necessary normalization by velocity step. It was used to illustrate the dissimilarity of the measured distributions, and to identify reliable biomarker candidates for basic cell changes linked to over-expression of membrane proteins in *S. cerevisiae*, and stress response induced by medium pH variation and heat shock in K562 cells. The quantified Wasserstein distance spectra, denoted as Wasserstein signatures, were linked to specific cell states. The combination of 2DEP Cytometry, DE and Wasserstein signatures represents a unique tool enabling identification of reliable biomarkers for cell changes.

Chapter 6

Epilogue

6.1 Summary

State of the art Dielectrophoretic (DEP) technologies for cytometry purposes were investigated, the concepts were described, and the current technology limitations were formulated. To overcome these limitations, improvements were searched through improvements of fabrication processes of microfluidic devices enabling high precision alignment of microchannel structures with underlying electrodes permitting use of fast and relatively cheap prototyping fabrication technology based on Poly(dimethylsiloxane) (PDMS). Subsequently, a novel method enabling label-free, non-invasive, continuous probabilistic measurements of live cell Dielectric (DE) signatures was developed to show Dielectrophoresis (DEP) is sensitive enough to be used for cytometry purposes, and for identification of reliable biomarkers for cell changes.

In Chapter 3, the importance of precise alignment of microchannels with microelectrode structures was formulated for precision requiring applications. A benchmark problem of DEP-driven cell sorting in microfluidics was defined. The benchmark problem was characterised numerically to show that high sorting efficiencies can be achieved only with precise alignment. Alignment of the microchannel above the electrode structures must be in the order of the sorted cell size in order to achieve meaningful sorting efficiencies. Hence, the standard PDMS soft lithography fabrication process comprising a manual alignment stage is not suitable. A novel fabrication process enabling rapid prototyping of microfluidic devices with integrated electrodes and with high precision alignment was presented. The process enables faster development of DEP-based microfluidic technology achieving higher efficiencies and fully utilizing its real potential. The fabrication process was developed in ENS Cachan, Laboratory of Systems & Applications of Information & Energy Technologies (SATIE).

Chapter 4 describes the newly developed method called Distributed Dielectrophoretic Cytometry (2DEP Cytometry). It uses a DEP-induced vertical translation of live cells in conjunction with Particle Image Velocimetry (PIV) in order to measure probabilistic distribution of DEP forces on an entire cell population, and to identify reliable biomarkers for cell changes. The method was integrated in a microfluidic device. The presented method enables simultaneous and high-throughput collection of hundreds of single-cell responses in a single frame. In addition, PIV may be further integrated with fluorescence measurements yielding correlations between DE signatures and intracellular processes. Custom electric signal generator based on Direct Digital Synthesis (DDS) was designed and fabricated. Definition of complex signal profiles enables complete automation of 2DEP Cytometry data collection. An interface platform providing necessary mechanical support, and electrical and fluidic interconnections, enabling full encapsulation for precise control of the Carbon Dioxide (CO_2) and humidity levels was developed. 2DEP Cytometry was used to quantify the DE signature of a *Saccharomyces cerevisiae* (*S. cerevisiae*) population and Human Immortalised Myelogenous Leukemia (K562) cell line. It showed that DEP-induced cell translation along the parabolic velocity profile can be measured by PIV with sub-micron precision, enabling identification of individual cell DE signatures. It was possible to analyse more than 5 thousand cells within 1 minute with the actual experimental setup. The high-throughput enabled measurement of DE signatures at 20 different frequencies in almost real-time. Applications of 2DEP Cytometry in synthetic biology and cancer research were demonstrated. 2DEP Cytometry was used to perform comparative study on genetically modified *S. cerevisiae* cell populations and stressed K562 cell lines.

Chapter 5 addresses the problem of statistical analysis of 2DEP Cytometry data. Kernel Density Estimation (KDE) was used to overcome to finite nature of the measured data. The disparity between DE signatures of cells in different cells states was illustrated by adjusted Wasserstein pseudometrics. The KDE and Wasserstein pseudometric were adjusted to include the normalization by velocity step, which is necessary for correct interpretation of the data. The comparative study identified frequencies, where less and more significant differences between the measured DE signatures were observed. The obtained Wasserstein spectra, denoted as Wasserstein signatures, may be used as reliable biomarkers for cell changes measurable by 2DEP Cytometry.

6.2 Major contributions

Major contributions achieved in the presented work are listed in the following list:

1. A novel highly precise SU-8 fabrication technology was employed to construct microfluidic devices for sensitive DEP manipulation of *S. cerevisiae* cells. A benchmark microfluidic live cell sorting system was presented, and the effect of microchannel misalignment above electrode topologies on live cell DEP is discussed in detail. Simplified model of budding *S. cerevisiae* yeast cell was presented and validated experimentally in fabricated microfluidic devices. A novel fabrication process enabling rapid prototyping of microfluidic devices with well-aligned integrated electrodes was presented and the process flow was described.

2. A novel method called 2DEP Cytometry was developed. It uses a DEP-induced vertical translation of live cells in conjunction with PIV in order to measure probabilistic distribution of live cell DE signatures on an entire cell population. The method was integrated in a microfluidic device and validated on *S. cerevisiae* cell population and K562 cell line. 2DEP Cytometry was used to detect differences in molecular expression on cells by differential analysis of *a*) *S. cerevisiae* cells, and *b*) K562 cell line. First, the effect of over-expression of certain membrane protein was studied in *S. cerevisiae* cells. Measured distribution of DE signatures was compared to distribution of DE signatures of *S. cerevisiae* cell population expressing cytoplasmic protein at the same rate. Second, 2DEP Cytometry was applied to, and validated on, K562 cell line. Effects of stress response triggered by heat shock and pH variations on the DE signature of the cell line were analysed.

3. KDE was used to overcome to finite nature of the data measured by 2DEP Cytometry. Wasserstein pseudometrics from sampled data was used as a measure of dissimilarity between DE signature distributions in the comparative studies. Both, the KDE and the Wasserstein pseudometrics were adjusted to include the normalization by velocity step, which is required for correct interpretation of the 2DEP Cytometry data. The Wasserstein pseudometrics identifies frequencies, where less and more significant differences between the measured DE signatures are observed. The individual Wasserstein distance spectra, denoted as Wasserstein signatures, may be linked to certain cell states and used for later autonomous cell state identification. The degree of similarity between the measured Wasserstein signature and the ones that are linked to certain cell state then corresponds to the probability of the cells being in that specific cell state. In addition, 2DEP Cytometry is a unique tool that enables fast and almost autonomous collection of live cell DE signatures for numerous cell phenotypes, and the Wasserstein signatures of cells in individual cell states, enabling construction of large database of the individual cell DE and Wasserstein signatures that may be used as reliable biomarkers for cell state identification using 2DEP Cytometry.

4. In conclusion, 2DEP Cytometry in combination with the statistical data analysis showed it is sensitive enough to identify reliable biomarkers for certain changes in cell states.

6.3 Conclusion

Label-free and non-invasive DEP is a promising alternative to conventional flow cytometry. DEP already showed it is capable to distinguish between different cell phenotypes as well as cells in different cell states or cell undergoing certain cell changes suggesting DEP has great potential in sensitive cytometry applications. Although the DE signatures may contain whole set of useful biomarkers for cell changes, there is no efficient and universal method enabling measurement of the live cell DE signatures on a population level. Driven by the needs in current biotechnology, this thesis is trying to contribute to the field by **1)** providing a novel fast prototyping fabrication process suitable for DEP cytometry purpose requiring high precision, **2)** development of a new method called 2DEP Cytometry enabling label-free, non-invasive, continuous probabilistic measurements of live cell DE signatures on an entire cell populations, and **3)** providing powerful statistical analytical tools that enable fast automated identification of reliable biomarkers for cell changes in the measured samples.

Improvements of the current state of the art methods was first searched through fabrication of the microfluidic devices. It was shown that sensitivity of the DEP-based cell sorting in microfluidic devices can be highly dependent on the precision of the fabrication processes depending on the selected topology, and precision of the alignment of microchannels to the underlying electrodes must be on the order of the cell size in order to achieve meaningful sorting efficiencies. An innovative fabrication process for rapid prototyping of microfluidic devices providing high precision alignment of microchannels to underlying electrode structures was presented. Devices fabricated by the presented method showed close to perfect alignment, while the standard PDMS soft lithography fabrication process comprising a manual alignment stage proved not to be suitable. It was shown that permanent bonding of SU-8 to PDMS can be achieved by simple and efficient wet chemical silanization step in combination with oxygen plasma treatment. The presented method is easily reproducible and enables simple, low cost, fast prototyping of microfluidic devices suitable for live cell handling.

A novel force equilibrium method called 2DEP Cytometry enabling label-free, non-invasive, continuous probabilistic measurements of live cell DE signatures was developed, and it was shown 2DEP Cytometry is sensitive enough to be used for cytometry purposes. The presented method does not require any cell labelling, and is non-invasive. In addition,

the PIV is based on imaging and the measured DE signatures can be further correlated with other fluorescence and optical data providing deeper insight into each measured single cell properties and cellular processes that govern the cell behavior. Resolution of the method was roughly estimated in terms of z-resolution as well as sensitivity to individual cell DE properties. 2DEP Cytometry in combination with presented statistical data analysis provide unique tool for fast identification of reliable biomarkers for changes in cell states.

Applications of 2DEP Cytometry may be found for instance in cellular and synthetic biology, immunology, and cancer research. 2DEP Cytometry in combination with construction of database of DE and Wasserstein signatures could be a valuable tool, which may lead to better understanding of changes in cell states under various inducers, effect of certain therapies on cancer cells, or development of Multidrug Resistance (MDR) in cancer cells and subsequent improvement of personal medicine.

6.4 Future work

The PIV is based on imaging and the measured DE signatures can be further correlated with other fluorescence and optical data providing deeper insight into each measured single cell properties and cellular processes that govern the cell behavior. Fluorescence levels may be linked to specific functional products enabling mapping of certain protein levels. Eventually, combination of 2DEP Cytometry with fluorescence measurements might be beneficial in distinguishing multiple subpopulations within single analyzed sample.

2DEP Cytometry is a unique tool enabling relatively easy collecting of large quantities of data that may lead to construction of robust database containing DE signatures of cells of different phenotypes and genotypes; including Wasserstein signatures for identification of individual changes in cell states making 2DEP Cytometry more powerful tool in the biotechnology field giving biologists the opportunity to use the DE biomarkers for various purposes.

Both, the resolution and the sensitivity of 2DEP Cytometry may be significantly increased by using more suitable CMOS technology instead of CCD used in the presented experiments. Eventually, using lens-free CMOS technology for 3D on-chip tomography [57] would be interesting approach providing even finer resolution as well as much higher throughput due to significantly larger field of view, shorter times necessary for individual measurements, and minimization of both the initial price, and the room requirements. The combination of 2DEP Cytometry and the on-chip tomography would bring the opportunity to perform static, zero-flow-rate experiments, that could be used

for true time lapse single cell DEP analysis, while the amount of single cell analysis obtained at single moment would remain unchanged or would even increase (hundreds to thousands of cells).

Sensitivity of 2DEP Cytometry might be further increased by combining DEP with Dielectric Spectroscopy (DS) on single chip. Recently, DS measurements expanded and found application in Impedimetric Flow Cytometry (IFC), cancer and stem cell research, or drug dosing assays. Impedance analysis was used to measure cell proliferation in real-time and showed that it is faster than commonly used image based analysis in detecting drug-induced cellular activities [6]. Microfluidic-based impedance cytometer was also used to characterise *S. cerevisiae* sub-cellular morphology of single cells. The capabilities were demonstrated by discrimination of wild-type *S. cerevisiae* cells from mutants [49]. IFC is able to analyze massive number of cells in short time, but it is not yet sensitive enough to replace the standard flow cytometry as it cannot differentiate between cell types with similar morphology [107]. Although sensitivity of the DEP-based cell analysis may be improved with DS, no one yet combined these two technologies on a single chip for this purpose.

List of publications

6.5 Journal papers

1. P. Fikar, G. Lissorgues, L. Rousseau, O. Francais, B. Le Pioufle, F. S. Hamdi, V. Georgiev, D. Georgiev *Su-8 microchannels for live cell dielectrophoresis improvements.* Microsystem Technologies, ISSN 0946-7076, DOI 10.1007/s00542-015-2725-y, July 2015.

6.6 Conference papers

1. P. Fikar et al. *Distributed dielectrophoretic cytometry: measuring dielectric signature distribution in cell populations.* In Proceedings of Dielectrophoresis 2016, July 2016

2. P. Fikar, G. Lissorgues, L. Rousseau, O. Francais, B. Le Pioufle, F. S. Hamdi, V. Georgiev, D. Georgiev *Su-8 microchannels for live cell dielectrophoresis improvements.* In Proceedings of DTIP - Design, Test, Integration and Packaging of MEMS/MOEMS. IEEE, April 2015

3. P. Fikar et. al. *Dependence of dielectrophoretic forces on membrane proteins.* In Proceeding of BioBricks Foundation Synthetic Biology Conference (SB6.0), July 2013

4. P. Fikar. *Micro-fluidic device for dielectrophoretic sorting of live cells.* In Elektrotechnika a informatika 2013, Part 2., Electronics. Pilsen: University of West Bohemia, 2013, pg. 29-32, ISBN: 978-80-261-0232-8

5. P. Fikar. *Standard methods for computer modeling and simulation of live cells dielectrophoresis.* In Elektrotechnika a informatika 2012, Part 2., Electronics. Pilsen: University of West Bohemia, 2012, pg. 33-36, ISBN: 978-80-261-0119-2

Bibliography

[1] Valera A. Tracking and synchronization of the yeast cell cycle using dielectrophoretic opacity. *Lab chip*, 11:1754–1760, 2011.

[2] Daniel L Adams, Peixuan Zhu, Olga V Makarova, Stuart S Martin, Monica Charpentier, Saranya Chumsri, Shuhong Li, Platte Amstutz, and Cha-Mei Tang. The systematic study of circulating tumor cell isolation using lithographic microfilters. *RSC advances*, 4(9):4334–4342, 2014.

[3] M. Alshareef. Separation of tumor cells with dielectrophoresis-based microfluidic chip. *Biomicrofluidics*, 7, 2013.

[4] Marianna Alunni-Fabbroni. Circulating tumour cells in clinical practice: Methods of detection and possible characterization. *Methods*, 50:289–297, 2010.

[5] Dan E. Angelescu. *Highly Integrated Microfluidic Design.* Artech House, Norwood, 2011.

[6] L Renea Arias, Carla A Perry, and Liju Yang. Real-time electrical impedance detection of cellular activities of oral cancer cells. *Biosensors and Bioelectronics*, 25(10):2225–2231, 2010.

[7] Koji Asami. Characterization of biological cells by dielectric spectroscopy. *Journal of Non-Crystalline Solids*, 305(1):268–277, 2002.

[8] Koji Asami, Eugen Gheorghiu, and Takeshi Yonezawa. Dielectric behavior of budding yeast in cell separation. *Biochimica et Biophysica Acta (BBA)-General Subjects*, 1381(2):234–240, 1998.

[9] Garsha Bahrieh, Murat Erdem, Ebru Özgür, Ufuk Gündüz, and Haluk Külah. Assessment of effects of multi drug resistance on dielectric properties of k562 leukemic cells using electrorotation. *RSC Advances*, 4(85):44879–44887, 2014.

[10] E Balciunas. Lithographic microfabrication of biocompatible polymers for tissue engineering and lab-on-a-chip applications. *Biophotonics: Photonic Solutions for Better Health Care III.*, 2012.

[11] J.P. Beech. Sorting cells by size, shape and deformability. *Lab on a Chip*, 12(6):1048–1051, 2012.

[12] David Botstein, Steven A Chervitz, and J Michael Cherry. Yeast as a model organism. *Science (New York, NY)*, 277(5330):1259, 1997.

[13] William A Braff, Dana Willner, Philip Hugenholtz, Korneel Rabaey, and Cullen R Buie. Dielectrophoresis-based discrimination of bacteria at the strain level based on their surface properties. *PloS one*, 8(10):e76751, 2013.

[14] Henrik Bruus. *Theoretical microfluidics*. MIC Department of Micro and Nanotechnology Technical University of Denmark, 2006.

[15] Esther G Cen, Colin Dalton, Youlan Li, Sophia Adamia, Linda M Pilarski, and Karan VIS Kaler. A combined dielectrophoresis, traveling wave dielectrophoresis and electrorotation microchip for the manipulation and characterization of human malignant cells. *Journal of microbiological methods*, 58(3):387–401, 2004.

[16] H.S. Chang. Electro-kinetics: A viable micro-fluidic platform for miniature diagnostic kits. *The Canadian Journal of Chemical Engineering*, 84(2):146–160, 2006.

[17] T. Chen. Fabrication and package of microfluidic dielectrophoretic chip for trapping two particles. *Industrial Electronics and Applications (ICIEA), 2013 8th IEEE Conference on. IEEE*, 2013.

[18] Yuchao Chen. Rare cell isolation and analysis in microfluidics. *Lab on a chip*, 14:626–645, 2014.

[19] Sue Chin, Michael P Hughes, Helen M Coley, and Fatima H Labeed. Rapid assessment of early biophysical changes in k562 cells during apoptosis determined using dielectrophoresis. *international Journal of nanomedicine*, 1(3):333–337, 2006.

[20] S.H. Cho. Biocompatible su-8-based microprobes for recording neural spike signals from regenerated peripheral nerve fibers. *IEEE Sensors Journal*, 8(11), 2008.

[21] Davey CL and Kell DB. The low-frequency dielectric properties of biological cells. *Bioelectrochemistry of cells and tissues*, pages 159–207, 1995.

[22] Helen M Coley, Fatima H Labeed, Hilary Thomas, and Michael P Hughes. Biophysical characterization of mdr breast cancer cell lines reveals the cytoplasm is critical in determining drug sensitivity. *Biochimica et Biophysica Acta (BBA)-General Subjects*, 1770(4):601–608, 2007.

[23] Ronald B Corley. *A guide to methods in the biomedical sciences*. Springer Science & Business Media, 2005.

[24] Massimo Cristofanilli, Giovanni De Gasperis, Lisha Zhang, Mien-Chie Hung, Peter RC Gascoyne, and Gabriel N Hortobagyi. Automated electrorotation to reveal dielectric variations related to her-2/neu overexpression in mcf-7 sublines. *Clinical Cancer Research*, 8(2):615–619, 2002.

[25] C Dalton, AD Goater, J Drysdale, and R Pethig. Parasite viability by electrorotation. *Colloids and Surfaces A: Physicochemical and Engineering Aspects*, 195(1):263–268, 2001.

[26] CL Davey, GH Markx, and DB Kell. On the dielectric method of monitoring cellular viability. *Pure and applied chemistry*, 65(9):1921–1926, 1993.

[27] A. del Campo. Su-8: a photoresist for high-aspect-ratio and 3d submicron lithography. *Journal of Micromechanics and Microengineering*, 17(6), 2007.

[28] N. Demierre. Focusing and continuous separation of cells in a microfluidic device using lateral dielectrophoresis. *Sensors and Actuators B: Chemical*, 132(2):388–396, 2008.

[29] Yağmur Demircan, Aziz Koyuncuoğlu, Murat Erdem, Ebru Özgür, Ufuk Gündüz, and Haluk Külah. Label-free detection of multidrug resistance in k562 cells through isolated 3d-electrode dielectrophoresis. *Electrophoresis*, 36(9-10):1149–1157, 2015.

[30] G. Destgeer. Continuous separation of particles in a pdms microfluidic channel via travelling surface acoustic waves (tsaw). *Lab on a Chip*, 13(21):4210–4216, 2013.

[31] Jabel Dinorin-Tellez-Giron, Raul Jacobo Delgado-Macuil, Claudia Patricia Larralde Corona, Francisco Javier Martinez Montes, Mayra de la Torre Martinez, and Victor Eric Lopez-Y-Lopez. Reactance and resistance: main properties to follow the cell differentiation process in bacillus thuringiensis by dielectric spectroscopy in real time. *Applied microbiology and biotechnology*, pages 1–12, 2015.

[32] L Duncan, H Shelmerdine, MP Hughes, HM Coley, Y Hübner, and FH Labeed. Dielectrophoretic analysis of changes in cytoplasmic ion levels due to ion channel blocker action reveals underlying differences between drug-sensitive and multidrug-resistant leukaemic cells. *Physics in medicine and biology*, 53(2):N1, 2007.

[33] O'Donnell EA. Multiparameter flow cytometry: advances in high resolution analysis. *Immune Network*, 13(2):43–54, 2013.

[34] F.H. Labeed et al. Assessment of multidrug resistance reversal using dielectrophoresis and flow cytometry. *Biophysical journal*, 85:2028–2034, 2003.

[35] Hortensia Ferrero, Francisco Delgado-Rosas, Carmen M Garcia-Pascual, Mercedes Monterde, Ralf C Zimmermann, Carlos Simón, Antonio Pellicer, and Raúl Gómez. Efficiency and purity provided by the existing methods for the isolation of luteinized granulosa cells: a comparative study. *Human reproduction*, 27(6):1781–1789, 2012.

[36] Lisa A Flanagan, Jente Lu, Lisen Wang, Steve A Marchenko, Noo Li Jeon, Abraham P Lee, and Edwin S Monuki. Unique dielectric properties distinguish stem cells and their differentiated progeny. *Stem cells*, 26(3):656–665, 2008.

[37] Kenneth R Foster, Friedrich A Sauer, and Herman P Schwan. Electrorotation and levitation of cells and colloidal particles. *Biophysical journal*, 63(1):180, 1992.

[38] O. Francais. 3d field focusing and defocusing geometries for cell trapping on a chip. *Design, Test, Integration & Packaging of MEMS/MOEMS, 2009. MEMS/-MOEMS'09. Symposium on. IEEE*, 2009.

[39] James Friend. Fabrication of microfluidic devices using polydimethylsiloxane. *Biomicrofluidics*, 4(2), 2010.

[40] Cevc G. Membrane electrostatics. *Bioelectrochemistry of cells and tissues*, 1031, 1990.

[41] Peter Gascoyne, Ronald Pethig, Jutamaad Satayavivad, Frederick F Becker, and Mathuros Ruchirawat. Dielectrophoretic detection of changes in erythrocyte membranes following malarial infection. *Biochimica et Biophysica Acta (BBA)-Biomembranes*, 1323(2):240–252, 1997.

[42] Peter R. C. Gascoyne. Dielectrophoretic separation of cancer cells from blood. *IEEE Trans Ind Appl.*, 33(3):670–678, 1997.

[43] Peter RC Gascoyne, Jamileh Noshari, Thomas J Anderson, and Frederick F Becker. Isolation of rare cells from cell mixtures by dielectrophoresis. *Electrophoresis*, 30(8):1388–1398, 2009.

[44] Peter RC Gascoyne and Sangjo Shim. Isolation of circulating tumor cells by dielectrophoresis. *Cancers*, 6(1):545–579, 2014.

[45] Peter RC Gascoyne, Sangjo Shim, Jamileh Noshari, Frederick F Becker, and Katherine Stemke-Hale. Correlations between the dielectric properties and exterior morphology of cells revealed by dielectrophoretic field-flow fractionation. *Electrophoresis*, 34(7):1042–1050, 2013.

[46] P.R.C. Gascoyne. Isolation of rare cells from cell mixtures by dielectrophoresis. *Electrophoresis*, 30(8):1388–1398, 2009.

[47] A. Ghubade. Dielectrophoresis assisted concentration of micro-particles and their rapid quantitation based on optical means. *Biomedical microdevices*, 11(5):987–995, 2009.

[48] Vishal Gupta, Insiya Jafferji, Miguel Garza, Vladislava O Melnikova, David K Hasegawa, Ronald Pethig, and Darren W Davis. Apostream, a new dielectrophoretic device for antibody independent isolation and recovery of viable cancer cells from blood. *Biomicrofluidics*, 6(2):024133, 2012.

[49] Niels Haandbæk, Sebastian C Bürgel, Fabian Rudolf, Flavio Heer, and Andreas Hierlemann. Microfluidic impedance cytometer for characterization of subcellular morphology of single cells. In *2013 Transducers & Eurosensors XXVII: The 17th International Conference on Solid-State Sensors, Actuators and Microsystems (TRANSDUCERS & EUROSENSORS XXVII)*, pages 1314–1317. IEEE, 2013.

[50] F.S. Hamdi. Low temperature irreversible poly (dimethyl) siloxane packaging of silanized su-8 microchannels: Characterization and lab-on-chip application. *IEEE*, pages 1015–1024, 2014.

[51] Ralph Holzel. Electrorotation of single yeast cells at frequencies between 100 hz and 1.6 ghz. *Biophysical journal*, 73(2):1103–1109, 1997.

[52] Ralph Holzel. Nystatin-induced changes in yeast monitored by time-resolved automated single cell electrorotation. *Biochimica et Biophysica Acta (BBA)-General Subjects*, 1425(2):311–318, 1998.

[53] MP Hughes, X-B Wang, FF Becker, PRC Gascoyne, and RBUK Pethig. Computer-aided analyses of electric fields used in electrorotation studies. *Journal of Physics D: Applied Physics*, 27(7):1564, 1994.

[54] S.C. Hur. High-throughput size-based rare cell enrichment using microscale vortices. *Biomicrofluidics*, 5(2):022206, 2011.

[55] Kyung A Hyun. Negative enrichment of circulating tumor cells using a geometrically activated surface interaction chip. *Analytical chemistry*, 85(9):4439–4445, 2013.

[56] S. Noorjannah Ibrahim. The quadrupole microelectrode design on a multilayer biochip for dielectrophoretic trapping of single cells. *Microelectronic Engineering*, 97:369–374, 2012.

[57] Serhan O Isikman, Waheb Bishara, Onur Mudanyali, Ikbal Sencan, Ting-Wei Su, Derek K Tseng, Oguzhan Yaglidere, Uzair Sikora, and Aydogan Ozcan. Lensfree

on-chip microscopy and tomography for biomedical applications. *IEEE Journal of Selected Topics in Quantum Electronics*, 18(3):1059–1072, 2012.

[58] Thomas B. Jones. Basic theory of dielectrophoresis and electrorotation. *IEEE engineering in medicine and biology magazine*, pages 34–42, 2003.

[59] J.G. Kralj. Continuous dielectrophoretic size-based particle sorting. *Analytical chemistry*, 78(14):5019–5025, 2006.

[60] S.N. Krylov. Single-cell analysis using capillary electrophoresis: Influence of surface support properties on cell injection into the capillary. *Electrophoresis*, 21:767–773, 2000.

[61] Johana Kuncova-Kallio. Pdms and its suitability for analytical microfluidic devices. In *Proceedings of the 28th IEEE EMBS Annual International Conference*, New York City, USA, 9 2006. IEEE.

[62] J. Kwon. Su-8-based immunoisolative microcontainer with nanoslots defined by nanoimprint lithography. *Journal of Vacuum Science & Technology B*, 27(6):2795–2800, 2009.

[63] Fatima H Labeed, Helen M Coley, and Michael P Hughes. Differences in the biophysical properties of membrane and cytoplasm of apoptotic cells revealed using dielectrophoresis. *Biochimica et Biophysica Acta (BBA)-General Subjects*, 1760(6):922–929, 2006.

[64] G.B. Lee. Hydrodynamic focusing for a micromachined flow cytometer. *Journal of fluids engineering*, 123(3):672–679, 2001.

[65] J.N. Lee. Solvent compatibility of poly(dimethylsiloxane)-based microfluidic devices. *Analytical Chemistry*, 75:6544–6554, 2003.

[66] S.W. Lee. Shrinkage ratio of pdms and its alignment method for the wafer level process. *Microsystem Technologies*, 14(2):205–208, 2008.

[67] K.F. Lei. Materials and fabrication techniques for nano-and microfluidic devices. *Microfluidics in Detection Science: Lab-on-a-chip Technologies*, pages 1–28, 2014.

[68] Nuttawut Lewpiriyawong, Kumaravel Kandaswamy, Chun Yang, Volodymyr Ivanov, and Roman Stocker. Microfluidic characterization and continuous separation of cells and particles using conducting poly (dimethyl siloxane) electrode induced alternating current-dielectrophoresis. *Analytical chemistry*, 83(24):9579–9585, 2011.

[69] J.M. Lopacinska. Poly(dimethylsiloxane) (pdms) affects gene expression in pc12 cells differentiating into neuronal-like cells. *PLoS ONE*, 8(1), 2013.

[70] Gerard H. Markx and Christopher L. Davey. The dielectric properties of biological cells at radiofrequencies: Applications in biotechnology. *Enzyme and Microbial Technology*, 25:161–171, 1999.

[71] Gerard H Markx, Mark S Talary, and Ronald Pethig. Separation of viable and non-viable yeast using dielectrophoresis. *Journal of Biotechnology*, 32(1):29–37, 1994.

[72] J.C. McDonald. Poly (dimethylsiloxane) as a material for fabricating microfluidic devices. *Accounts of chemical research*, 35(7):491–499, 2002.

[73] Hui-Sung Moon, Kiho Kwon, Seung-Il Kim, Hyunju Han, Joohyuk Sohn, Soohyeon Lee, and Hyo-Il Jung. Continuous separation of breast cancer cells from blood samples using multi-orifice flow fractionation (moff) and dielectrophoresis (dep). *Lab on a Chip*, 11(6):1118–1125, 2011.

[74] H Morgan. Large-area travelling-wave dielectrophoresis particle separator. *Journal of Micromechanics and Microengineering*, 7(2), 1997.

[75] Seiichi Morita, Hiroshi Umakoshi, and Ryoichi Kuboi. Characterization and on-line monitoring of cell disruption and lysis using dielectric measurement. *Journal of bioscience and bioengineering*, 88(1):78–84, 1999.

[76] HJ Mulhall, A Cardnell, KF Hoettges, FH Labeed, and MP Hughes. Apoptosis progression studied using parallel dielectrophoresis electrophysiological analysis and flow cytometry. *Integrative Biology*, 7(11):1396–1401, 2015.

[77] Sunitha Nagrath. Isolation of rare circulating tumour cells in cancer patients by microchip technology. *Nature*, 450:1235–1239, 2007.

[78] K.V. Nemani. In vitro and in vivo evaluation of su-8 biocompatibility. *Materials Science and Engineering C: Material for Biological Applications*, 33(7), 2013.

[79] Marija Nikolic-Jaric, Tim Cabel, Elham Salimi, Ashlesha Bhide, Katrin Braasch, Michael Butler, Greg E Bridges, and Douglas J Thomson. Differential electronic detector to monitor apoptosis using dielectrophoresis-induced translation of flowing cells (dielectrophoresis cytometry). *Biomicrofluidics*, 7(2):024101, 2013.

[80] Marija Nikolic-Jaric, Sean F Romanuik, Graham A Ferrier, Tim Cabel, Elham Salimi, David B Levin, Greg E Bridges, and Douglas J Thomson. Electronic detection of dielectrophoretic forces exerted on particles flowing over interdigitated electrodes. *Biomicrofluidics*, 6(2):024117, 2012.

[81] I.S. Noorjannah. The quadrupole microelectrode design on a multilayer biochip for dielectrophoretic trapping of single cells. *Microelectronic Engineering*, 97:369–374, 2012.

[82] In Soo Park, Jaewoo Lee, Gyudo Lee, Kihwan Nam, Taewoo Lee, Woo-Jin Chang, Hansung Kim, Sei-Young Lee, Jongbum Seo, Dae Sung Yoon, et al. Real-time analysis of cellular response to small-molecule drugs within a microfluidic dielectrophoresis device. *Analytical chemistry*, 87(12):5914–5920, 2015.

[83] R Pethig and MS Talary. Dielectrophoretic detection of membrane morphology changes in jurkat t-cells undergoing etoposide-induced apoptosis. *Iet Nanobiotechnology*, 1(1):2–9, 2007.

[84] Ronald Pethig, Richard S Lee, and Mark S Talary. Cell physiometry tools based on dielectrophoresis. *Journal of the association for laboratory automation*, 9(5):324–330, 2004.

[85] Yulia Polevaya, Irina Ermolina, Michael Schlesinger, Ben-Zion Ginzburg, and Yuri Feldman. Time domain dielectric spectroscopy study of human cells: Ii. normal and malignant white blood cells. *Biochimica et Biophysica Acta (BBA)-Biomembranes*, 1419(2):257–271, 1999.

[86] Erica D Pratt, Chao Huang, Benjamin G Hawkins, Jason P Gleghorn, and Brian J Kirby. Rare cell capture in microfluidic devices. *Chemical engineering science*, 66(7):1508–1522, 2011.

[87] Sittisak Pui-ock, Mathuros Ruchirawat, and Peter Gascoyne. Dielectrophoretic field-flow fractionation system for detection of aquatic toxicants. *Analytical chemistry*, 80(20):7727–7734, 2008.

[88] Kanatip Ratanachoo, Peter RC Gascoyne, and Mathuros Ruchirawat. Detection of cellular responses to toxicants by dielectrophoresis. *Biochimica et Biophysica Acta (BBA)-Biomembranes*, 1564(2):449–458, 2002.

[89] Christoph Reichle, Torsten Muller, Thomas Schnelle, and Gunter Fuhr. Electrorotation in octopole micro cages. *Journal of Physics D: Applied Physics*, 32(16):2128, 1999.

[90] Jose Luis Sebastian Franco, Aranzazu Sanchis Otero, José Roldan Madronero, and Sagrario Munoz San Martin. Dielectric characterization of the yeast cell budding cycle. *Progress In Electromagnetics Research*, 134:1–22, 2013.

[91] Jose Luis Sebastian Franco, Aranzazu Sanchis Otero, José Roldan Madronero, and Sagrario Munoz San Martin. Dielectric characterization of the yeast cell budding cycle. *Progress In Electromagnetics Research*, 134:1–22, 2013.

[92] Y. Shiine. Soft-lithographic methods for the fabrication of dielectrophoretic devices using molds by proton beam writing. *Microelectronic Engineering*, 87(5):835–838, 2010.

[93] Sangjo Shim. Antibody-independent isolation of circulating tumor cells by continuous-flow dielectrophoresis. *Biomicrofluidics*, 7(1), 2013.

[94] Sangjo Shim. Dielectrophoresis has broad applicability to marker-free isolation of tumor cells from blood by microfluidic systems. *Biomicrofluidics*, 7(1), 2013.

[95] Shi-Yang Tang, Pyshar Yi, Rebecca Soffe, Sofia Nahavandi, Ravi Shukla, and Khashayar Khoshmanesh. Using dielectrophoresis to study the dynamic response of single budding yeast cells to lyticase. *Analytical and bioanalytical chemistry*, 407(12):3437–3448, 2015.

[96] S. Tay. Single-cell nf-kb dynamics reveal digital activation and analogue information processing. *Nature*, 466:267–271, 2010.

[97] David Thorsley and Eric Klavins. Model reduction of stochastic processes using wasserstein pseudometrics. In *2008 American Control Conference*, pages 1374–1381. IEEE, 2008.

[98] Tian Y Tsong. Electroporation of cell membranes. *Biophysical journal*, 60(2):297, 1991.

[99] M. D. Vahey and J. Voldman. High-throughput cell and particle characterization using isodielectric separation. *Analytical Chemistry*, 81(7):2446–2455, 2009.

[100] Michael D Vahey and Joel Voldman. An equilibrium method for continuous-flow cell sorting using dielectrophoresis. *Analytical chemistry*, 80(9):3135–3143, 2008.

[101] A. Valero. A unified approach to dielectric single cell analysis: Impedance and dielectrophoretic force spectroscopy. *Lab on a Chip*, 17:2216–2225, 2010.

[102] L. Wang. Su-8 microstructure for quasi-three-dimensional cell-based biosensing. *Sensors and Actuators B: Chemical*, 140:349–355, 2009.

[103] X-B Wang, Ying Huang, Ralph Holzel, Julian PH Burt, and R Pethig. Theoretical and experimental investigations of the interdependence of the dielectric, dielectrophoretic and electrorotational behaviour of colloidal particles. *Journal of Physics D: Applied Physics*, 26(2):312, 1993.

[104] Xiao-Bo Wang. Cell separation by dielectrophoretic field-flow-fractionation. *Analytical Chemistry*, 72(4):832–839, 2000.

[105] Xujing Wang, Frederick F Becker, and Peter RC Gascoyne. Membrane dielectric changes indicate induced apoptosis in hl-60 cells more sensitively than surface phosphatidylserine expression or dna fragmentation. *Biochimica et Biophysica Acta (BBA)-Biomembranes*, 1564(2):412–420, 2002.

[106] Ieong Wong. Surface molecular property modifications for poly(dimethylsiloxane) (pdms) based microfluidic devices. *Microfluid Nanofluid*, 7:291–306, 2009.

[107] Youchun Xu, Xinwu Xie, Yong Duan, Lei Wang, Zhen Cheng, and Jing Cheng. A review of impedance measurements of whole cells. *Biosensors and Bioelectronics*, 77:824–836, 2016.

[108] Huang Y. Differences in the ac electrodynamics of viable and non-viable yeast cells determined through combined dielectrophoresis and electrorotation. *Phys Med Bio*, 37:1499–1517, 1992.

[109] Jun Yang, Ying Huang, Xiao-Bo Wang, Frederick F Becker, and Peter RC Gascoyne. Differential analysis of human leukocytes by dielectrophoretic field-flow-fractionation. *Biophysical Journal*, 78(5):2680–2689, 2000.

[110] Liju Yang, Padmapriya P Banada, Mohammad R Chatni, Kwan Seop Lim, Arun K Bhunia, Michael Ladisch, and Rashid Bashir. A multifunctional micro-fluidic system for dielectrophoretic concentration coupled with immuno-capture of low numbers of listeria monocytogenes. *Lab on a Chip*, 6(7):896–905, 2006.

[111] S.M. Yang. Precise cell trapping with structure-confined dielectrophoresis. *Solid-State Sensors, Actuators and Microsystems Conference (TRANSDUCERS), 2011 16th International. IEEE*, 2011.

[112] F. Yi. Design, fabrication and experiment of microfluidic cell culture for cancer and neurobiology research. *Doctoral Thesis, University of East Paris*, 2014.

Dielectrophoretic cytometry for measurement of live cell dielectric signatures on population level

Keywords: Dielectrophoresis, microfluidics, cytometry

The use of Dielectrophoresis (DEP) generated by non-uniform electric fields showed to be an interesting alternative to standard flow cytometry technology enabling non-invasive label-free cell measurements. This thesis investigates Dielectrophoretic (DEP) cytometry from three perspectives.

First, the importance of precise alignment of microchannels with microelectrode structures was formulated for precision requiring applications. A novel highly precise SU-8 fabrication technology suitable for fast prototyping was employed to construct microfluidic devices for sensitive DEP manipulation of live cells.

Second, a novel method called Distributed Dielectrophoretic Cytometry (2DEP Cytometry) was developed and integrated in a microfluidic device. It uses a DEP-induced vertical translation of live cells in conjunction with Particle Image Velocimetry (PIV) in order to measure probabilistic distribution of DEP forces on an entire cell population. Applications of 2DEP Cytometry in synthetic biology and cancer research were demonstrated by performing comparative study on genetically modified *Saccharomyces cerevisiae* cell populations and stressed Human Immortalised Myelogenous Leukemia (K562) cell lines.

Finally, statistical analytical tools were applied to quantify the dissimilarity between population signatures of cells in different cell states in terms of Wasserstein distance spectra, denoted as Wasserstein signatures. It was shown these signatures may be used as reliable biomarkers for cell changes.

Cytométrie diélectrophorétique pour les mesures des signatures diélectriques de cellules vivantes au niveau d'une population

Mots clés: Diélectrophorèse, microfluidique, cytométrie

L'utilisation de la diélectrophorèse (DEP) générée par des champs électriques non-uniformes a montré être une alternative intéressante à la technologie de cytométrie de débit standard permettant des mesures non-invasives et sans marquage de différentes cellules. Cette thèse étudie la cytométrie diélectrophorétique (DEP) selon trois axes.

Tout dabord, l'importance de l'alignement précis des micro-canaux avec des structures de microélectrodes a été démontrée pour des applications exigeantes en précision. Une nouvelle technologie de fabrication avec résine SU-8 adaptée au prototypage rapide a été utilisée pour construire des dispositifs microfluidiques permettant des manipulations de cellules vivantes par DEP à haute sensibilité.

Deuxièmement, une nouvelle méthode appelée Cytométrie Diélectrophorétique Distribuée (cytométrie 2DEP) a été développée. Elle utilise un effet de diélectrophorèse induite par translation verticale de cellules vivantes en liaison avec la vélocimétrie par image de particules (PIV) afin de mesurer la répartition probabiliste de forces DEP sur une population cellulaire entière. La méthode a été intégrée dans un dispositif microfluidique. Les applications de cytométrie 2DEP en biologie synthétique et en recherche sur le cancer ont été démontrées en réalisant une étude comparative sur des populations cellulaires de *Saccharomyces cerevisiae* génétiquement modifiées et sur des lignées cellulaires stressées *Human immortalise leucemie myeloide* (K562).

Enfin, des outils d'analyse statistique ont été développés pour quantifier les dissemblances entre les signatures des populations cellulaires à différents stades à l'aide de spectres en distance de Wasserstein, notés signatures Wasserstein. Il a été montré que ces signatures peuvent être utilisées comme marqueurs biologiques fiables pour certains changements cellulaires.